

N715 H.C. 83.00

NASA CONTRACTOR REPORT



NASA CR-2133

NASA CR-2133

FACILITY FORM 602	<u>N73-16133</u> (ACCESSION NUMBER)	<u>H.C. 83.00</u> (THRU)
	<u>110</u> (PAGES)	<u>H1</u> (CODE)
	<u>CR 2133</u> (NASA CR OR TMX OR AD NUMBER)	<u>07</u> (CATEGORY)

HIGH PERFORMANCE S-BAND HORN ANTENNAS FOR RADIOMETER USE

by R. Caldecott, C. A. Mentzer, L. Peters, and J. Toth

Prepared by
THE OHIO STATE UNIVERSITY
ELECTROSCIENCE LABORATORY
Columbus, Ohio 43212
for Langley Research Center

1. Report No. NASA CR-2133	2. Government Accession No.	3. Recipient's Catalog No.	
4. Title and Subtitle HIGH PERFORMANCE S-BAND HORN ANTENNAS FOR RADIOMETER USE		5. Report Date January 1973	
		6. Performing Organization Code	
7. Author(s) R. Caldecott, C. A. Mentzer, L. Peters and J. Toth		8. Performing Organization Report No.	
		10. Work Unit No. 160-20-54-03	
9. Performing Organization Name and Address The Ohio State University ElectroScience Laboratory Columbus, Ohio 43212		11. Contract or Grant No. NAS1-10040	
		13. Type of Report and Period Covered Contractor Report	
12. Sponsoring Agency Name and Address National Aeronautics and Space Administration Washington, D.C. 20546		14. Sponsoring Agency Code	
		15. Supplementary Notes	
16. Abstract <p>Horn antennas of four types: pyramidal corrugated, conical corrugated, pyramidal dual mode and conical dual mode, have been constructed and evaluated for use as S-band radiometer antennas. Each of the structures is described and radiation patterns and impedance and resistive loss measurements including a layer of foreign material on a thin radome, are presented. A precision method for determining reflection losses is described using a multiprobe reflectometer technique. The same technique is also applied to the measurement of resistive losses by closing the ends of the antennas with short circuit plates and determining the losses from an accurate measurement of the reflection coefficient. The radiation patterns were recorded with the aid of a real-time digital computer. The stored patterns were then processed to yield gain and beam efficiency.</p> <p>It was concluded that it is possible to design a highly efficient antenna for radiometer use and to measure its parameters precisely. However, it was found that it is necessary to modify the conventional definition of beamwidth somewhat if this term is to be meaningful for radiometer applications.</p>			
17. Key Words (Suggested by Author(s)) Antennas Radiometer Antennas, Corrugated Horn Antennas		18. Distribution Statement Unclassified - Unlimited	
19. Security Classif. (of this report) Unclassified	20. Security Classif. (of this page) Unclassified	21. No. of Pages 110	22. Price* \$3.00

TABLE OF CONTENTS

	Page
I. INTRODUCTION	1
II. DISCUSSION OF THE REQUIRED PARAMETERS	2
III. ANTENNA TYPES AND RADIATION PATTERN CHARACTERISTICS	3
A. <u>The Conical Corrugated Horn Antenna</u>	4
B. <u>The Pyramidal Corrugated Horn Antenna</u>	9
C. <u>The Conical Dual Mode Horn Antenna</u>	25
D. <u>The Pyramidal Dual Mode Horn Antenna</u>	38
E. <u>Comparisons with a Paraboloidal Antenna</u>	38
IV. MEASURING TECHNIQUES	43
A. <u>The Reflectometer System</u>	43
(i) The three probe reflectometer	45
(ii) The four probe reflectometer	48
(iii) Self checking systems	50
B. <u>Impedance Measurements</u>	53
C. <u>Resistive Loss Measurements</u>	57
D. <u>Beam Efficiency Measurements</u>	63
V. NEAR FIELD STUDIES	65
VI. RADOME LOSS MEASUREMENTS	78
VII. GEOMETRICAL DIFFRACTION THEORY APPLIED TO DUAL MODE HORN DESIGN	100
A. <u>The Pyramidal Dual Mode Horn</u>	101
B. <u>The Conical Dual Mode Horn</u>	101
VIII. CONCLUSIONS	106
REFERENCES	108

I. INTRODUCTION

The objective of this program has been to design a horn antenna of high quality for use with an S-band radiometer. The antenna is to have a symmetrical circularly polarized beam with a half-power beamwidth of 25° . In itself, this is not too difficult a task. However, the ultimate intention of this research is to examine the limitations introduced by the antenna for radiometer systems with a capability of observing noise temperatures to an accuracy of better than 1°K . This requires that the field of view of the antenna must be controlled and known to a very high degree of accuracy. The term field of view is used here in a very broad sense. Of course it includes the field of interest, that which lies within the main beam. In addition it includes the side and backlobes. If these are not to introduce substantial errors, they must be kept to an absolute minimum, i.e., the beam efficiency must be high. A further contributor to the observed noise, though not viewed by the antenna in the conventional sense, is resistive loss within the antenna structure. The contribution from this source depends on the loss (or alternatively the emission coefficient) of the antenna and on its physical temperature. If both these are known, a correction can be made. Thus, while it is not necessary to keep the loss extremely low (though this simplifies the measurement problem), it is necessary to evaluate it with a high degree of accuracy. A final contributor to the noise observed by the antenna results from its own mismatch. Any noise originating in the front end of the radiometer will be partially reflected back into the system by any mismatch at the antenna terminals. The effect is similar to that of the resistive loss. If the magnitude of the mismatch and the temperature of the radiometer front-end are known then correction can be made. However, it is first desirable to keep the mismatch to a minimum and then to know the residual mismatch to a high degree of accuracy.

It is evident from the foregoing that both the design of a high quality antenna and a precision evaluation of its characteristics are required. Target parameters for the antenna design were a symmetrical beam with a half-power beamwidth of 25° , sidelobes below 30 dB (preferably 35 dB), and a beam efficiency in the order of 97%. The target for evaluation of loss and mismatch was 0.01 dB. If such loss were assumed to occur at 300°K , 0.01 dB would correspond to an accuracy of 0.72°K . The 0.01 dB figure is the permissible loss of radiated power referred to the input power if the antenna were operating as a transmitter.

II. DISCUSSION OF THE REQUIRED PARAMETERS

Some of these parameters appear to be rather awesome and others depend on the definition of the quantity. The 0.01 dB accuracy figure of the antenna matching can be satisfied if the antenna VSWR is kept below 1.1. The antenna absorption losses must of course be measured to an accuracy of 0.01 dB of the forward power in the antenna, when transmitting.

Satisfaction of the beam efficiency condition depends on how the beam efficiency is defined. The common definition consisting of the ratio of the power radiated in the main beam (the region enclosed by the first null) to the total power radiated is not applicable to antenna patterns void of nulls, since this definition would always give 100% beam efficiency. An alternate definition for the beam efficiency B of the form

$$B = \frac{\int_0^{2\pi} \int_0^{\theta_1} S \sin^2 \theta \, d\theta \, d\phi}{\int_0^{2\pi} \int_0^{\pi} S \sin^2 \theta \, d\theta \, d\phi} ,$$

where S is the transmitted power density, is suggested. For example, the main beam may be fixed arbitrarily so that it includes twice the half power beamwidth, i.e., $\theta_1 = \theta_{\text{HPBW}}$. If the back lobe radiation is taken at a practical level of 40 dB below the pattern maximum for this half power beamwidth, this leads to an efficiency on the order 90% for the case of a rotationally symmetric pattern of the form of the H-plane pattern. (Further decreasing the back lobe level has only a minor effect on the beam efficiency.) Increasing the region of the main beam to include three times the half-power beamwidth ($\theta_1 = 1.5 \times \theta_{\text{HPBW}}$) yields a 99% beam efficiency. These values are relatively independent of the aperture phase taper (or H-plane horn geometry) once the phase distribution is such that the desired H-plane antenna pattern is obtained. This rotationally symmetric antenna pattern can be obtained and is needed to obtain the desired circular polarization over the main beam. In other words, the area to be observed or the "footprint" should be the angular region covered by approximately 35° from the polar axis for this particular low side lobe antenna to maintain the desired beam efficiency. Also it is only necessary to maintain the circular polarization over this angular region corresponding approximately to the -15 dB pattern level. These requirements appear too excessive in that the extent of the footprint would be almost twice the altitude of the antenna. Of course, the contribution from the extreme edges of the footprint would be reduced by the pattern level (-15 dB) but would look at a larger area per increment of polar angle. The use of a narrower antenna beam would require a larger aperture and a longer horn but a lower backlobe radiation level can be achieved. This reduces the angular extent required to achieve the 99% efficiency.

It should be noted that while backlobes 40 dB below the main beam produce a negligible effect on the present antennas, this would not be true for antennas with a narrower beam. The narrower beam antenna has a higher gain and therefore, though the absolute level of the backlobe radiation remains the same, the level relative to the main beam will be lower. For 1% radiation in the back pattern the approximate back lobe level in dB, relative to the main beam, is given by:

$$DB = 10 \log_{10} \left[\frac{4\pi}{\text{Beam Area Within Half Power Points}} \right] + 17$$

III. ANTENNA TYPES AND RADIATION PATTERN CHARACTERISTICS

The requirements for this application are a symmetrical circularly polarized beam with low side and backlobes. The requirement of symmetry obviously suggests a symmetrical antenna structure. The H-plane pattern of a simple horn has the desired characteristics: namely low side and backlobes. These result from a tapered aperture distribution, which reduces the sidelobes, and zero field at the horn walls which, since it reduces edge diffraction at the aperture, minimizes the sidelobes and backlobes. All of the antenna types considered are designed to produce a similar field configuration in the E- as well as the H-plane.

Two basic methods were used to produce the desired taper in the E-plane. The first of these employed the concept of a corrugated surface¹ to suppress the surface ray along the E walls. In this method slots are cut into the walls normal to both the surface and the direction of propagation. These slots are between a quarter and a half wavelength in depth and are therefore capacitive. It has been established for rectangular waveguides that the boundary conditions cannot be satisfied for the case where the surface impedance is capacitive for all four walls. However, it is suggested by an analysis by Narashimhan² that this concept is not valid for the pyramidal horn geometry. Excellent horn performance has been achieved with corrugations on all four walls of a pyramidal horn. The hybrid modes in a circular corrugated horn are well defined modes. A balanced hybrid mode theory has been developed for the circular corrugated horn which has been applied to the case where corrugations are exactly $\lambda/4$ deep. However, several experiments^{3,4} have shown the horn is an excellent radiator over nearly a two to one bandwidth. Moreover, the reported input VSWR is quite high when the corrugations are $\lambda/4$ deep. At this time, the theory has not been developed to include the operation of the horn in the more appropriate operating band. The detailed design of these antennas and their performance characteristics are presented in a later section of this report.

The second method used to generate symmetrical E- and H-plane patterns was the dual mode technique⁵. In this method, a higher order mode is generated in the horn in addition to the fundamental mode. This is selected so that it undergoes one and a half phase reversals across the width of the aperture, and is in phase with the fundamental mode at the center while exactly cancelling at the edges. A circular horn has been constructed based on this principle. The modes in this case are the fundamental TE_{11} mode with the TM_{11} used to produce the desired taper. The TM_{11} mode is generated by a step in the throat of the horn. A square dual mode horn was also constructed and tested. This horn was essentially similar in construction employing the fundamental TE_{01} mode with a blend of the TM_{21} and the TE_{21} used to produce the desired taper. The field configuration in this case bears a strong physical resemblance to that in the circular dual mode horn. Design details and performance data for these horns will also be presented.

A. The Conical Corrugated Horn Antenna

The measured amplitude of the electric field in the aperture of the conical corrugated horn fits a cosine distribution in both the E- and the H-planes. Thus standard H-plane conical horn curves such as those given by Jasik⁶ may be used to obtain the pattern in the vicinity of the main beam for a conical corrugated horn. The "optimum horn" with diameter 3.4λ and slant length 3.9λ was selected since it presented a compromise on physical size and pattern qualities. This resulted in an aperture 25.4 cm in diameter and a 56° flare angle.

From past experience, good antenna patterns are obtained for corrugation depths between $\lambda/4$ and $\lambda/2$ and for more than five corrugations per wavelength for a horn several wavelengths long. Eight corrugations per wavelength and a corrugation depth of 0.43λ were chosen for this relatively short horn. The corrugation depth has little effect on the radiation pattern in the range $0.25 < d/\lambda < 0.375$ but affects the antenna impedance. For depths approaching 0.5λ the radiation pattern deteriorates slightly while the impedance match improves. The 0.43λ depth was chosen to yield low VSWR. The antenna, pictured in Fig. 1, was machined from an aluminum billet specially cast for this purpose.

Aperture distribution measurements at 3.7 GHz, both amplitude and phase, appear in Figs. 2, 3 and 4 for cuts corresponding to the H-plane, E-plane and 45° plane respectively. These measurements were obtained using a nulled radar system and probing the fields with a small sphere. These data show that, in the aperture, the phase front is essentially that of a point source at the cone vertex. Calculated phase points for this assumed phase center are shown for comparison. It is interesting to note that this horn has an aperture distribution which is nearly circularly symmetrical about its axis. Thus its far field patterns should also be nearly symmetrical.

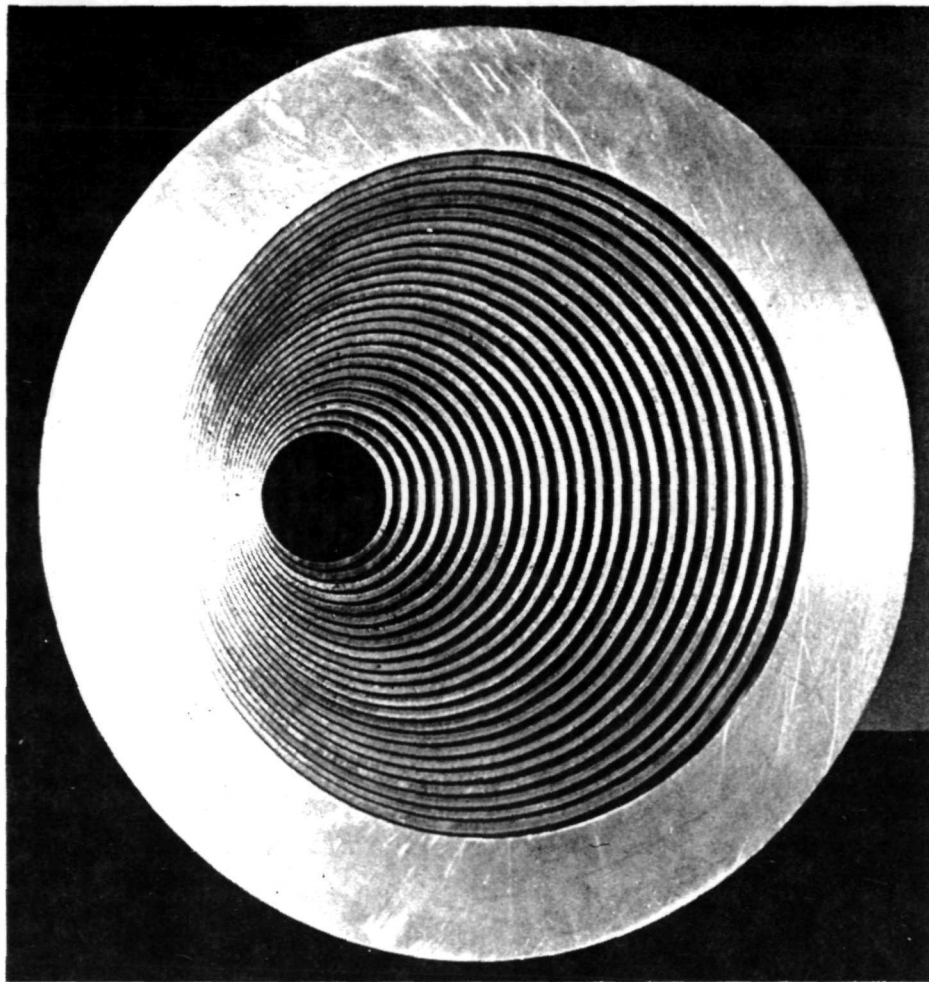


Fig. 1. The conical corrugated horn antenna.

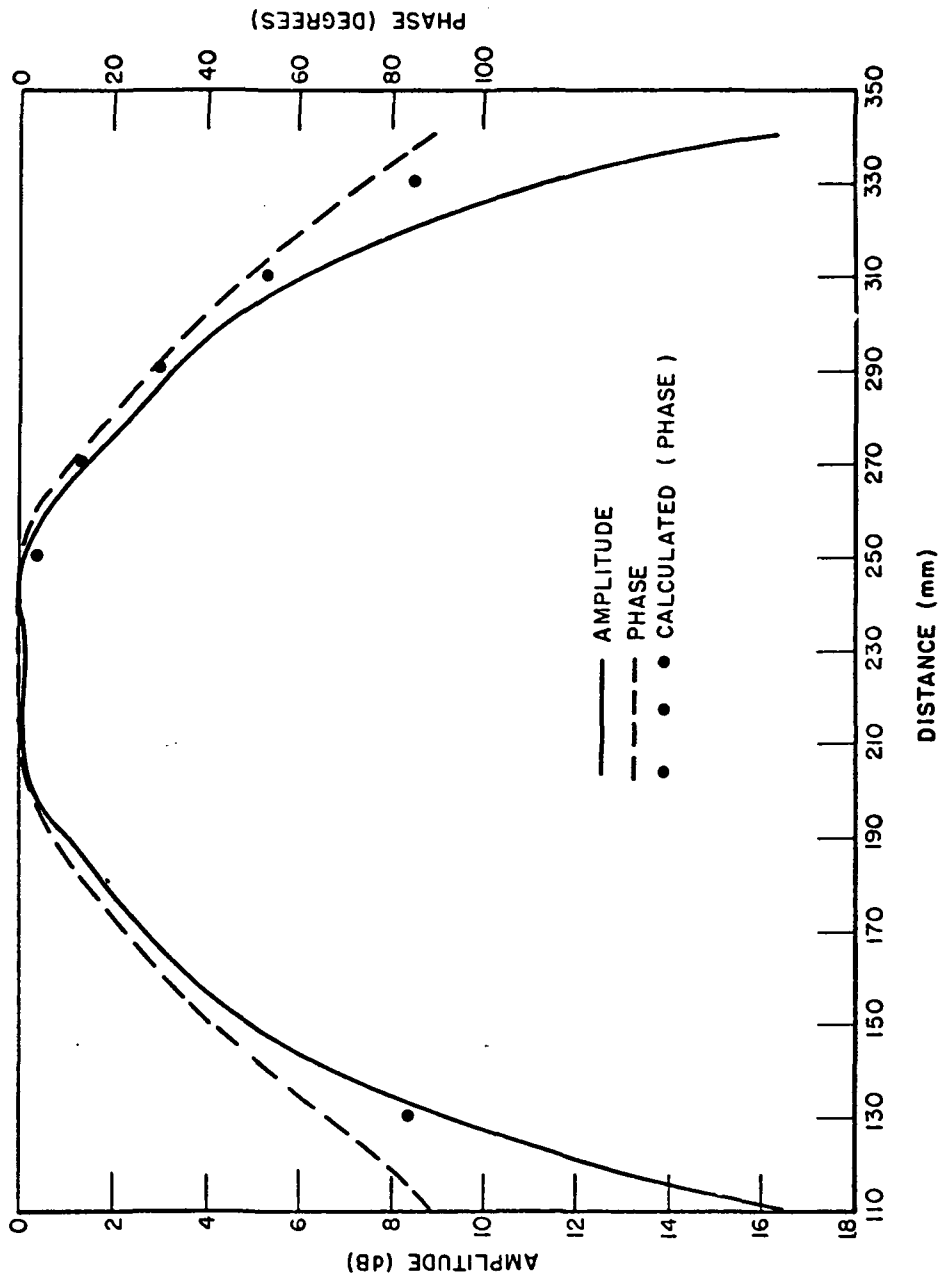


Fig. 2. Aperture distribution for the conical corrugated horn (H-plane).

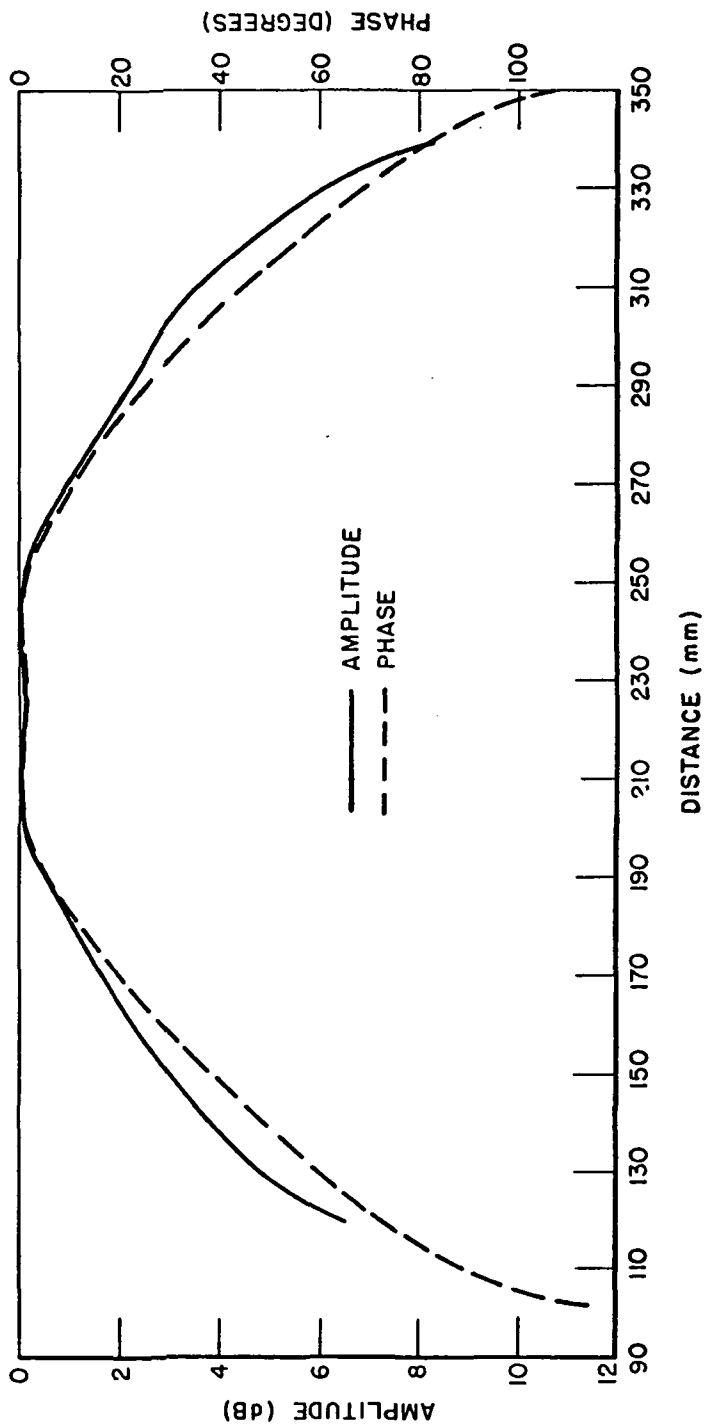


Fig. 3. Aperture distribution for the conical corrugated horn (E-plane).

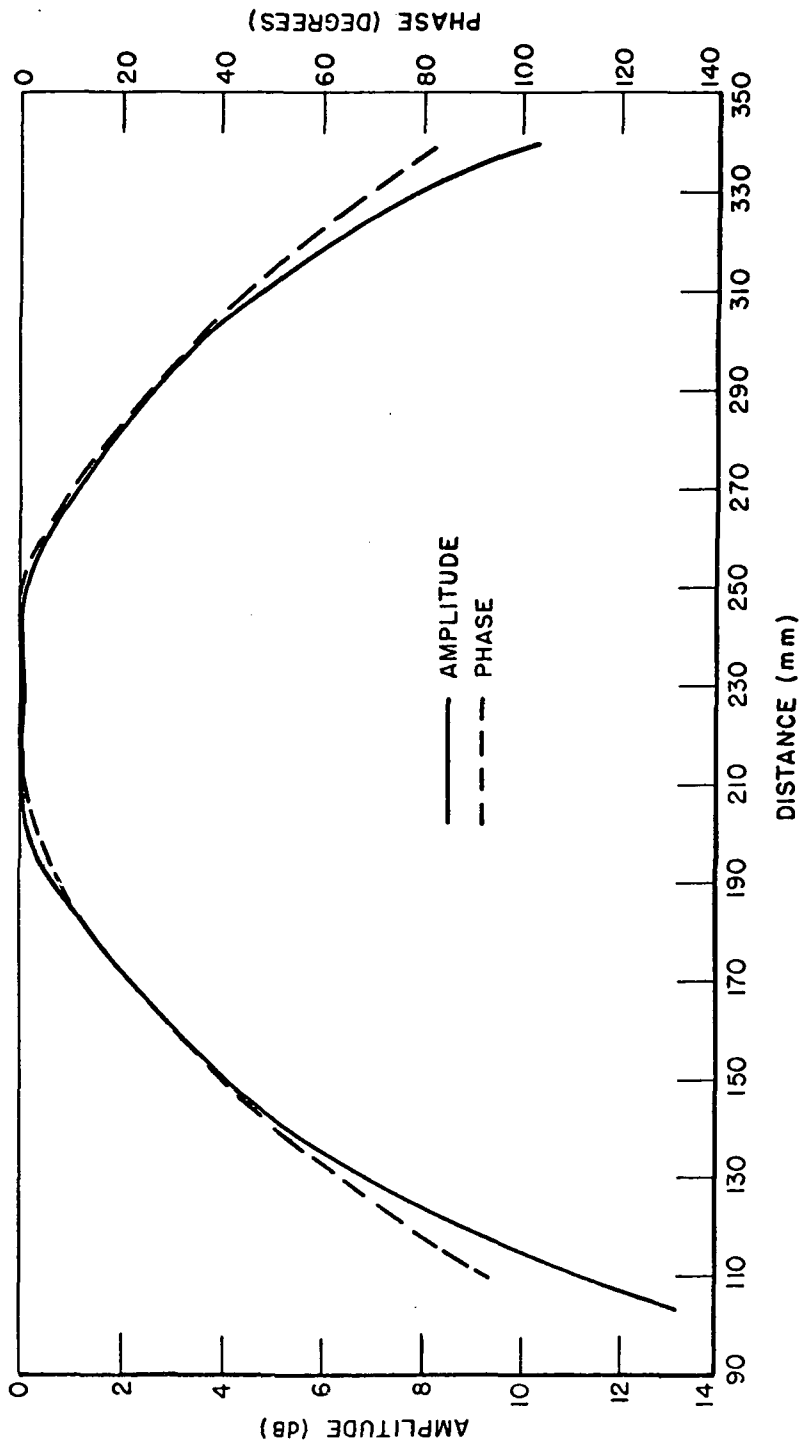


Fig. 4. Aperture distribution for the conical corrugated horn (45°-plane).

The E and H plane radiation patterns for the antenna are shown in Fig. 5. These were recorded using a digital computer to store the data. Patterns were recorded in planes at $22\frac{1}{2}^\circ$ intervals in addition to the E and H planes. The average pattern of these various cuts for both parallel and crossed polarization is shown in Fig. 6. Averaging was performed in the computer after all the patterns had been recorded. The data were further processed to yield beam efficiency, defined here as the fraction of the total radiated power (the antenna is considered to be transmitting) contained within a cone of any given angle from the beam axis. The cross polarized energy may be considered as desirable or undesirable depending on the particular application. The beam efficiency was therefore calculated both ways and is presented in Figs. 7 and 8.

In Fig. 5 shoulders are apparent at -27 dB on the E-plane pattern. At lower frequencies, these are lower while at 3.9 GHz the shoulders are at -23 dB. These shoulders illustrate the pattern deterioration as the corrugation depth approaches $\lambda/2$ at 4.28 GHz. This slight compromise in radiation pattern was made to obtain a good impedance match. An expanded radiation pattern of the main beam at 3.9 GHz with the antenna set up to receive circular polarization appears in Fig. 9. Shown here is the received pattern for vertical transmitted polarization, and, at selected points, lines obtained by rotating the transmitted polarization 180° while the receiving antenna is stationary. The length of this line is $20 \log b/a$ where "b" and "a" are the major and minor axes of the polarization ellipse. The axial ratio is approximately 1.8 in the region of 30° .

B. The Pyramidal Corrugated Horn Antenna

A pyramidal corrugated horn with a 56° flare angle and 10 inches square aperture was built. The horn, shown in Fig. 10, is fed by a 1-3/4 inches square waveguide and has corrugations which are 0.43λ deep at 3.8 GHz on all four walls. The large flare angle and deep corrugations were chosen, as in the case of the conical corrugated horn, to obtain a compact antenna and to provide a good impedance match, possibly at the cost of some slight deterioration in the radiation pattern.

Radiation patterns obtained with this antenna at 3.9 GHz are shown in Fig. 11. The H-plane pattern shows good agreement with typical horn design curves and changes only slightly from 3.8 GHz to 4.0 GHz. The E-plane pattern, however, is wider (28° at the 3 dB points) than the H-plane pattern (26° at the 3 dB points). It was also observed that this horn's E-plane radiation patterns exhibited a greater frequency dependence than expected. For example, at 4.0 GHz, the main beam sharpens up to match the 23° H-plane beamwidth while at 3.8 GHz a shoulder appears at -7 dB. Past work on corrugated horns has indicated that the frequency dependence should be much less than observed. For example, an X-band horn with two walls corrugated had nearly equal E- and H-plane beamwidths at both 3 and 10 dB over almost a 2:1 frequency range. At this point, the reason for this frequency dependence was not definitely known but was thought to be associated with the number and depth of the corrugations and possibly the short length of the horn.

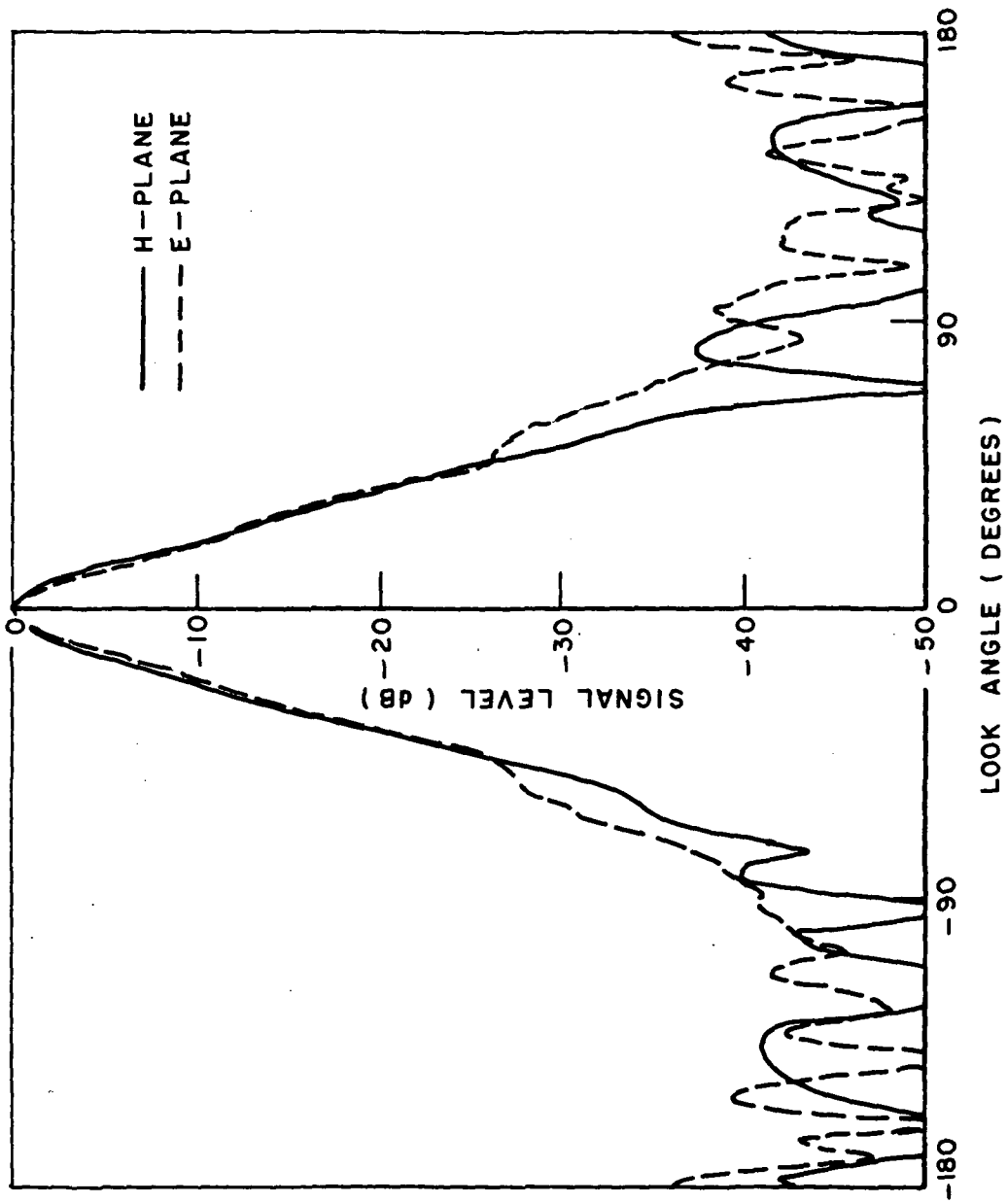


Fig. 5. Radiation patterns of the conical corrugated horn (3.7 GHz).

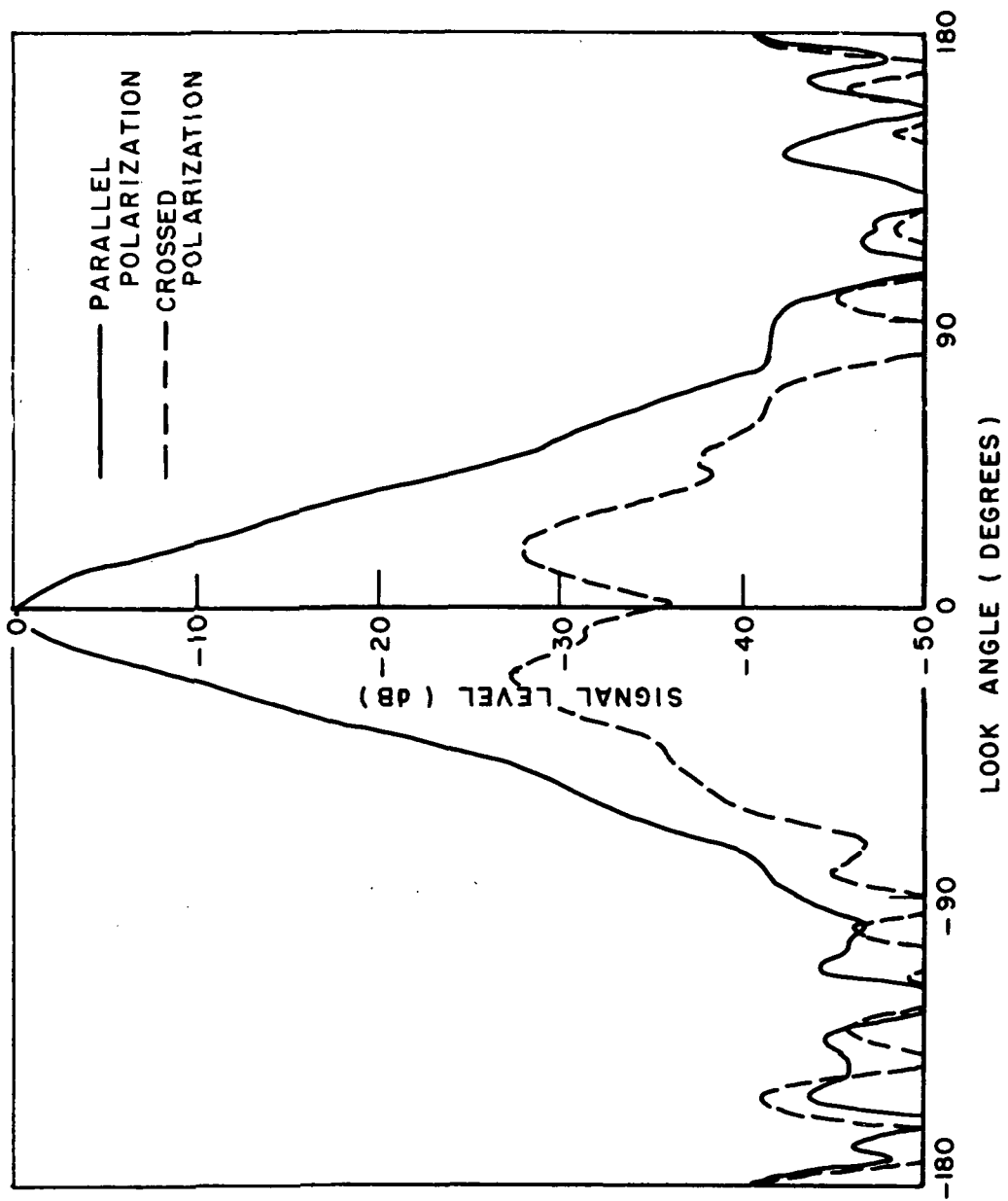


Fig. 6. Average parallel and crossed polarized radiation patterns for the conical corrugated horn (3.7 GHz).

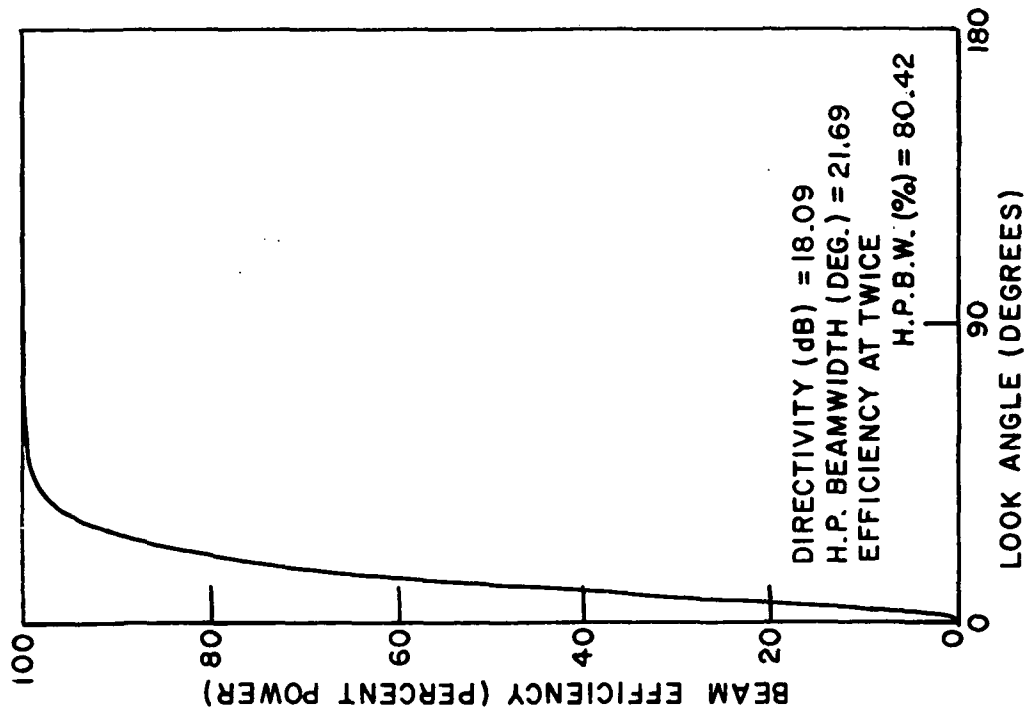


Fig. 7. Beam efficiency of the conical corrugated horn, crossed polarized energy considered desirable (3.7 GHz).

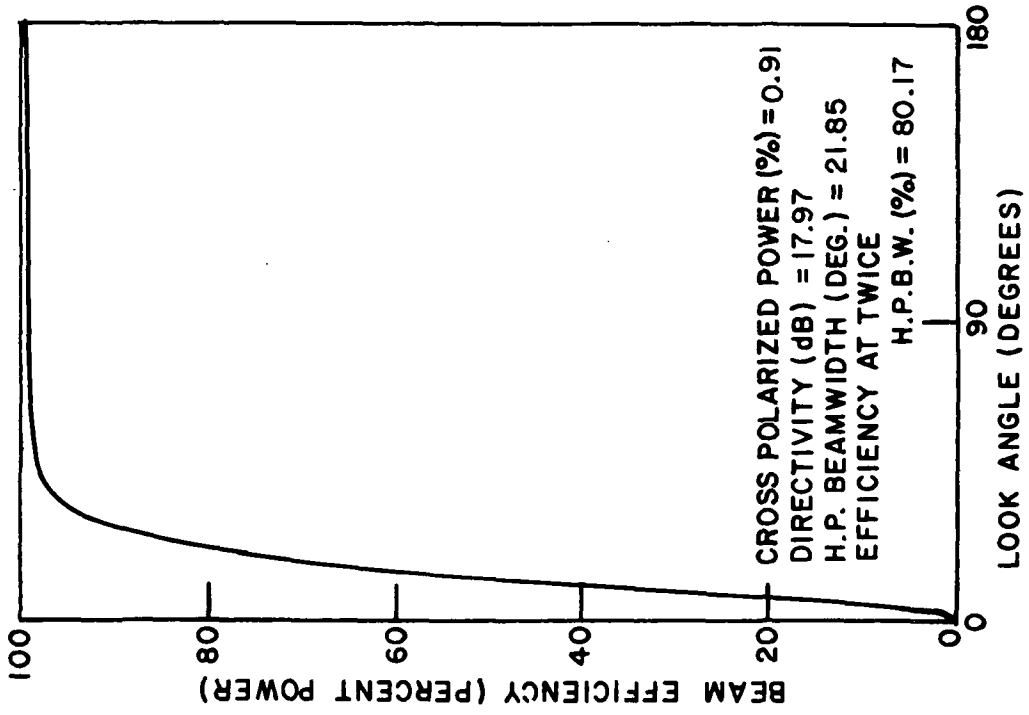


Fig. 8. Beam efficiency of the conical corrugated horn, crossed polarized energy considered undesirable (3.7 GHz).

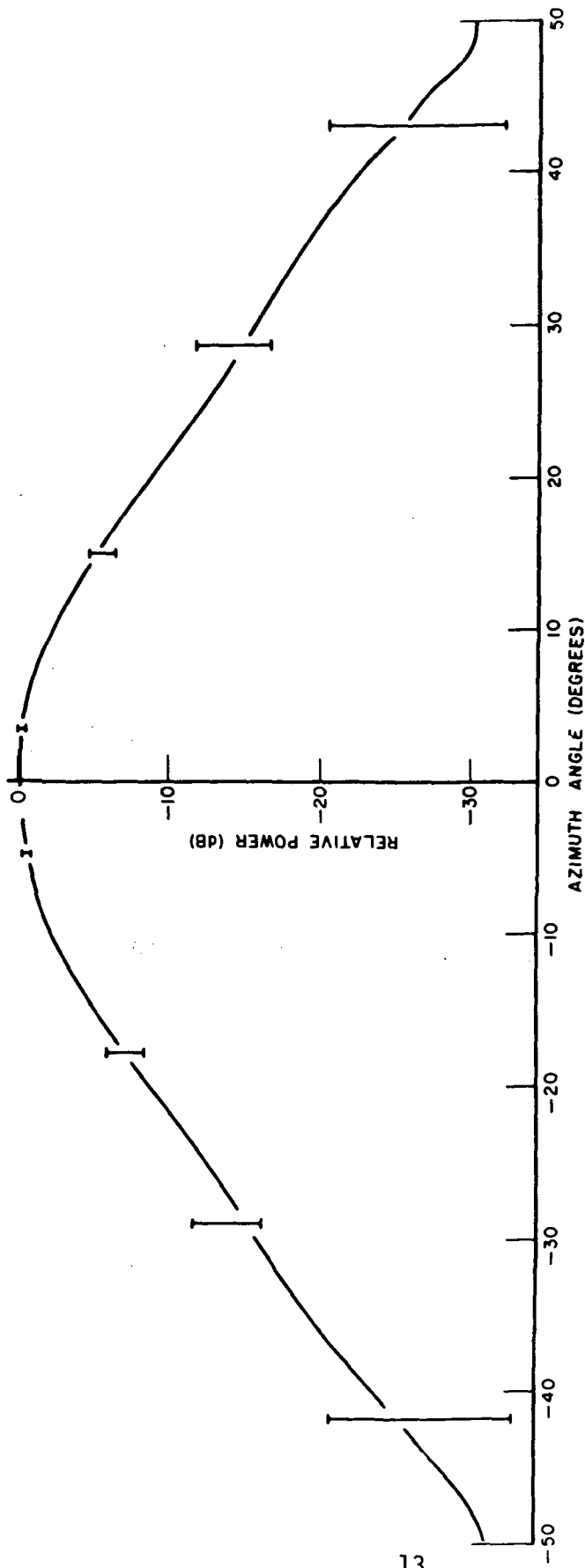


Fig. 9. Pattern showing the quality of the circular polarization for the conical corrugated horn (3.9 GHz).

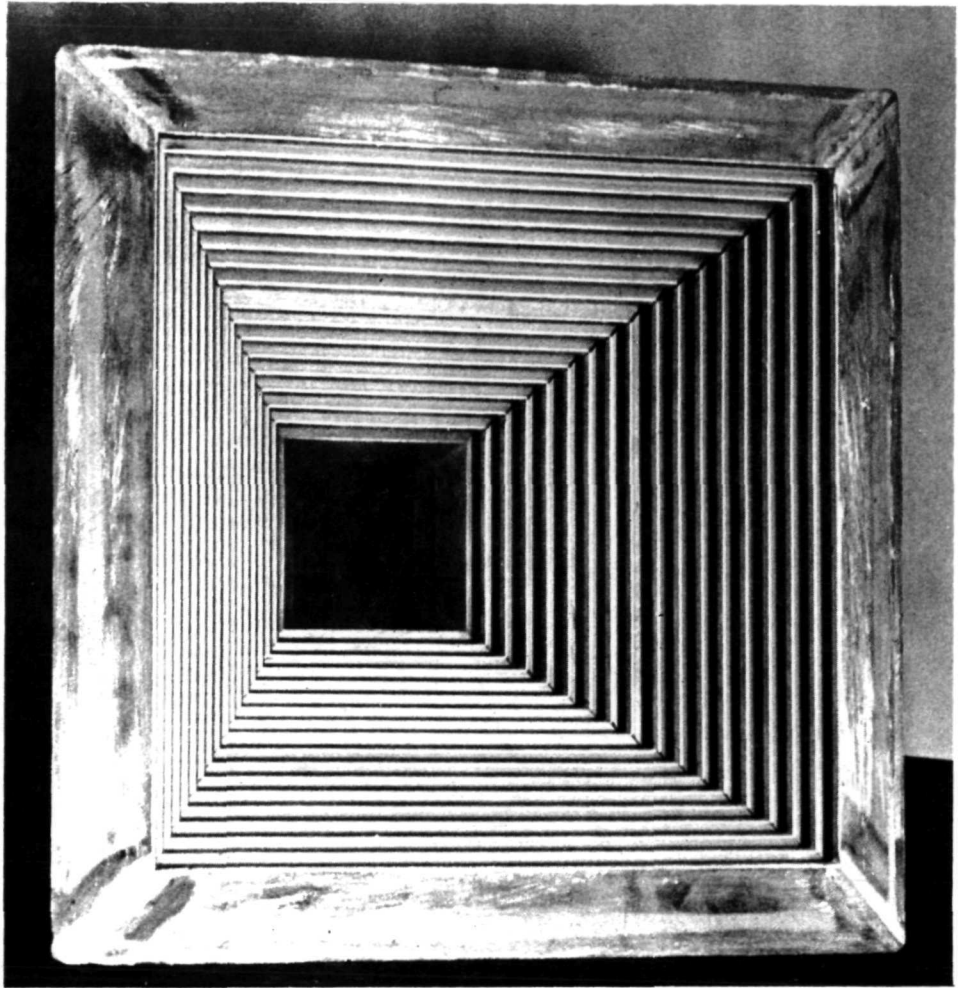


Fig. 10. The pyramidal corrugated horn antenna.

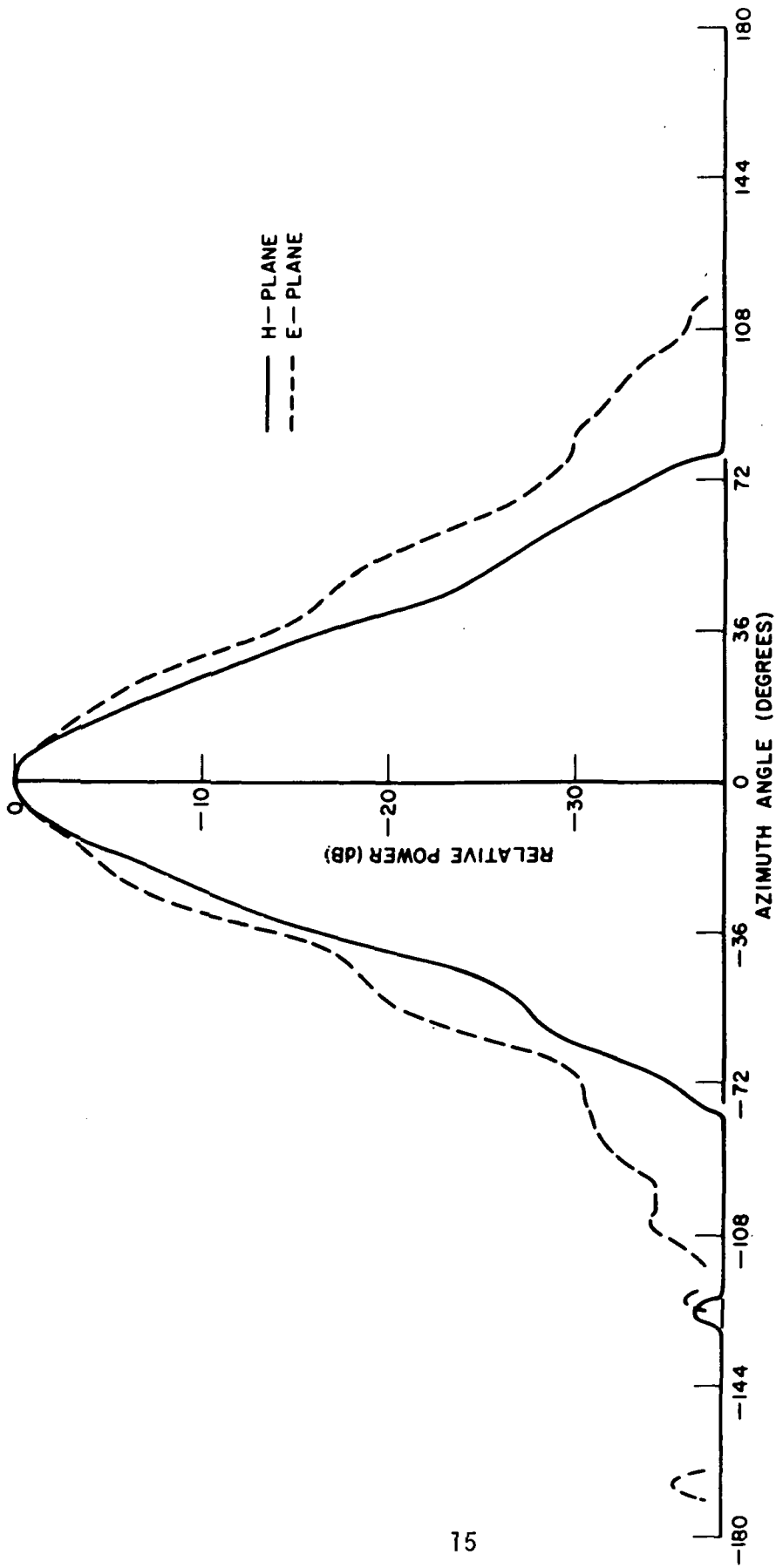


Fig. 11. Radiation patterns of the pyramidal corrugated horn (3.9 GHz, linear polarization, 550 flare angle, 6 teeth per wavelength).

This non-stationary behavior of the E-plane pattern is evidently caused by higher order modes which are generated at the position where the corrugations are initiated. If the surface could be truly represented by the capacitive impedance condition, these modes should be sufficiently attenuated. This is indicated by earlier measurements made by Peters and Lawrie¹ for a horn of nearly the same geometry. The major difference was that their horn had 15 teeth per wavelength at the center frequency in lieu of the 6 teeth per wavelength for this horn. To further validate this conclusion that the number of teeth is significant, a longer horn with 6 teeth per wavelength was considered. This was an X-band horn with the desirable property of nearly identical E and H plane patterns, a 29° flare angle instead of the previous 55°, and 8.75 inches long. The patterns for this horn together with the computed average patterns and efficiency curves are shown in Figs. 12-15. The end of this horn was then removed to make it approximately the same length as the above horn and again the same erratic behavior of the E-plane pattern appeared.

The conclusion then was that the corrugation density should be increased. A horn geometry was constructed having the same proportions as the original horn, except for the number of corrugations per wavelengths which was set at 15. The horn size was scaled down by a factor of 2½ to facilitate machining and the measurements made at X-band. Radiation patterns were measured at a frequency interval of 500 MHz from 8.5 to 11.5 GHz. The back level was maintained at -40 dB or lower over the entire frequency band. The E-plane patterns were substantially improved when compared to the patterns of conventional E-plane horns. While there was somewhat less variation in the E-plane pattern than before, the beamwidth still varied. The two most extreme patterns are shown in Figs. 16 and 17. It is interesting to note that they occur quite close in frequency, the E-plane changing from being wider than the H-plane to being narrower quite quickly. A further change in frequency in either direction produces a slow change in beamwidth back to the other condition. The most symmetrical pattern was obtained at 8.95 GHz and is shown in Fig. 18. The computed average patterns and beam efficiency for this case are shown in Figs. 19-21.

It is evident from these measurements that the pyramidal corrugated horn has a less stable mode structure than the conical corrugated horn. In order to achieve a symmetrical beam over a wide band it is necessary to use a low flare angle and a relatively large number of corrugations. It appears that the number of corrugations per wavelength is less important than the total number present.

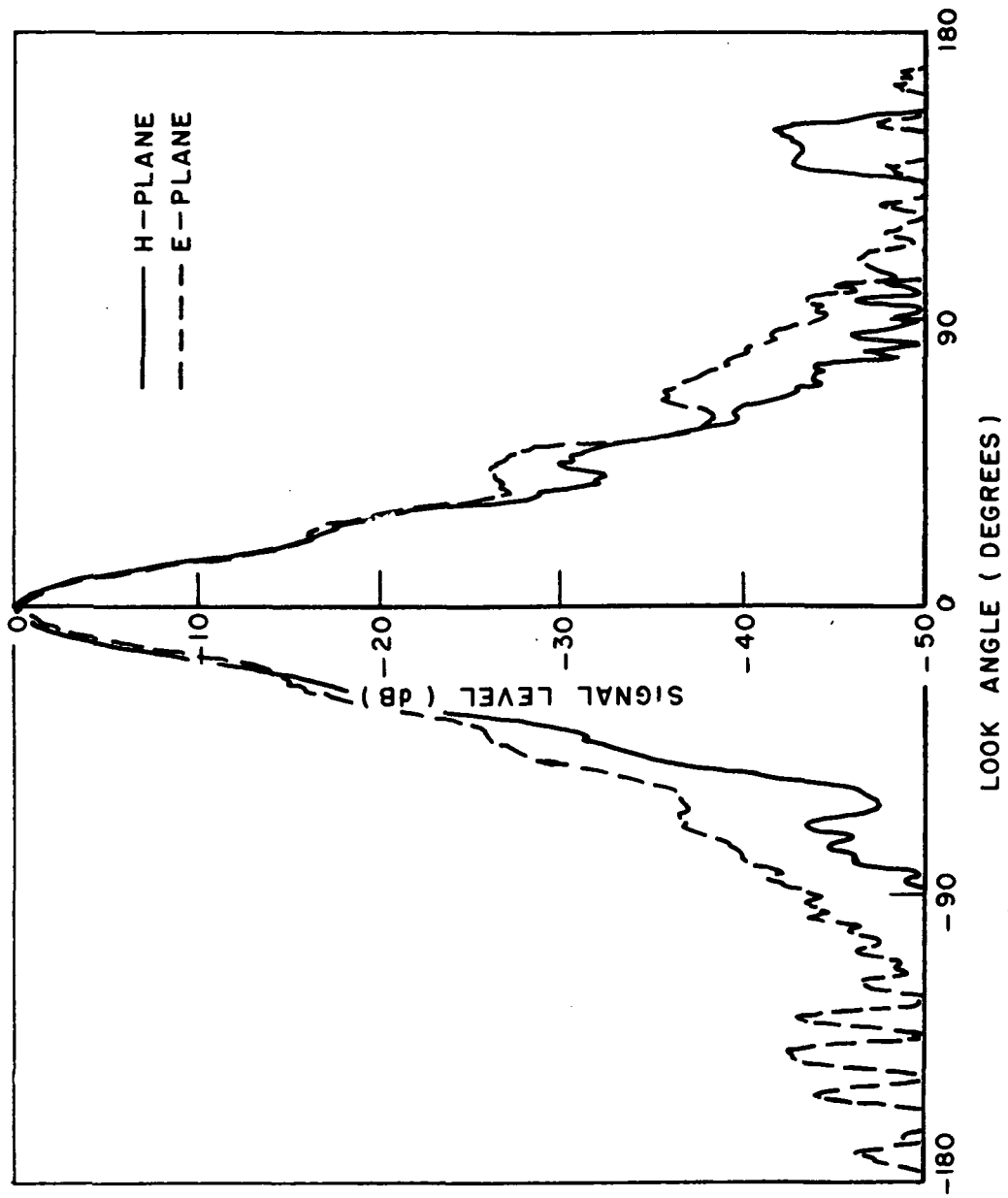


Fig. 12. Radiation patterns of a pyramidal corrugated horn (29° flare angle, 8.55 GHz, 6 teeth per wavelength).

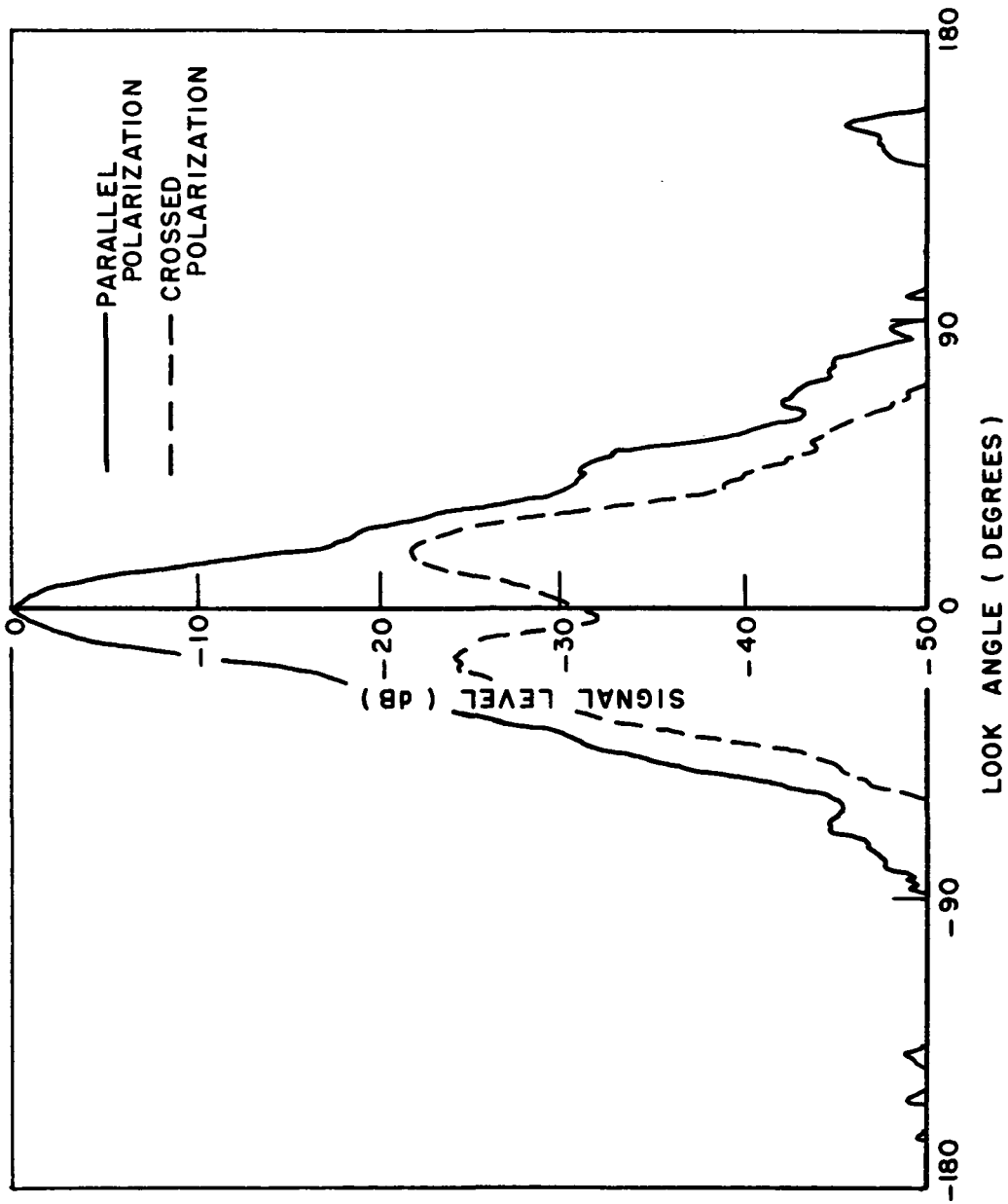


Fig. 13. Average radiation patterns of a pyramidal corrugated horn (29° flare angle, 8.55 GHz, 6 teeth per wavelength).

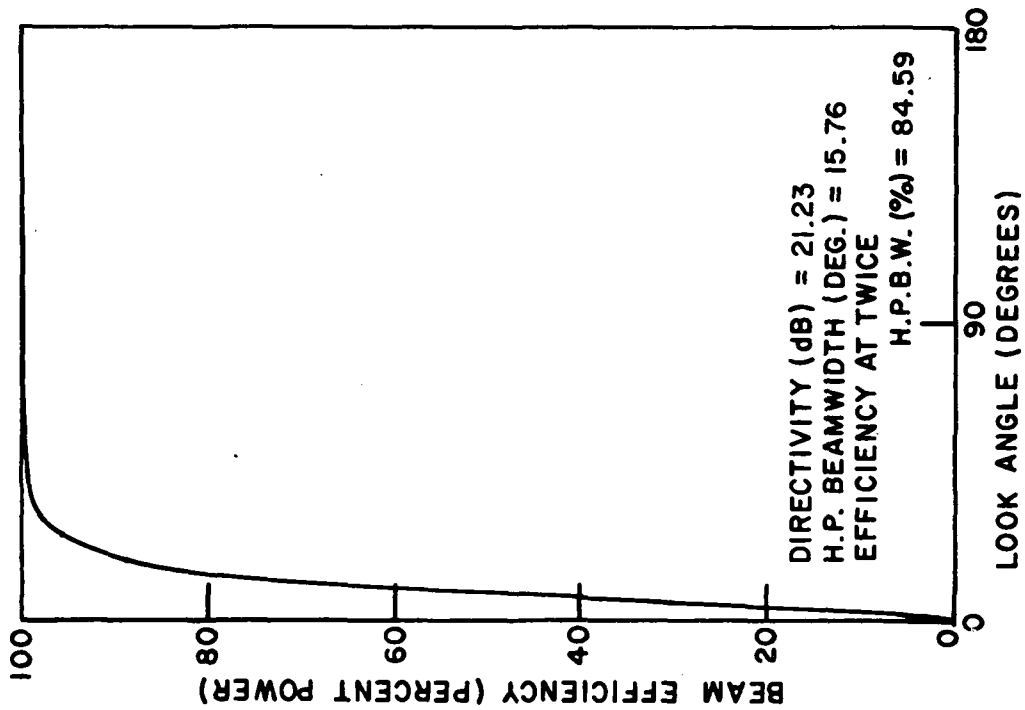


Fig. 14. Beam efficiency of a pyramidal corrugated horn, cross polarized energy considered desirable (290 flare angle, 8.55 GHz, 6 teeth per wavelength).

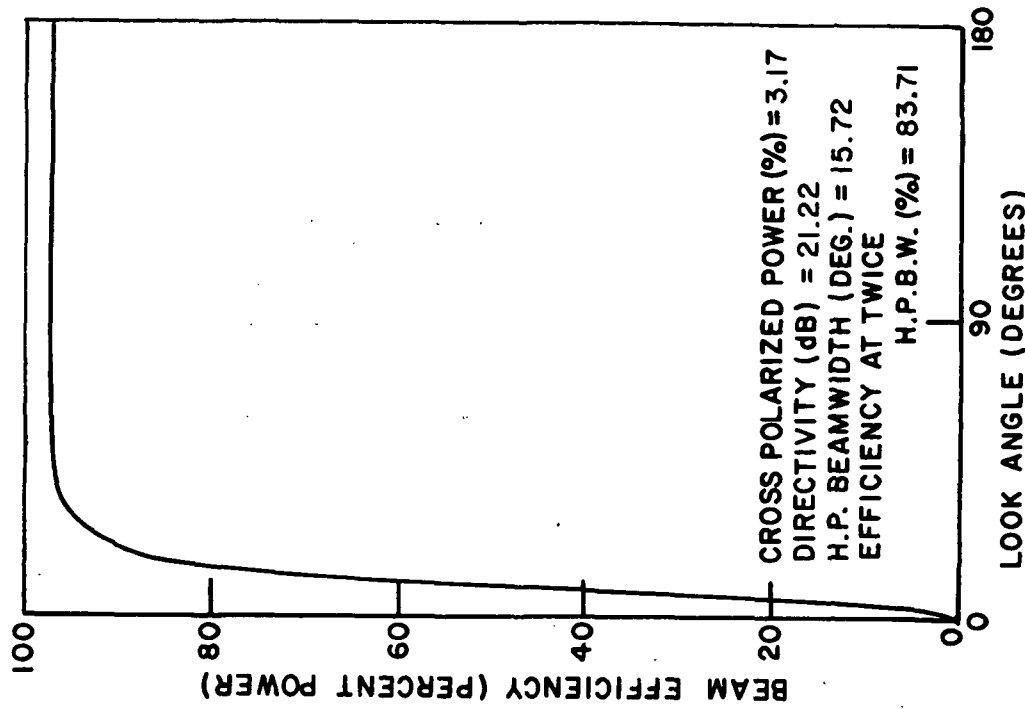


Fig. 15. Beam efficiency of a pyramidal corrugated horn, cross polarized energy considered undesirable (290 flare angle, 8.55 GHz).

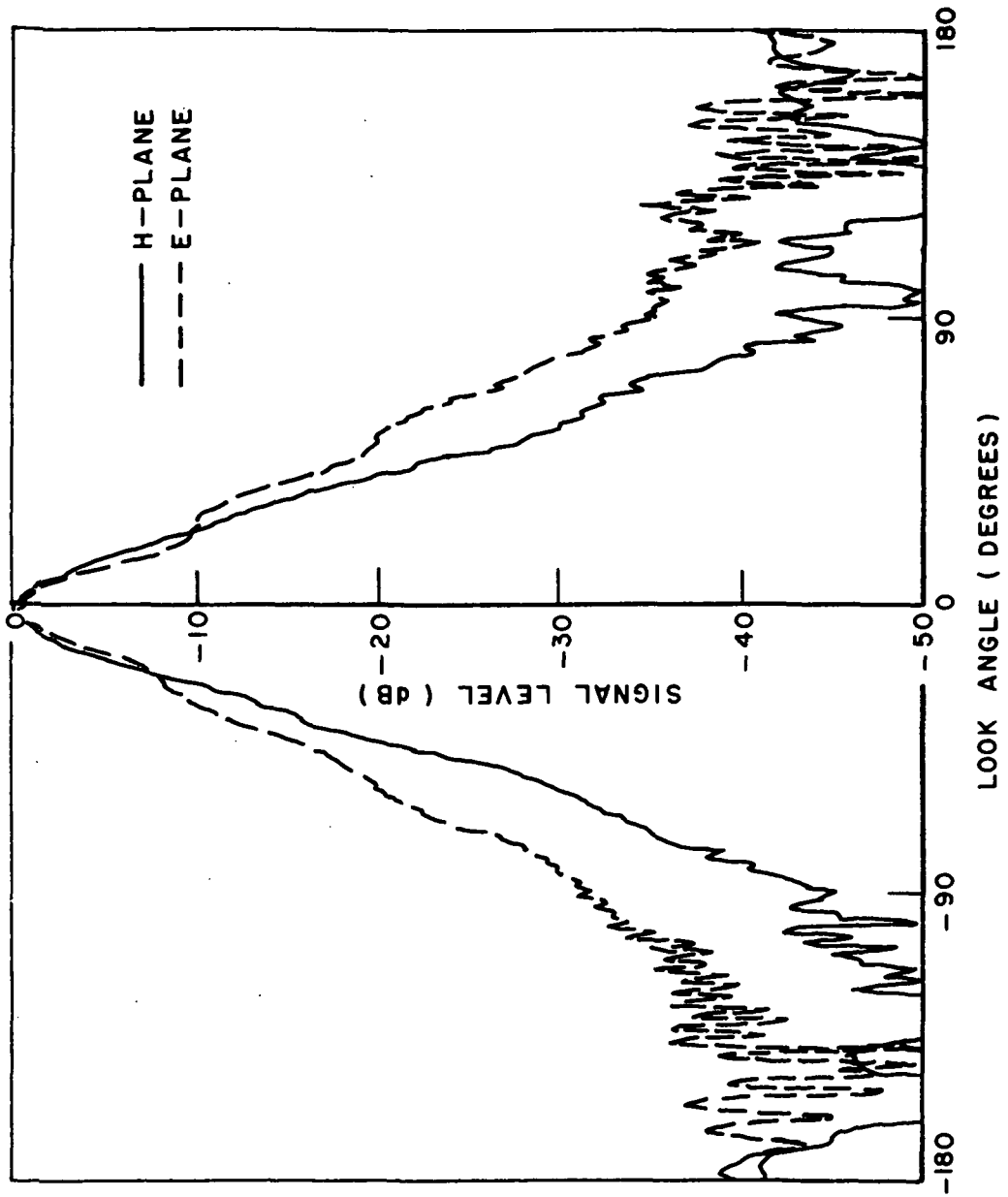


Fig. 16. Radiation patterns of a pyramidal corrugated horn (550 flare angle, 15 teeth per wavelength, 9.5 GHz).

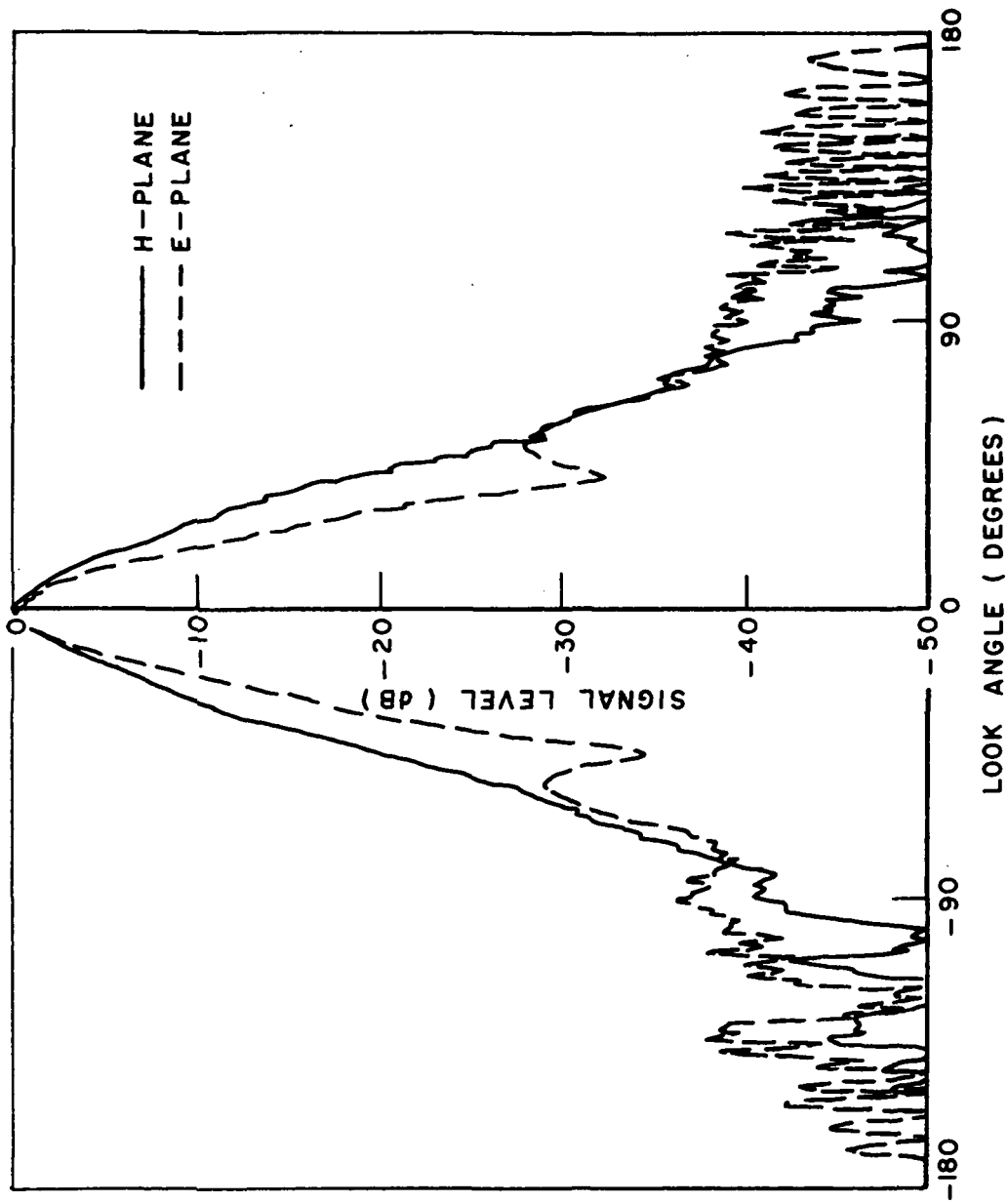


Fig. 17. Radiation patterns of a pyramidal corrugated horn (55° flare angle, 15 teeth per wavelength, 10.0 GHz).

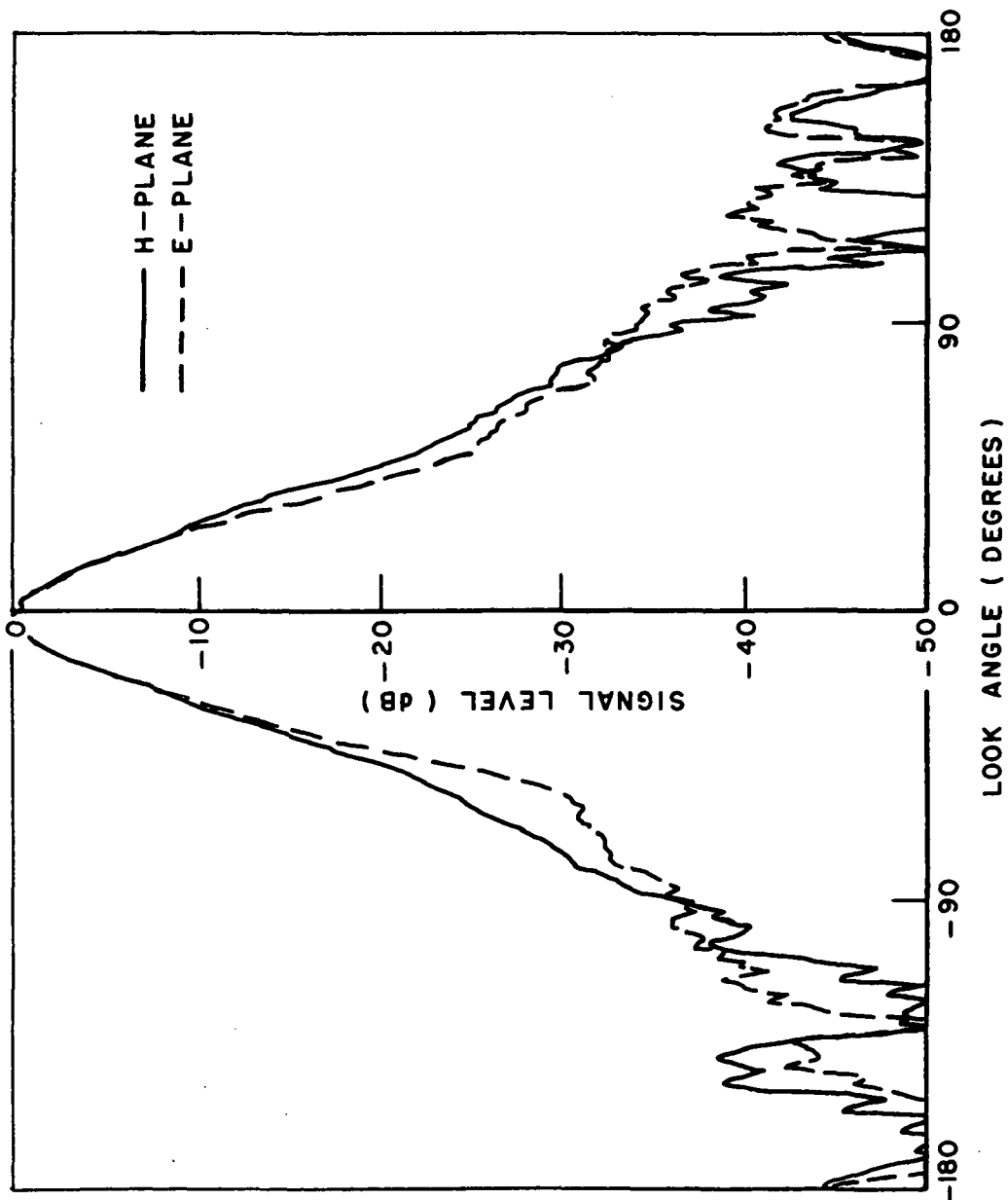


Fig. 18. Radiation patterns of a pyramidal corrugated horn (55° flare angle, 15 teeth per wavelength, 8.95 GHz).

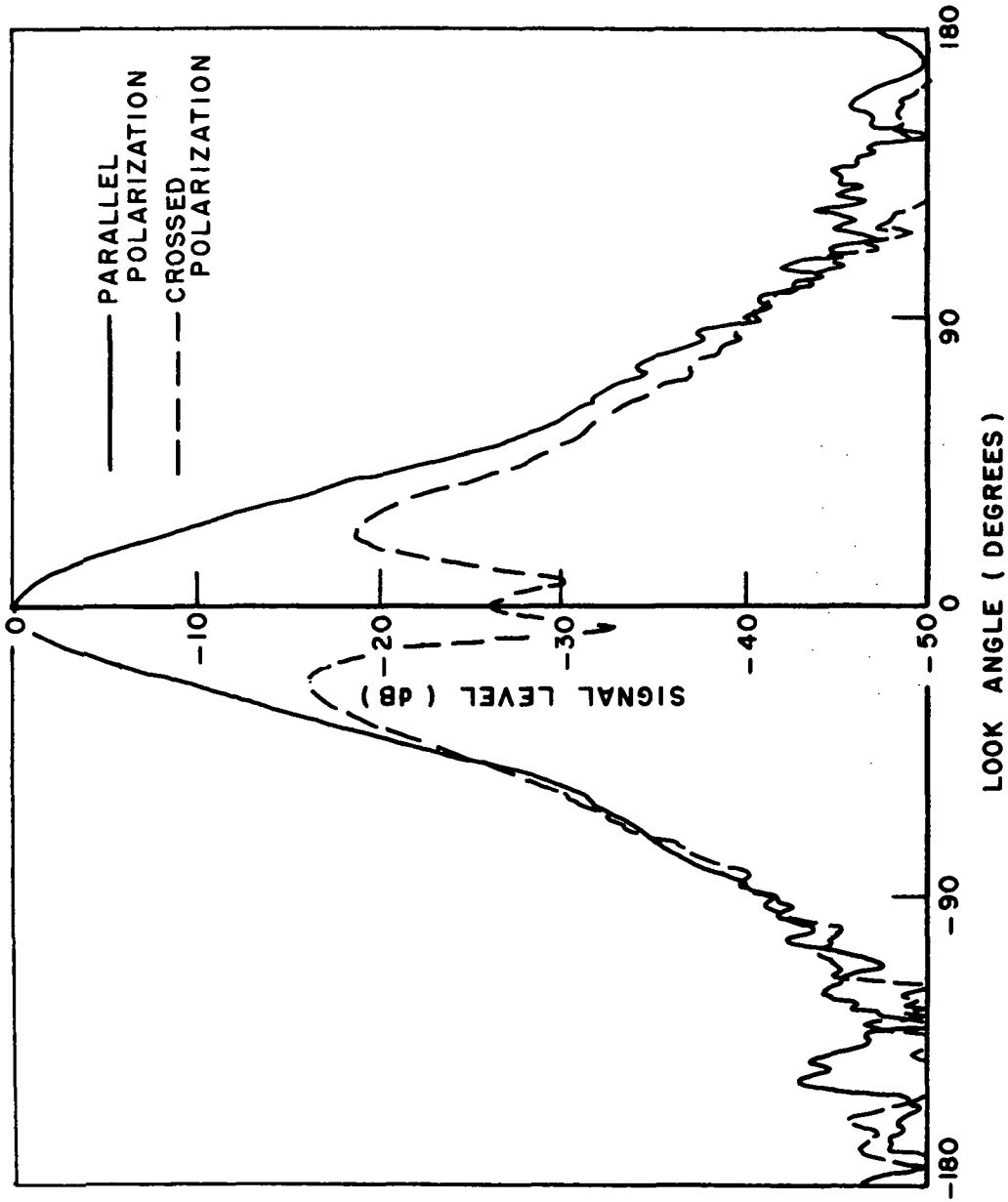


Fig. 19. Average radiation patterns for the pyramidal corrugated horn (550 flare angle, 15 teeth per wavelength, 8.95 GHz).

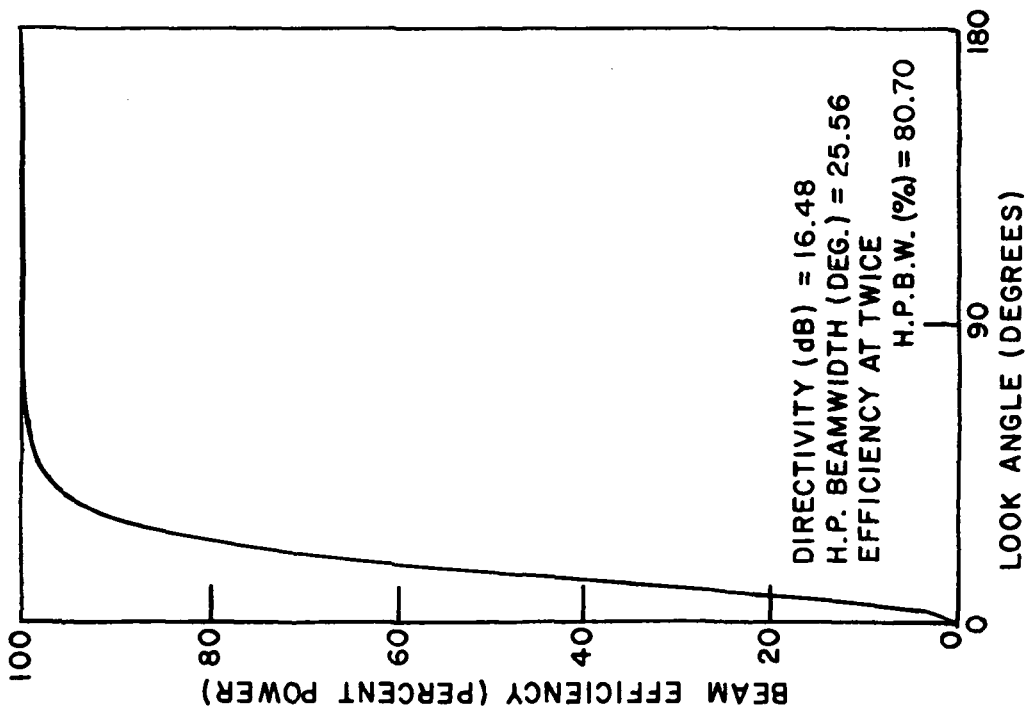


Fig. 20. Beam efficiency of a pyramidal corrugated horn, cross polarization considered desirable (550 flare angle, 15 teeth per wavelength, 8.95 GHz).

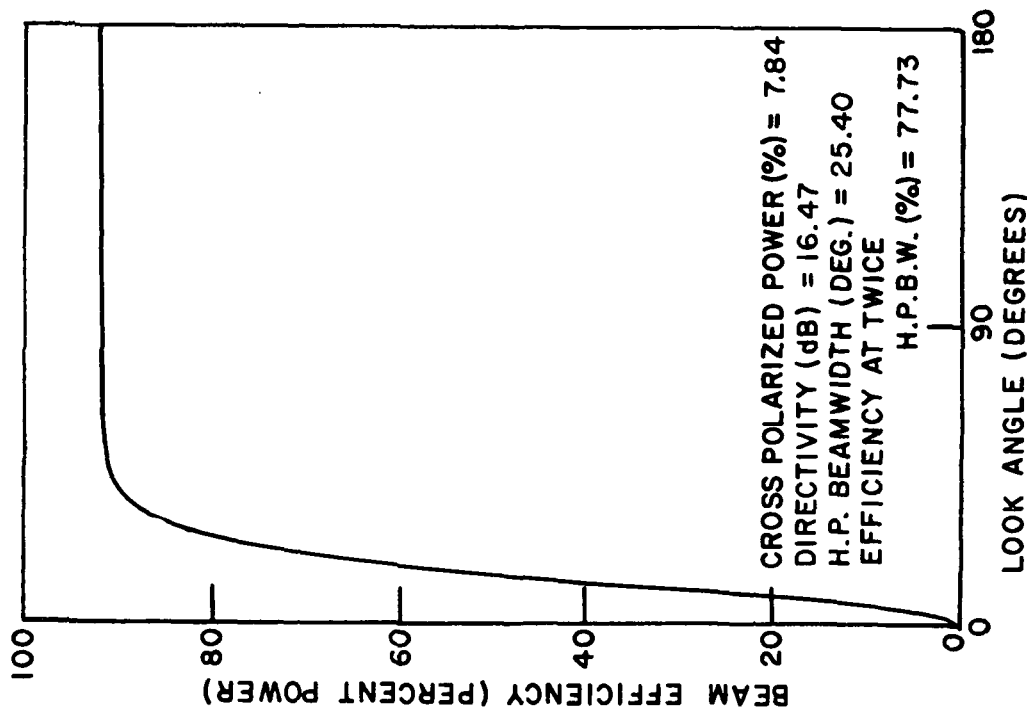


Fig. 21. Beam efficiency of a pyramidal corrugated horn cross polarization considered undesirable (550 flare angle, 15 teeth per wavelength, 8.95 GHz).

C. The Conical Dual Mode Horn Antenna

A dual mode horn was constructed based directly on the design described by Potter.⁵ The dimensions of the step and aperture were scaled directly from those given in Reference 5 with a further adjustment of the aperture width to yield the desired beamwidth. Some further changes were made, however, to reduce the overall size of the horn as far as possible. Potter found empirically that when the TM_{11} mode was generated at the step, it differed in phase from the fundamental TE_{11} mode by about 0.16λ . He therefore arranged the flare and an additional cylindrical section to yield an additional differential phase shift between the two modes of about 1.84λ between the step and the aperture to produce the desired aperture distribution. To minimize the length, the present horn was designed with an additional differential phase shift of only 0.84λ . Since the aperture and step dimensions were already determined this resulted in a flare angle of 10.4° . The same angle was used for the transformer section between the input waveguide and the step. There was no particular reason for using the same angle other than it seemed reasonable for the purpose. The transformer taper was felt to be sufficiently gradual that the cylindrical section prior to the step, used by Potter as a mode filter, could be omitted. The dimensions of the resulting horn are shown in Fig. 22 and a photograph in Fig. 23. The throat section was machined from solid stock. The flare section was rolled from sheet and welded. Two annular ribs were welded to the outside (one of these is visible in Fig. 23), also a threaded ring to mate with the throat section, the junction being at the step. After welding the inside of the flare was machined to the final dimensions.

The radiation patterns for the Conical Dual Mode Horn for linear polarization at a frequency of 3.8 GHz are shown in Fig. 24. The computed average patterns and beam efficiency curves are shown in Figs. 25-27. Figure 28 shows the C.P. performance at 3.9 GHz. The figure shows the main beam on an expanded scale with the horn set up to receive C.P. The transmitter was linearly polarized. At a number of points in the pattern the receiving antenna was stopped and the transmitter polarization rotated. The vertical lines so produced indicate the ellipticity of the polarization. The best C.P. for this horn was obtained at 3.8 GHz as shown in Fig. 29. The C.P. at 4.0 GHz was similar to that at 3.9 GHz.

At 3.8 GHz, the polarization is comparable or slightly superior to that of the conical corrugated horn. However, for 0.1 GHz shift in frequency, the polarization properties deteriorate to an axial ratio of the order of 10 dB at an angle of 30° . The beam efficiency is also better than that of the conical corrugated horn at 3.8 GHz. This results from the presence of a null in the radiation pattern, which does not exist for the corrugated horn pattern, producing a sharper fall off at the beam edge. Again, of course, it should be stressed that the dual mode horn is a much narrower band structure.

The aperture distributions for the conical dual mode horn are shown in Figs. 30 and 31 for the H- and E-planes respectively.

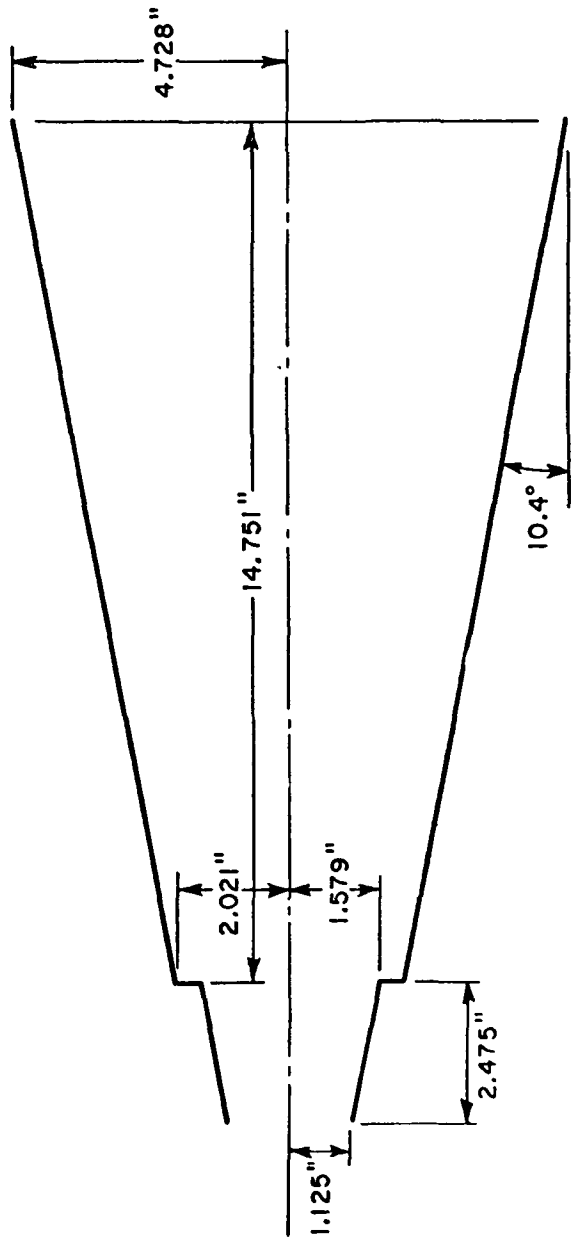


Fig. 22. Dimensions of the conical dual mode horn.



Fig. 23. The conical dual mode horn.

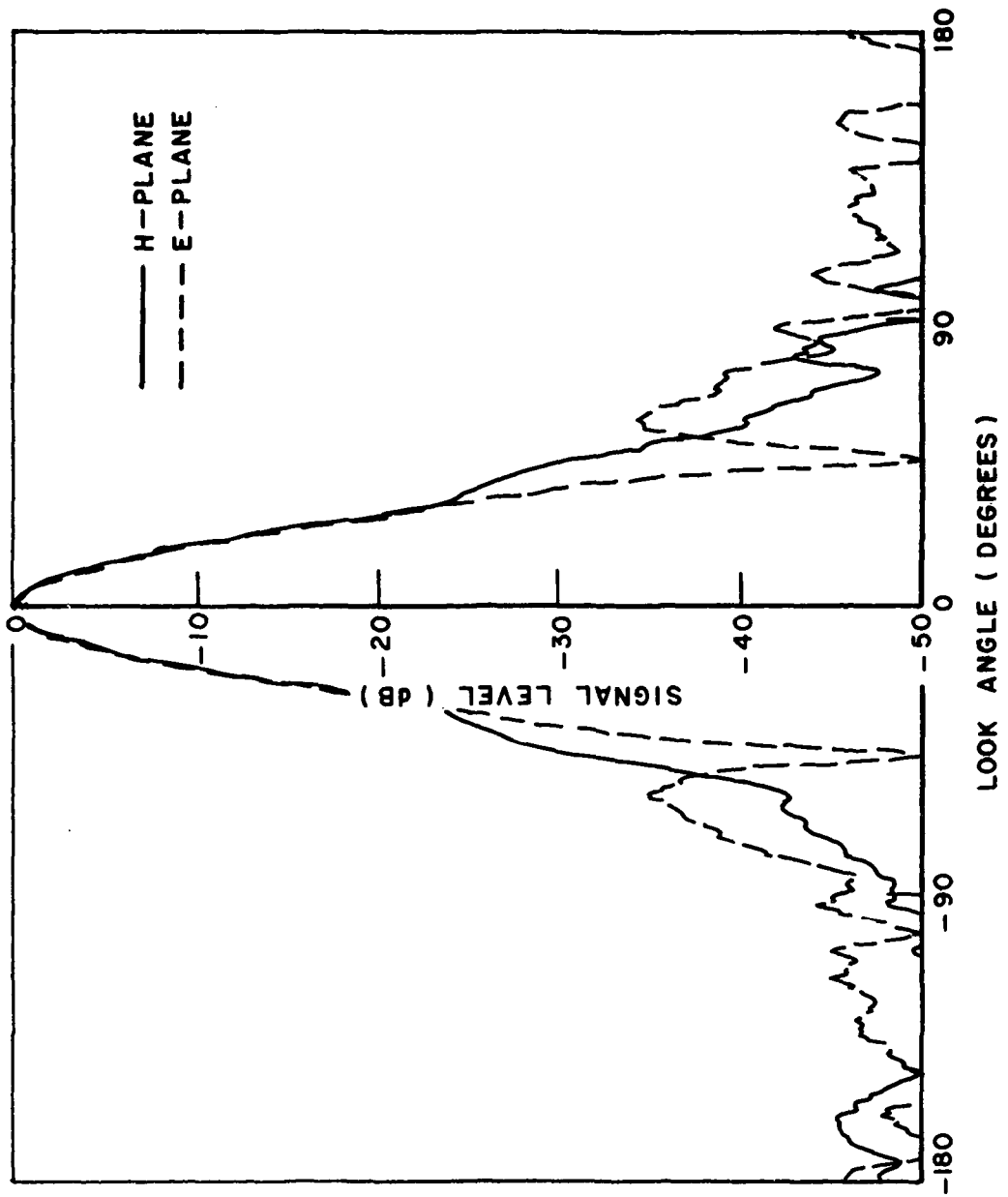


Fig. 24. Radiation patterns of the conical dual mode horn (3.8 GHz, linear polarization).

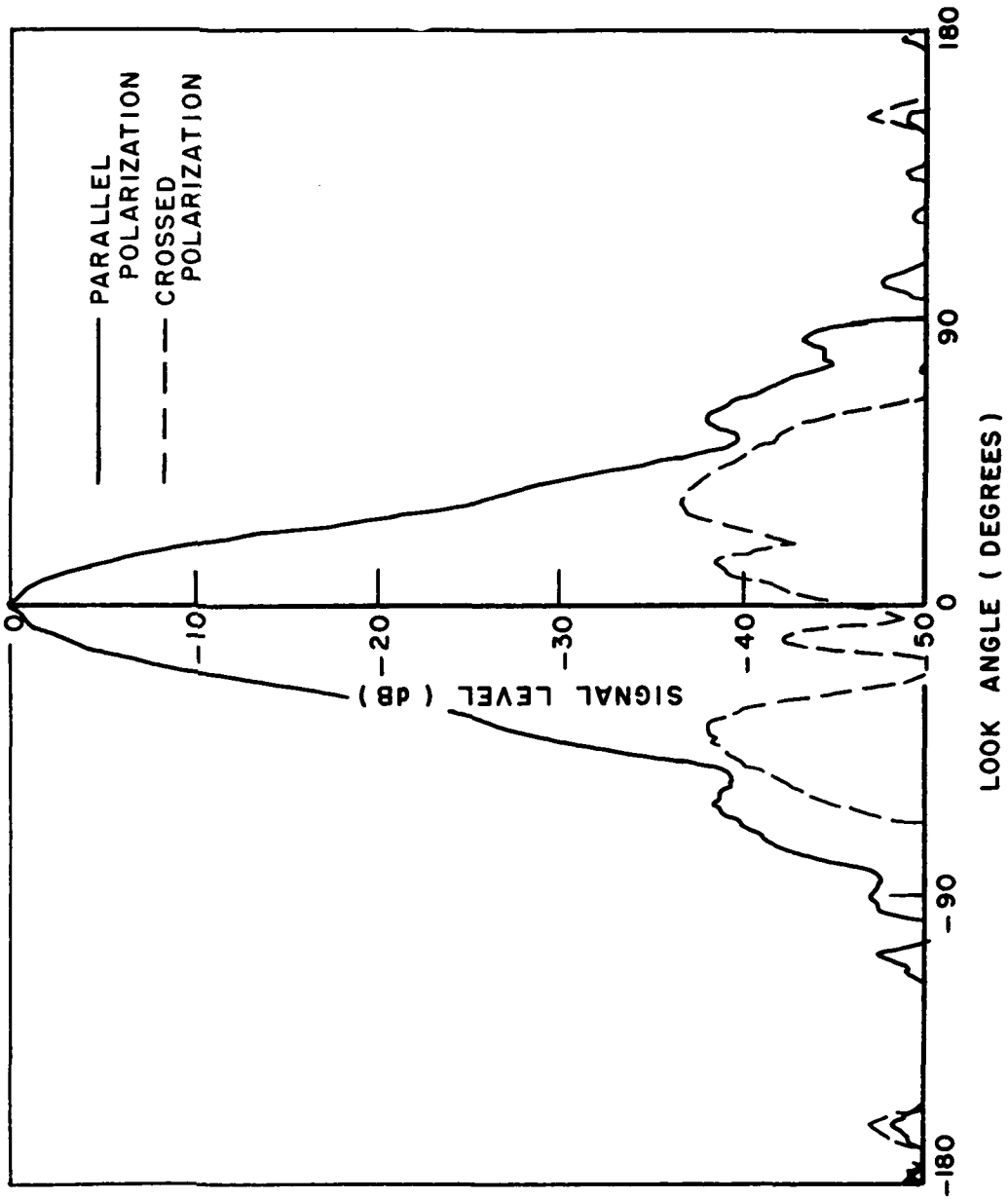


Fig. 25. Average radiation patterns of the conical dual mode horn (3.8 GHz, Linear polarization).

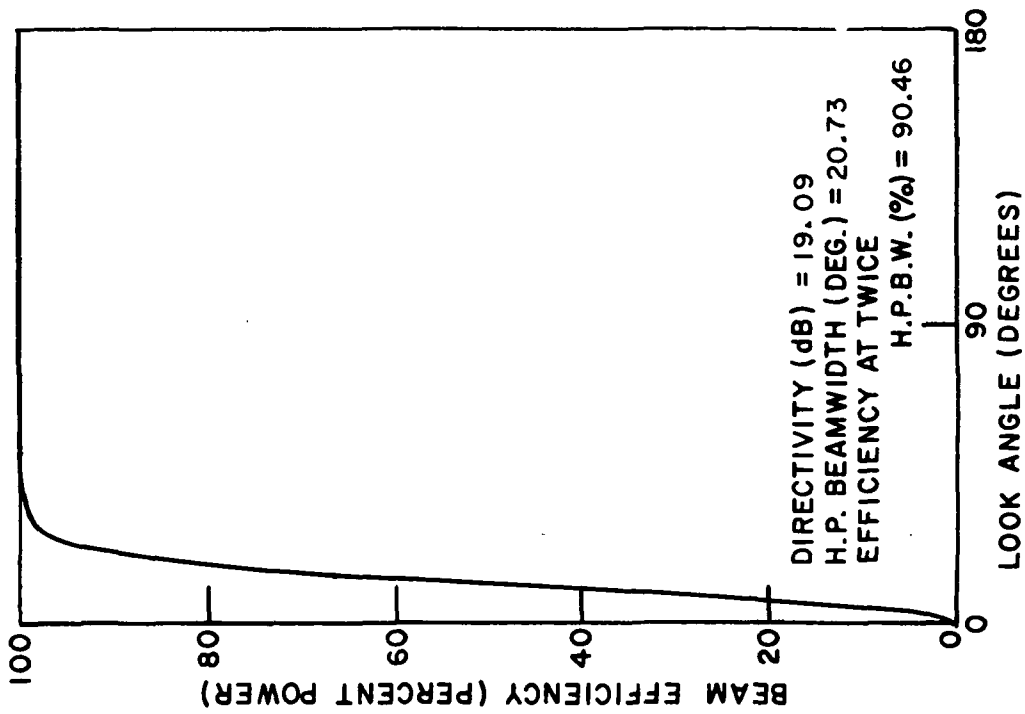


Fig. 26. Beam efficiency of the conical dual mode horn, cross polarization considered desirable (3.8 GHz, linear polarization).

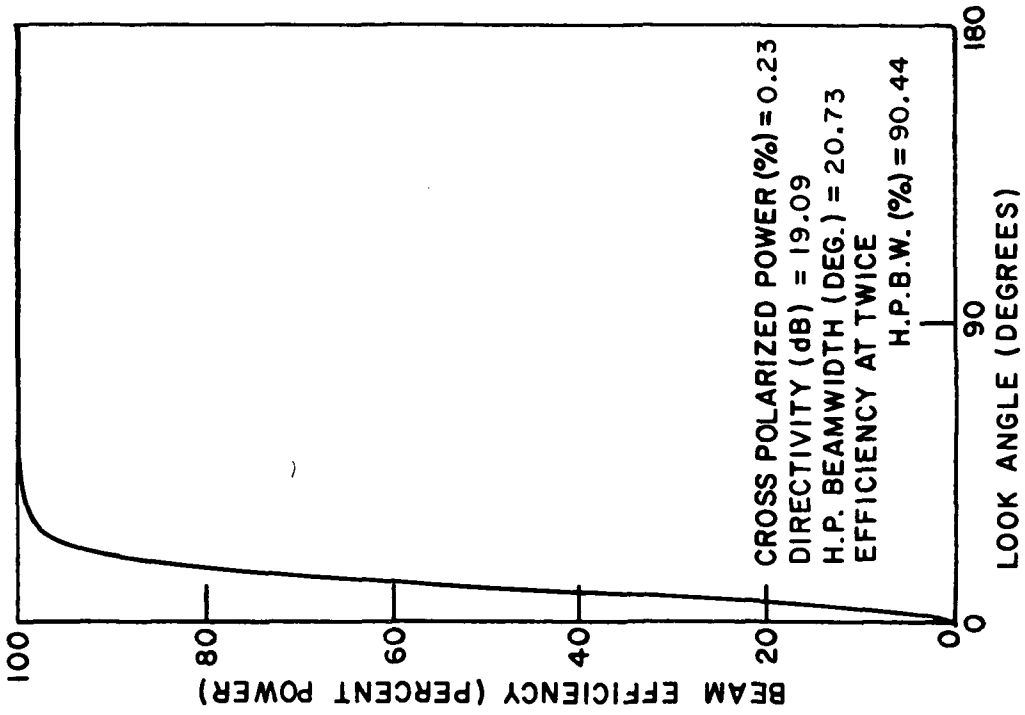


Fig. 27. Beam efficiency of the conical dual mode horn, cross polarization considered undesirable (3.8 GHz, linear polarization).

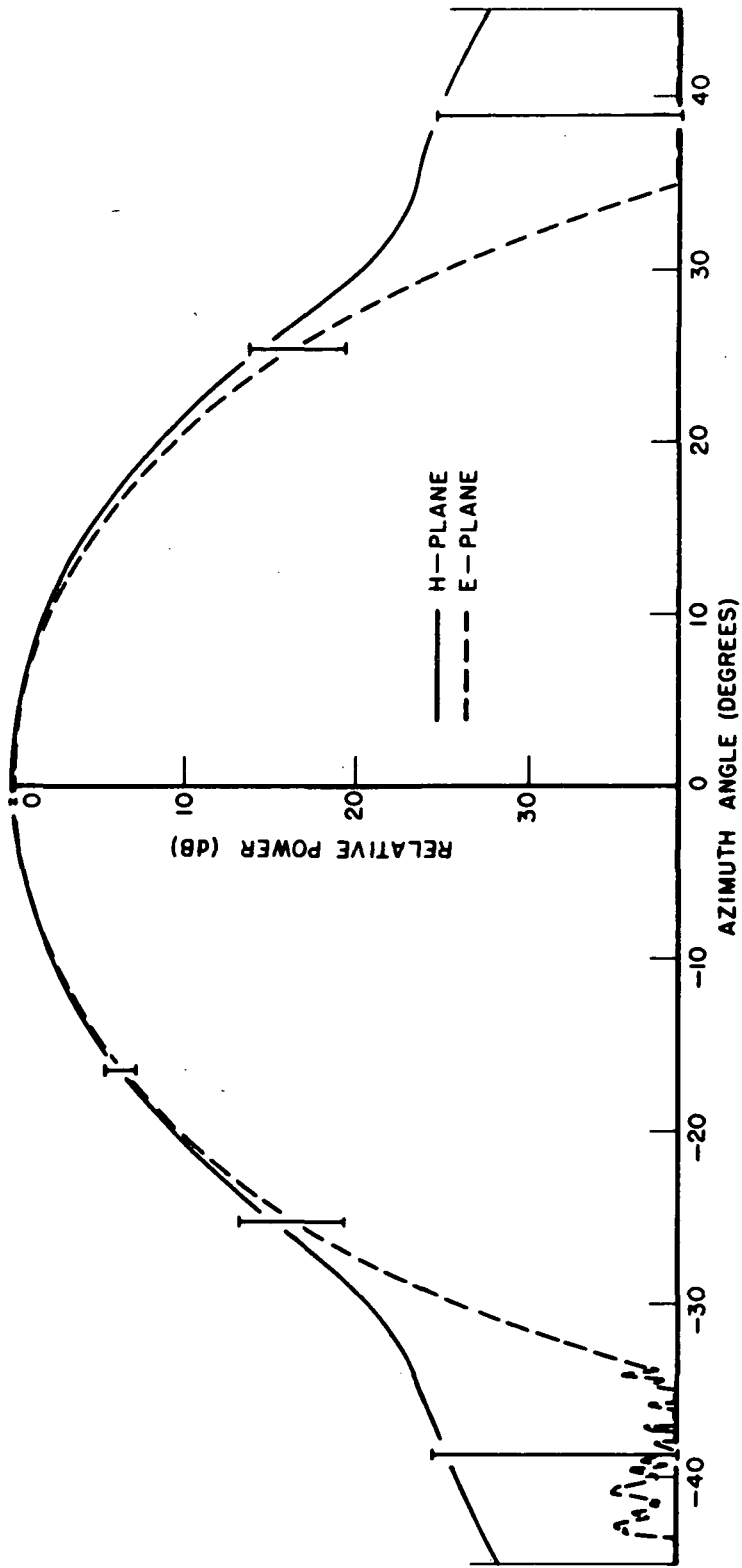


Fig. 28. Pattern showing the quality of the circular polarization for the conical dual mode horn (3.9 GHz).

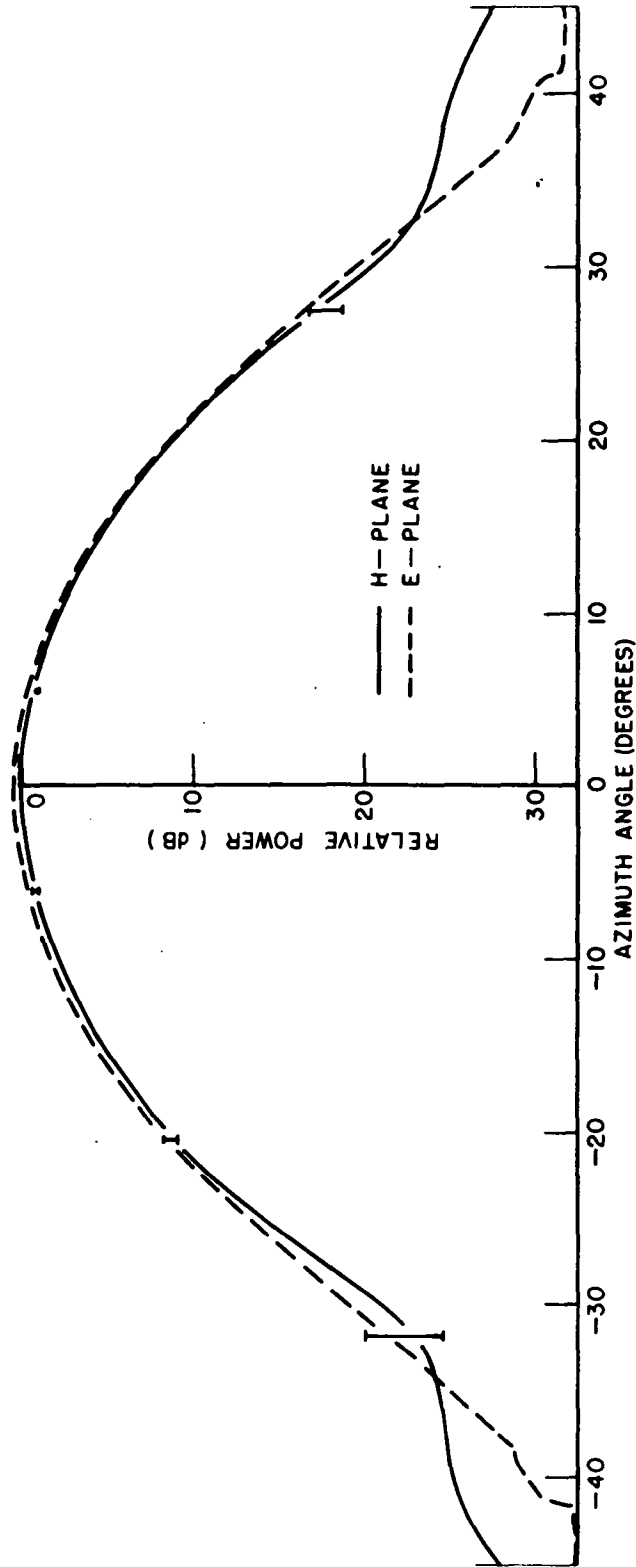


Fig. 29. Pattern showing the quality of the circular polarization for the conical dual mode horn (3.8 GHz).

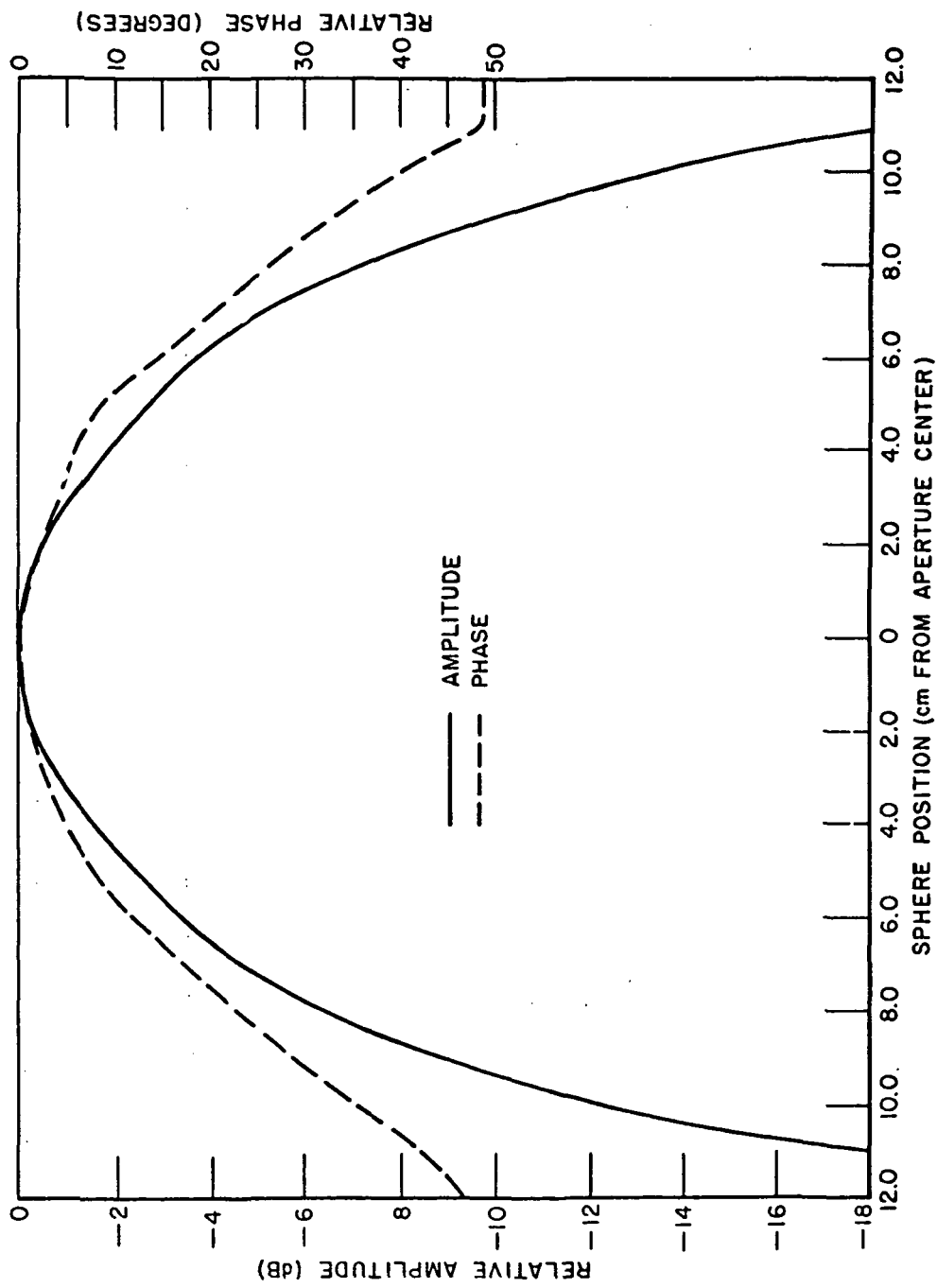


Fig. 30. Aperture distribution of the conical dual mode horn (H-plane, 3.9 GHz).

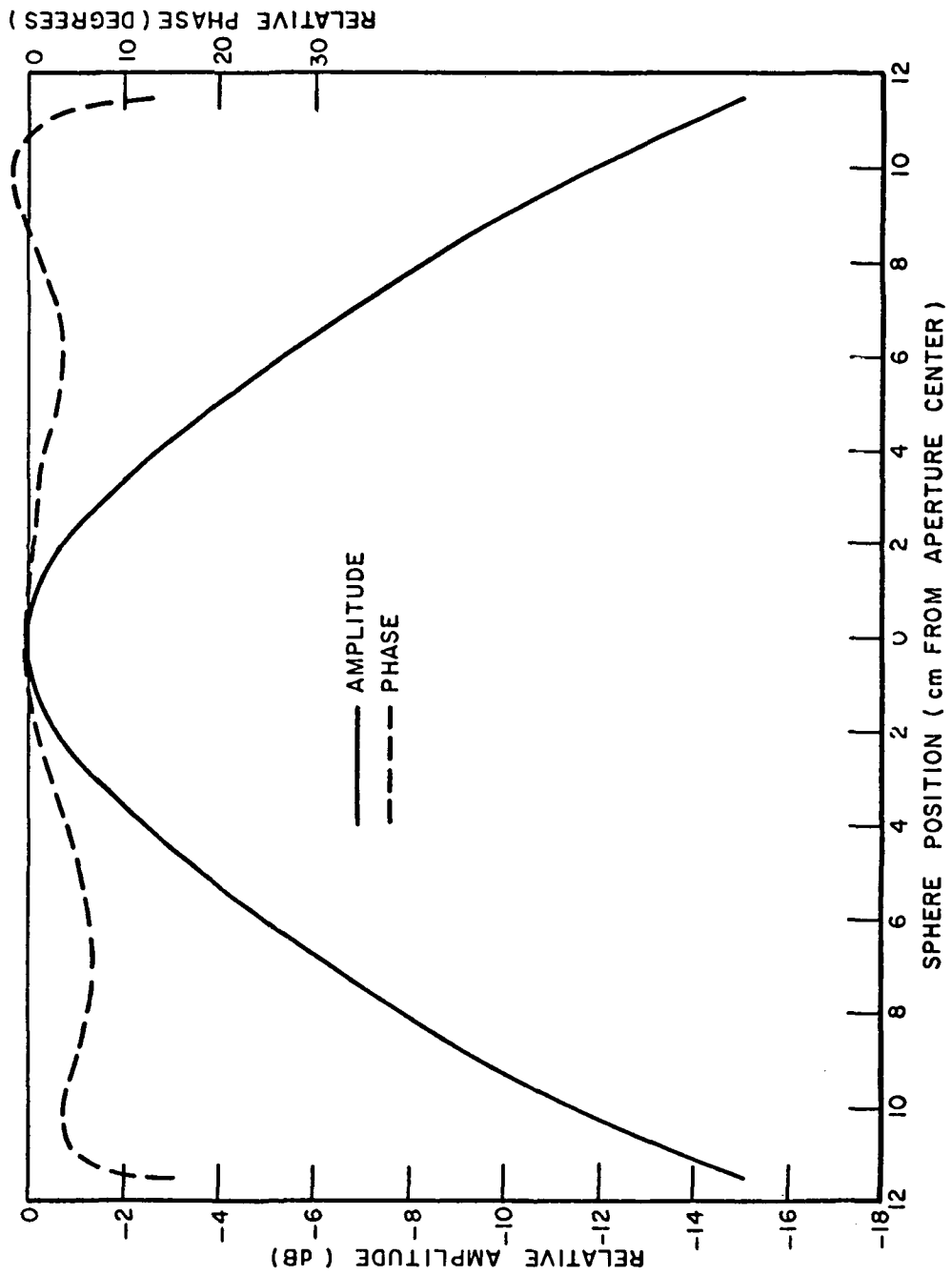


Fig. 31. Aperture distribution of the conical dual mode horn (E-plane, 3.9 GHz).

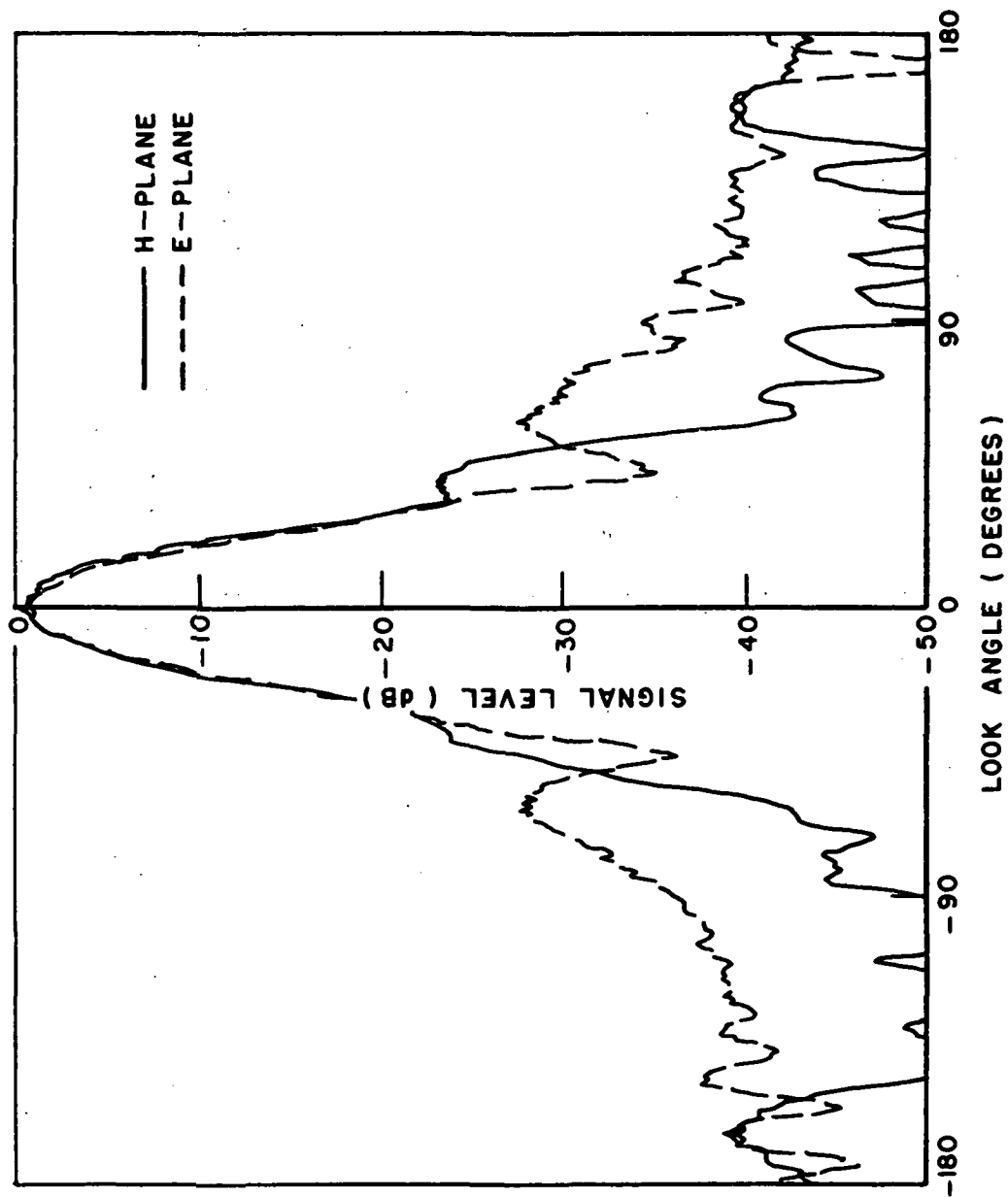


Fig. 32. Radiation patterns of the pyramidal dual mode horn (3.7 GHz).

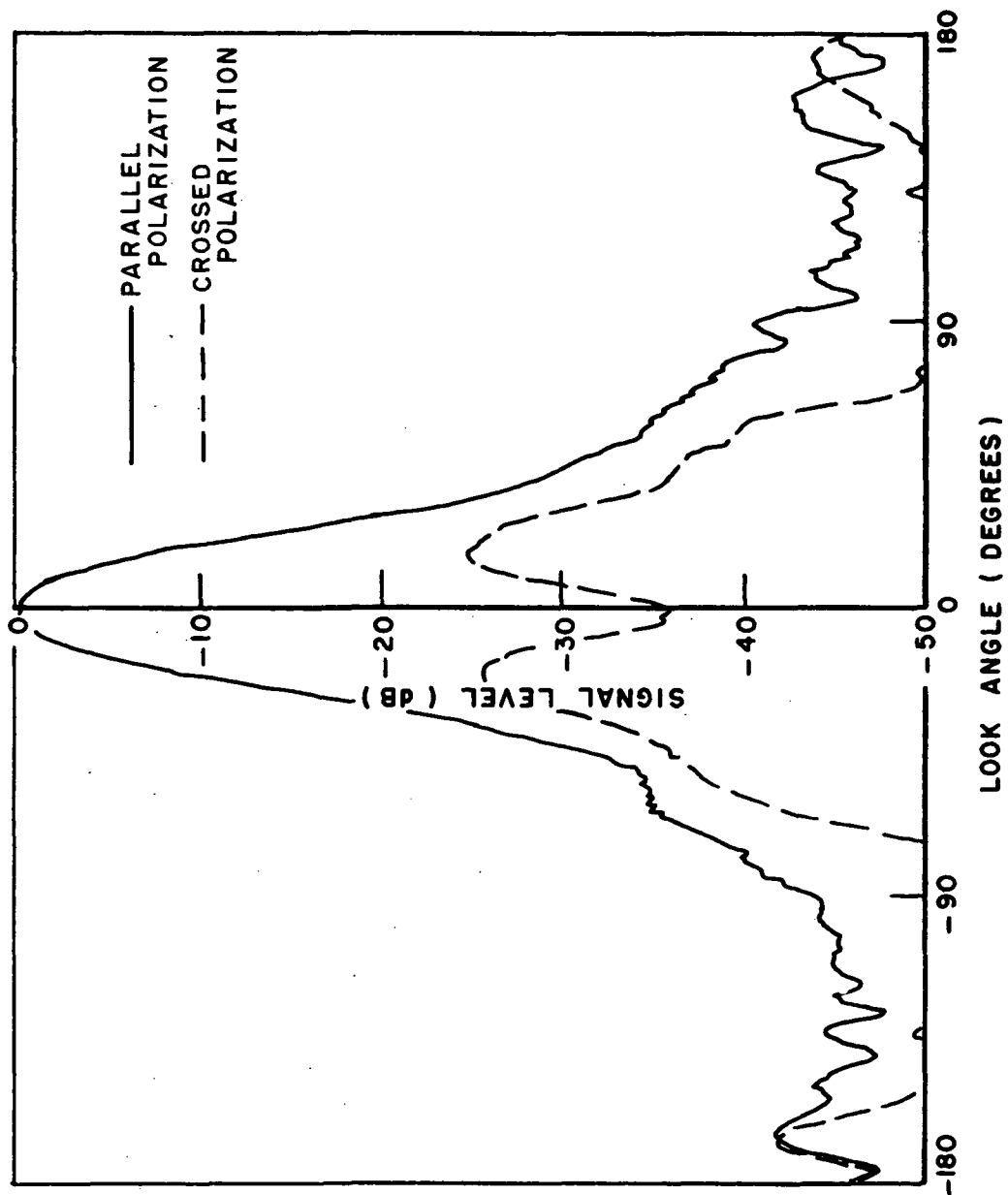


Fig. 33. Average radiation patterns for the pyramidal dual mode horn (3.7 GHz).

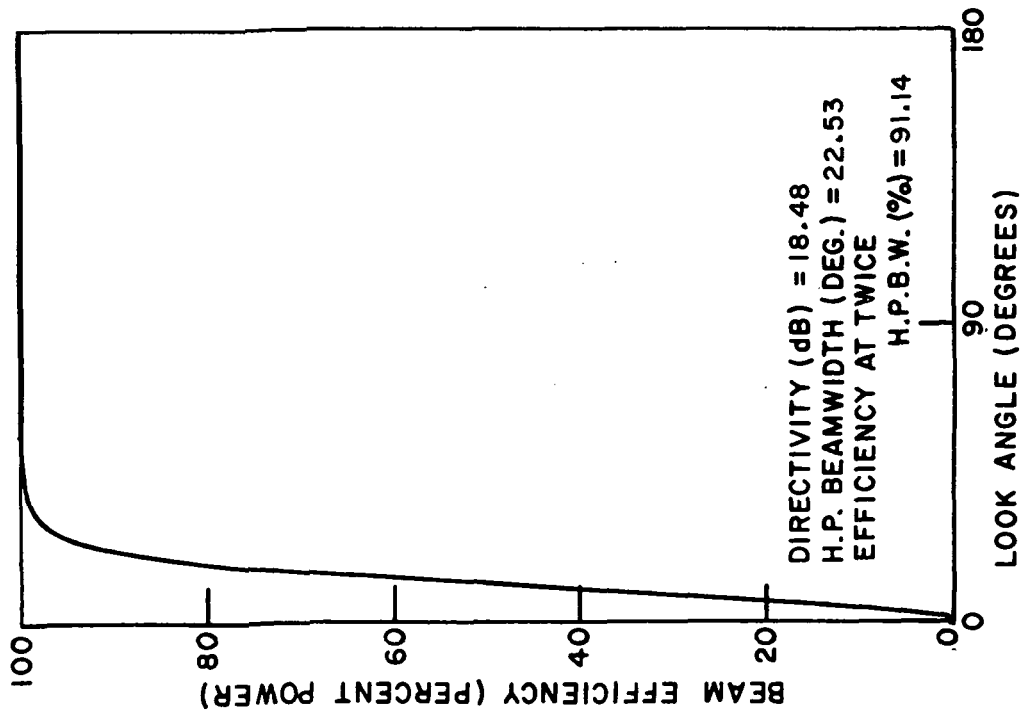


Fig. 34. Beam efficiency of the pyramidal dual mode horn, cross polarization considered desirable (3.7 GHz).

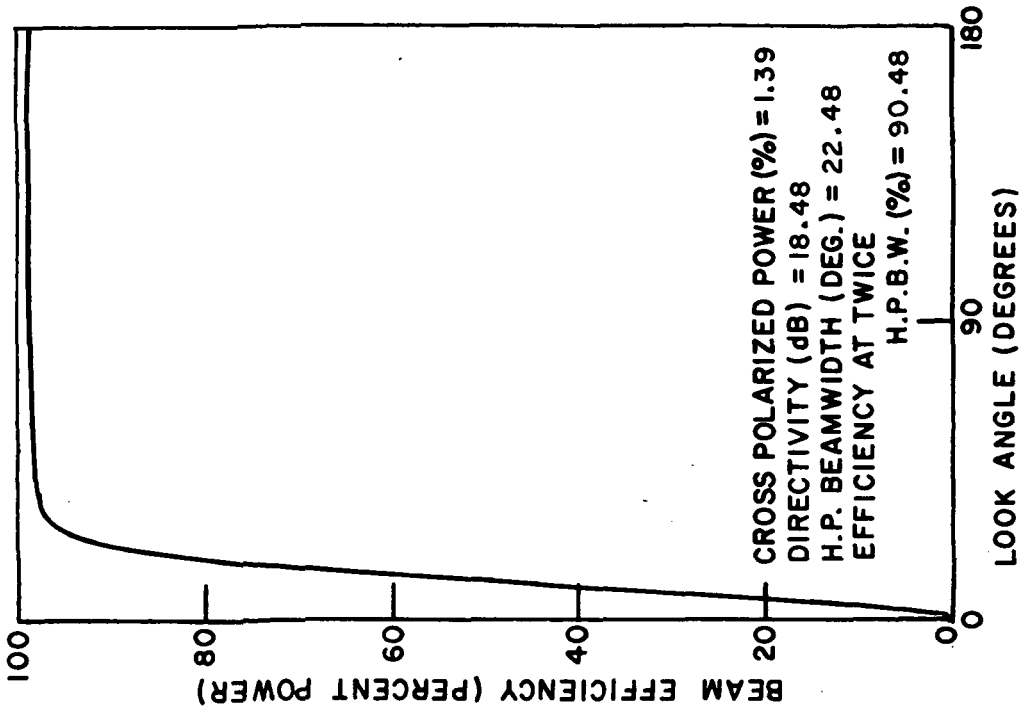


Fig. 35. Beam efficiency of the pyramidal dual mode horn, cross polarization considered undesirable (3.7 GHz).

D. The Pyramidal Dual Mode Horn Antenna

In order to complete the quartet of antenna types a square dual mode horn was also constructed. Since Potter had found it necessary to adjust the phase of the various modes empirically for the circular dual mode horn, it was decided that to avoid a tedious trial and error design procedure an attempt should be made to "square" the conical horn.

In the conical horn, the fundamental mode is the TE_{11} and the higher order mode used to produce the desired aperture taper is the TM_{11} . These should have the same amplitude and phase at the aperture. In the square horn the fundamental mode is the TE_{01} . If the TE_{12} and TM_{12} are now generated, each at half the amplitude of the TE_{01} mode a field configuration results which is very similar to that in the circular geometry. It was decided that the most critical factors in generating the modes in the correct proportions and phases were the area ratio of the waveguides across the step and the guide wavelength for the higher order modes after the step. The guide wavelength of the fundamental mode is relatively insensitive to guide size at this point since the guide dimension is considerably greater than that which will produce cut off. The guide size after the step was thus chosen to produce the same guide wavelength for the TE_{12} and TM_{12} modes as existed in the circular horn for the TM_{11} mode. This resulted in a guide of 3.706 inches on a side. The area ratio across the step was made the same which resulted in the smaller dimension at the step being 2.895 inches. The aperture of the horn was set to give the same 25° half power beamwidth based on a tapered aperture distribution and resulted in a dimension of 8.563 inches. It was further assumed that a differential phase shift between the step and the aperture of 0.84λ would be required as before. This resulted in a flare angle of 9.795° and a length of 14.07 inches from the step to the aperture. A 3.0 inch long taper was used to feed the step section from the 1.75 inch waveguide.

This horn was constructed using quarter inch aluminum sheet for the sides of the large section and brass for the step and taper sections. The resulting antenna patterns are shown in Fig. 32 for a frequency of 3.7 GHz which was found to be the best frequency for this particular horn. The average patterns and beam efficiency curves are shown in Figs. 33-35.

E. Comparisons with a Paraboloidal Antenna

In order to show how much better all of the antennas just discussed are for the intended application than the ever popular paraboloid some comparative measurements of beam efficiency were made. It should be mentioned that the antenna used for comparison is not a particularly good specimen for the purpose since it has a rather small focal length to diameter ratio (1:4). A shallow reflector would show a better performance since the feed would have a better defined phase center over the extent of the parabola. It was selected because its 14 inch diameter gives approximately the same beamwidth as the other antennas tested and

because it was equipped with a dipole feed suitable for use at 3.7 GHz. Its radiation patterns and beam efficiency curves are shown in Figs. 36-39. It will be noticed that the beam efficiency is very low, less than 60%. This is in part due to the quality of this particular antenna, but mainly due to the high side lobes which do not exist on the other antennas. However, 65 to 68% is about the maximum obtainable from a paraboloid. The cross polarized radiation is also very high. This again is in part due to the low f/d ratio. It is impossible to obtain a beam efficiency of 90% at any angle because of the cross polarized component.

In summary it may be said of the pattern characteristics of the antenna types tested that:

- (a) For wide band applications the corrugated structures perform best, i.e., bandwidths of 50% or greater.
- (b) For narrower band (5%) the dual mode structures have the advantage of a sharper drop off in the beam skirts, probably due in part to the smaller flare angle. Thus the percentage of power contained in twice the half-power beamwidth is greater.
- (c) The circular structures have a lower cross polarized component of radiation than do the square structures and they may be expected to perform better in a circularly polarized system.
- (d) The square corrugated structures for these small wide flare angle horns have been found to be critically dependent on: flare angle, total number of corrugations, and number of corrugations per wavelength. Considerable care must be exercised in the choice of these parameters to obtain proper performance.
- (e) All the antennas tested far out perform such well known basics as the paraboloid.

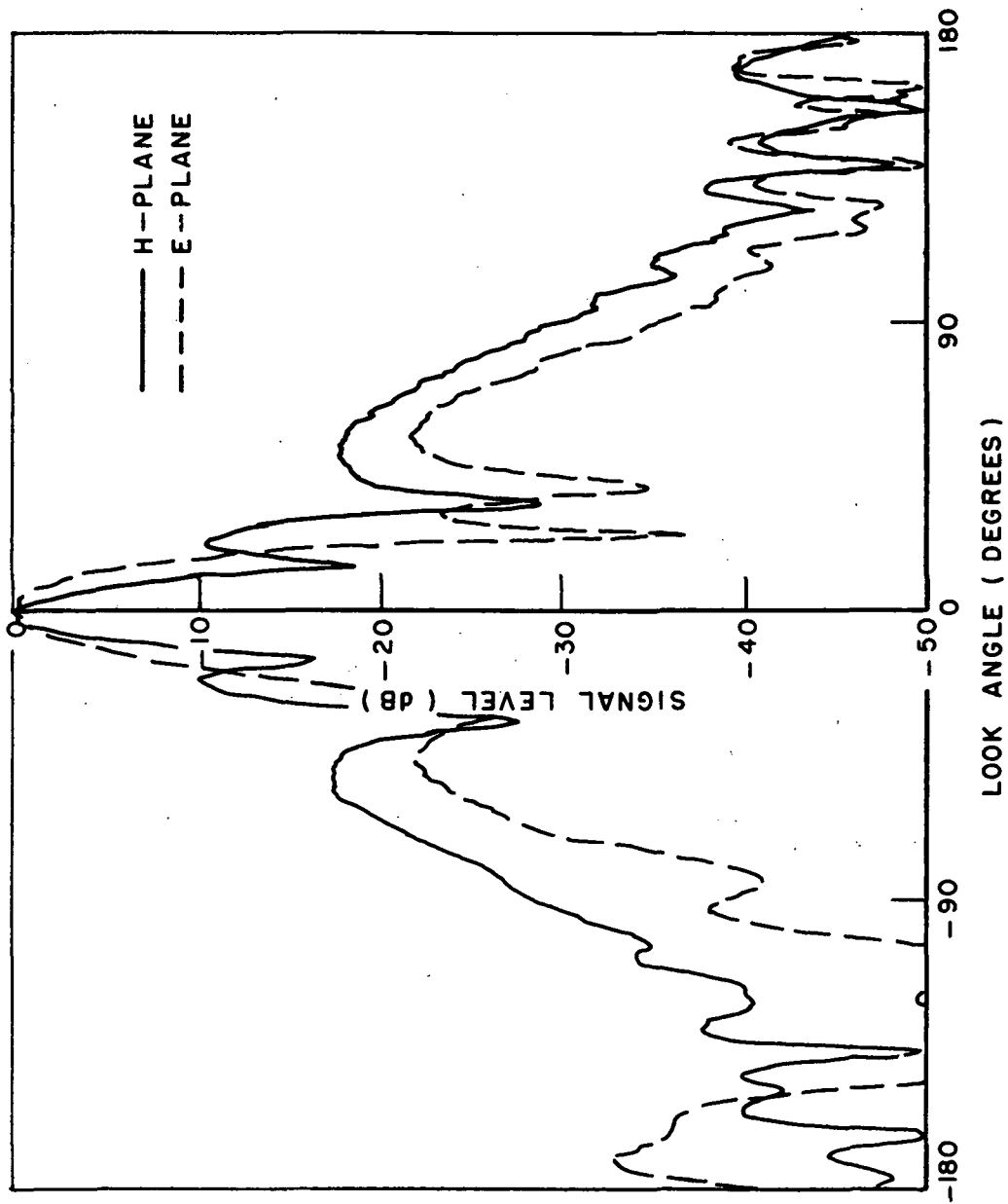


Fig. 36. Radiation patterns of a 14 inch paraboloid ($f:d = 1:4$) at 3.7 GHz.

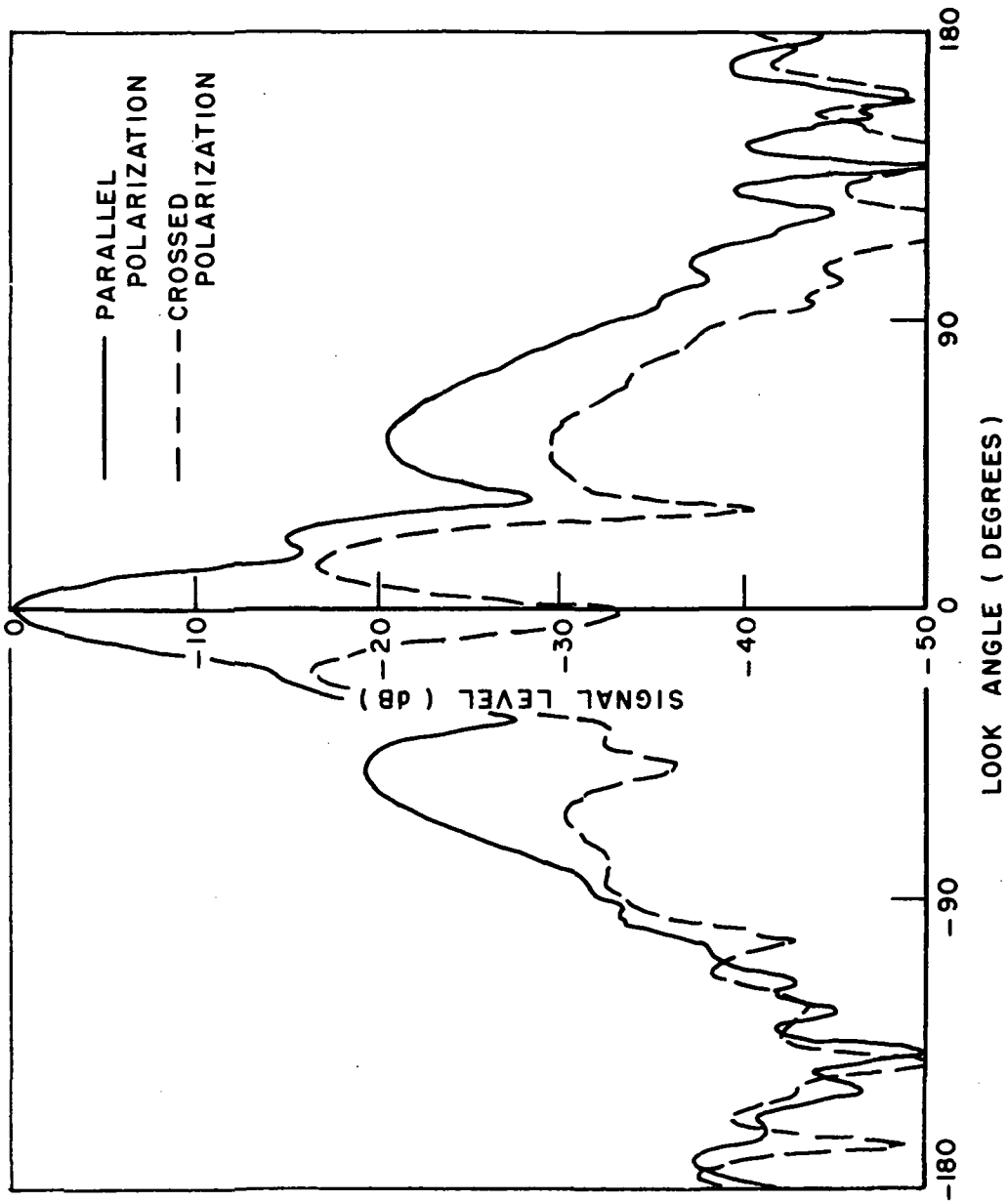


Fig. 37. Average radiation patterns of a 14 inch paraboloid (3.7 GHz).

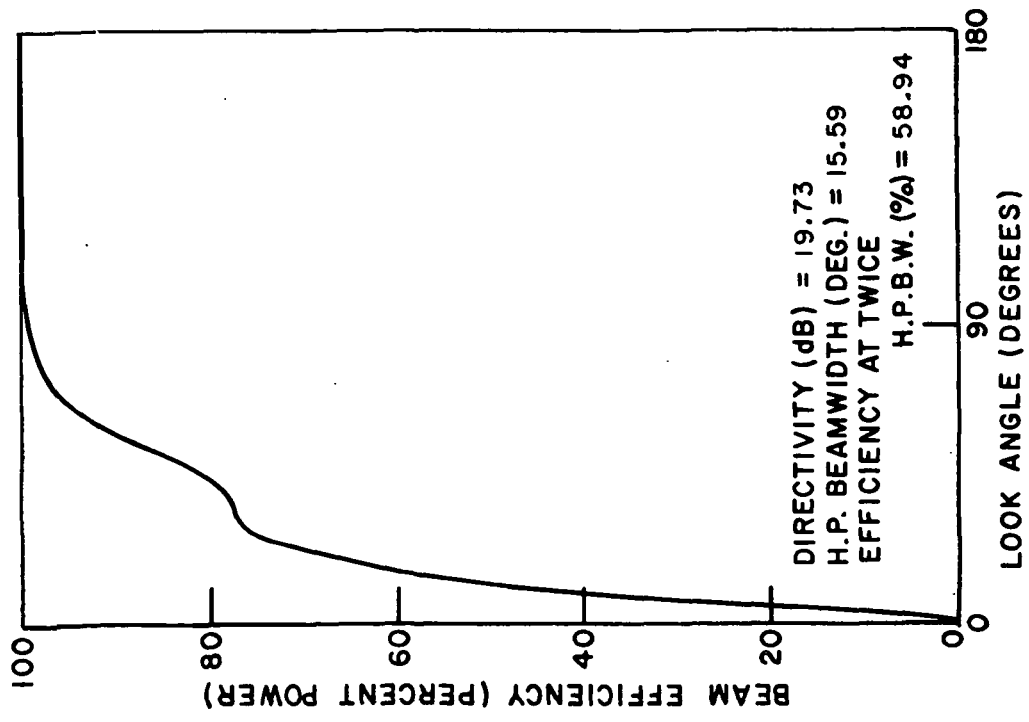


Fig. 38. Beam efficiency of a 14 inch paraboloid cross polarization considered desirable (3.7 GHz).

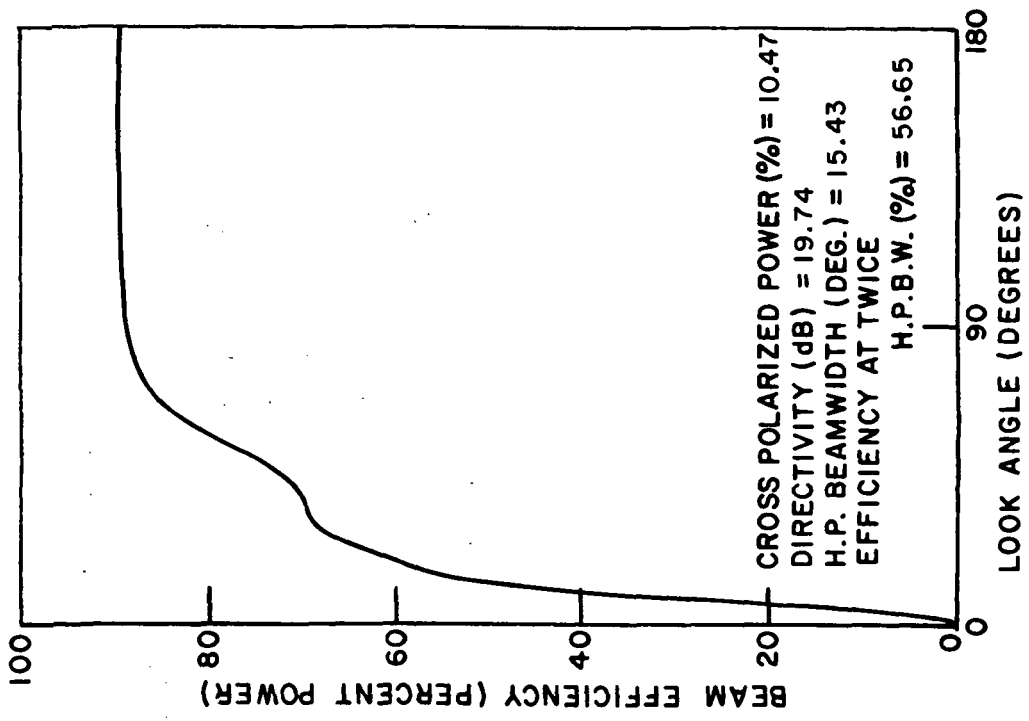


Fig. 39. Beam efficiency of a 14 inch paraboloid cross polarization considered undesirable (3.7 GHz).

IV. MEASURING TECHNIQUES

As indicated in the introduction, a major part of the program at least as important as antenna design is the precise evaluation of the resulting antennas. In addition to reducing reflection and resistive losses to a minimum, it is necessary that the residual losses be measured to 0.01 dB (referred to the forward power when the antenna is operated in a transmitting mode). Further, a beam efficiency of around 97% is needed which in turn requires a method capable of measuring efficiencies of this order. The methods developed for making measurements of the required accuracy will now be described.

A. The Reflectometer System

A fundamental problem in the present case is that all the antennas being considered use either round or square waveguide and no slotted lines or other reflection measuring devices are commercially available for these geometries. If the voltage reflection coefficient is kept below 1.1 then the reflected power will be less than 0.01 dB of the incident power and the accuracy is unimportant. However, as the reflection goes up the accuracy becomes more of a problem and the reflection coefficient ρ must be measured to within approximately $0.0012/\rho$. Even with the best slotted line available the necessary transformers would preclude sufficient accuracy.

One possibility is to construct a special slotted line in the waveguide used for the antennas. However, this requires very close tolerances and two such lines would have to be made. In addition, the presence of a slot in the waveguide is somewhat objectionable since it prevents circular polarization being used with the slotted line in place. To overcome this problem use was made of a method originally proposed for plasma sheath diagnostics, and further developed for the present purpose, employing a multiprobe reflectometer. The multiprobe reflectometer consists of nothing more than a number of fixed probes loosely coupled to the waveguide in much the same way as the single moveable probe of the slotted line. Each of the probes is connected to the measuring system via a square law detector. It is necessary to assume that the coupling factor of each probe to the waveguide is the same or to provide an appropriate calibration curve. In the present application a single probe mounted in a saddle, which could be placed on the waveguide in any of four locations, was used (Fig. 40). It was then only necessary for the probe to enter the waveguide to the same depth in each position for the four probe positions to be considered identical. Additional holes were provided in the perpendicular plane for C.P. studies. It is also necessary for the detectors to be square law or to be calibrated. However, for small VSWR's most detectors will easily satisfy the square law requirement.

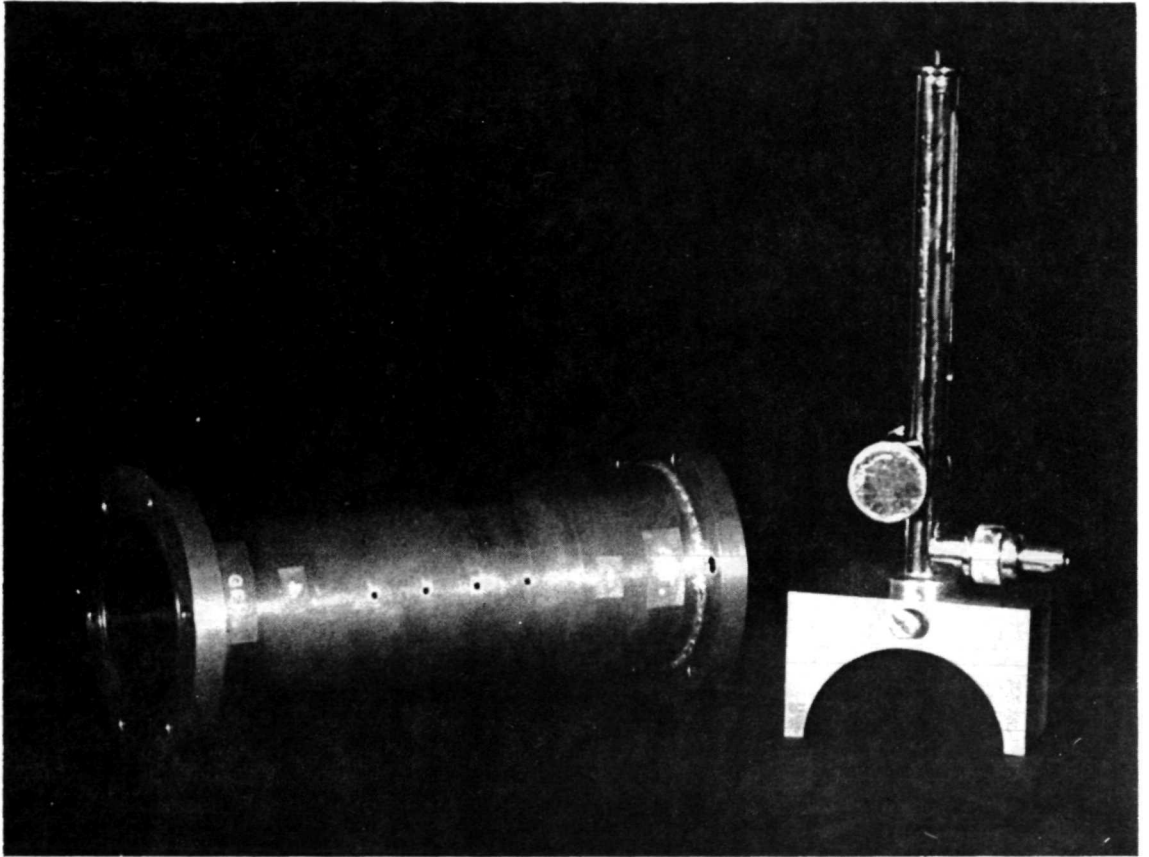


Fig. 40. The four-probe reflectometer.

(i). The three probe reflectometer

Consider first a situation where the frequency is known but the incident power and the phase and amplitude of the reflection coefficient are not known. There are three unknowns and the outputs from three probes are in general sufficient to evaluate them. There is one restriction and that is that no two of the probes shall be spaced at any multiple of $\lambda/2$. Otherwise the spacing of the probes is quite arbitrary, except for some practical limitations on accuracy which will be discussed later. Let V be the incident voltage and V_n the standing wave voltage on the transmission line at the location of the n th probe. Then:

$$(1) \quad V_n = V(1 + \rho e^{j(\theta - \phi_n)})$$

$$(2) \quad |V_n|^2 = V^2\{1 + \rho^2 + 2\rho \cos(\theta - \phi_n)\}$$

where ρ and θ are the modulus and angle of the reflection coefficient of the load and ϕ_n is the phase shift corresponding to the distance from the probe to the load and back, where ϕ_n is taken as positive. Then:

$$(3) \quad |V_n|^2 = V^2\{1 + \rho^2 + 2\rho(\sin \theta \sin \phi_n + \cos \theta \cos \phi_n)\}$$

or, writing $\sin \phi_n = S_n$ and $\cos \phi_n = C_n$ where S_n and C_n are constants for a given probe configuration,

$$(4) \quad |V_n|^2 = V^2\{1 + \rho^2 + 2\rho(S_n \sin \theta + C_n \cos \theta)\}.$$

It is worth noting at this point that if square law detectors are used for the probes the output from the n th probe will in fact be proportional to $|V_n|^2$. If for convenience we now write:

$$(5) \quad A = 2V^2\rho \cos \theta$$

$$(6) \quad B = 2V^2\rho \sin \theta$$

$$(7) \quad D = V^2(1 + \rho^2)$$

$$(8) \quad P_n = |V_n|^2$$

then for $n = 1, 2$ and 3 we have from Eq. (4):

$$(9) \quad D + C_1 A + S_1 B - P_1 = 0$$

$$(10) \quad D + C_2 A + S_2 B - P_2 = 0$$

$$(11) \quad D + C_3 A + S_3 B - P_3 = 0$$

Therefore,

$$(12) \quad \frac{D}{\begin{vmatrix} C_1 & S_1 & -P_1 \\ C_2 & S_2 & -P_2 \\ C_3 & S_3 & -P_3 \end{vmatrix}} = \frac{-A}{\begin{vmatrix} 1 & S_1 & -P_1 \\ 1 & S_2 & -P_2 \\ 1 & S_3 & -P_3 \end{vmatrix}} = \frac{B}{\begin{vmatrix} 1 & C_1 & -P_1 \\ 1 & C_2 & -P_2 \\ 1 & C_3 & -P_3 \end{vmatrix}} = \frac{-1}{\begin{vmatrix} 1 & C_1 & S_1 \\ 1 & C_2 & S_2 \\ 1 & C_3 & S_3 \end{vmatrix}}$$

and hence

$$(13) \quad A = - \left[\frac{P_1(S_3 - S_2) + P_2(S_1 - S_3) + P_3(S_2 - S_1)}{\sin(\phi_3 - \phi_2) + \sin(\phi_1 - \phi_3) + \sin(\phi_2 - \phi_1)} \right]$$

$$(14) \quad B = \frac{P_1(C_3 - C_2) + P_2(C_1 - C_3) + P_3(C_2 - C_1)}{\sin(\phi_3 - \phi_2) + \sin(\phi_1 - \phi_3) + \sin(\phi_2 - \phi_1)}$$

and

$$(15) \quad D = \frac{P_1 \sin(\phi_3 - \phi_2) + P_2 \sin(\phi_1 - \phi_3) + P_3 \sin(\phi_2 - \phi_1)}{\sin(\phi_3 - \phi_2) + \sin(\phi_1 - \phi_3) + \sin(\phi_2 - \phi_1)}$$

Now from Eqs. (5) and (6):

$$(16) \quad \theta = \arctan \frac{B}{A}$$

$$(17) \quad \rho = \frac{\sqrt{A^2 + B^2}}{2V^2}$$

and using Eq. (7)

$$(18) \quad V^2 \left(1 + \frac{A^2 + B^2}{4V^4} \right) = D$$

or

$$(19) \quad V^2 = \frac{D \pm \sqrt{D^2 - A^2 - B^2}}{2}$$

The root associated with the positive sign must be correct since if $\rho = 0$

$$(20) \quad A^2 + B^2 = 0 \text{ and } V^2 = D.$$

Therefore

$$(21) \quad V^2 = 1/2 \{ D + \sqrt{D^2 - A^2 - B^2} \}$$

and ρ may be found from Eq. (17).

V^2 , it should be noted, is proportional to the forward power and may be used as a measure of relative power level. With appropriate calibration it may be used to measure absolute power.

So far the treatment has been entirely general, no particular relationship between the probes being assumed. It will be noticed that Eqs. (13), (14), and (15) are symmetrical in 1, 2, and 3, as is to be expected for arbitrary probes. In a practical reflectometer, however, the probes will generally be spaced at equal intervals. Then let

$$(22) \quad \phi_3 - \phi_2 = \phi_2 - \phi_1 = \phi_s$$

and

$$(23) \quad \phi_1 - \phi_3 = -2\phi_s, \text{ probe number 1 being nearest the load (Fig. 41).}$$

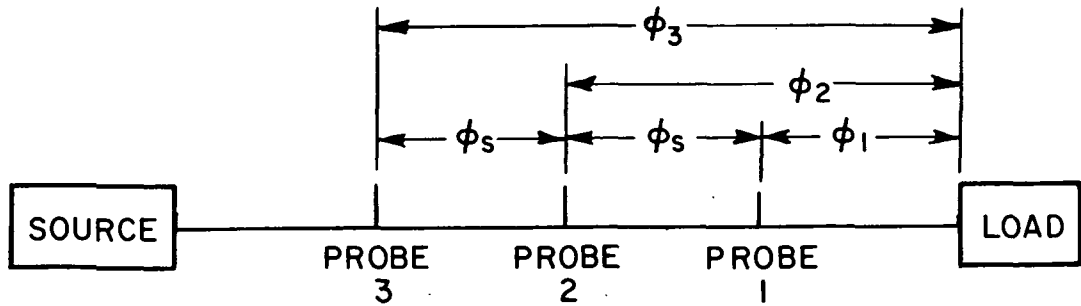


Fig. 41. A reflectometer with 3 equally spaced probes. (ϕ denotes the two way phase angle between indicated points.)

Equations (14), (15), and (16) then take the form

$$(24) \quad A = - \left[\frac{P_1(S_3 - S_2) + P_2(S_1 - S_3) + P_3(S_2 - S_1)}{2 \sin \phi_s - \sin 2\phi_s} \right]$$

$$(25) \quad B = \frac{P_1(C_3 - C_2) + P_2(C_1 - C_3) + P_3(C_2 - C_1)}{2 \sin \phi_s - \sin 2\phi_s}$$

$$(26) \quad D = \frac{(P_1 + P_3) \sin \phi_s - P_2 \sin 2\phi_s}{2 \sin \phi_s - \sin 2\phi_s}$$

(ii). The four probe reflectometer

With a fourth equally spaced probe it is also possible to determine the frequency. (The solution with unequal spacing is somewhat intractable, unless a best fit is found by iterative testing of different frequencies on a digital computer.) By advancing the subscripts in Eq. (26) to include a fourth probe:

$$(27) \quad D = \frac{(P_2 + P_4) \sin \phi_s - P_3 \sin 2\phi_s}{2 \sin \phi_s - \sin 2\phi_s}$$

Equating the numerators of Eqs. (26) and (27) yields

$$(28) \quad \cos \phi_S = 1/2 \left[\frac{P_1 - P_4}{P_2 - P_3} - 1 \right] .$$

Then if "a" is the probe spacing:

$$(29) \quad \phi_S = \frac{4\pi a}{\lambda} \quad \text{and}$$

$$(30) \quad \lambda = \frac{4\pi a}{\arccos \left[1/2 \left\{ \frac{P_1 - P_4}{P_2 - P_3} - 1 \right\} \right]}$$

where λ is the wavelength in the transmission line, or the guide wavelength in waveguide.

In a practical reflectometer a few restrictions must be imposed to avoid ambiguities and to obtain acceptable accuracy. From Eq. (28) it is evident that as long as ϕ_S remains in the first two quadrants no ambiguity arises in determining λ . However, if ϕ_S may possibly exceed π then there is more than one solution to Eq. (30). Thus, it is necessary to impose the restriction that:

$$0 < \phi_S < \pi$$

or

$$0 < a < \frac{\lambda}{4} .$$

It is worth noting that this condition includes the stipulation made at the outset that for a three probe reflectometer no two probes shall be spaced at a multiple of $\lambda/2$, a condition which makes A, B, and D indeterminate. In the case of four probes it is possible for the first and fourth probe to be spaced at $\lambda/2$ apart and still satisfy these conditions provided that both the first and fourth are not included in the calculation of A, B, and D.

The condition that ϕ_S be less than π may be relaxed if the approximate frequency is known since the correct quadrant for ϕ_S may then be determined in advance. In this case there is, in fact, an advantage in using large probe spacings in that it permits a proportionately more accurate frequency determination. Where the frequency is unknown two sets of probes; one at close spacing and one at wide spacing could be used to achieve the same end.

One further limitation exists and that is that if either a maximum or minimum of the standing wave pattern is located exactly midway between the second and third probes the frequency becomes indeterminate. This restriction does not apply if the frequency is already known or is measured independently.

In addition to these theoretical limitations there are some practical limitations which should be observed if accurate measurements are to be made. The frequency measurement tends to be inaccurate if the reflection coefficient is very small. In this event it is desirable either to measure the frequency independently or temporarily to introduce some mismatch to facilitate a frequency reading and then to remove it again for the reflection measurement. A further limitation is that if "a" is very small or approaches $\lambda/4$ the accuracy will be impaired. Maximum sensitivity exists for $a = \lambda/8$. A three to one bandwidth is obtainable for "a" between $\lambda/16$ and $3\lambda/16$ and a wider band could be used with care.

(iii) Self checking systems

So far only systems employing the minimum number of probes have been discussed: three if the frequency is known, four if it is not. By using additional probes it is possible to introduce a degree of redundancy and to make the system self checking.

Consider a system in which the frequency is known but in which four probes are used. It is possible to calculate V^2 , ρ and θ in four different ways using the probe outputs three at a time. Equations (13), (14), and (15) must be used since only two of the four combinations of probes are equally spaced. If the four results agree within acceptable limits, it is reasonable to assume that the measurement is accurate. Care must of course be taken in the practical application of this assumption. If for example, a common amplifier is used to monitor the probe outputs, a slow drift in gain could result in an error in V^2 while still yielding a self consistent set of results. ρ and θ would be correct in this case. A fast drift, that is one which changes between reading one probe and the next, would produce inconsistency in the outputs and hence be detected. Similarly a defect in one probe, with the others operating correctly, would be detectable, as also would a frequency error.

One extra probe provides the means of detecting errors but not of isolating them. In the case just discussed a defective probe would produce one correct set of outputs and three incorrect sets. It would not, however, be possible to identify the correct set. By introducing

a fifth probe in a system where the frequency is known it is possible to obtain ten sets of V^2 , ρ and θ . Four of these do not use the output from any one probe. Thus, if four sets are self consistent and the remaining six are not it is possible to identify not only the correct data but also the defective probe.

When some or all of the data sets agree within acceptable limits it is possible to improve the accuracy of the final result by averaging the values for V^2 and the reflection coefficient; the reflection coefficient is averaged by treating ρ and θ as a single complex quantity. This process, in effect, minimizes the mean square error in the observed standing wave voltages (V_n).

Similar arguments can of course be applied to systems where the frequency is regarded as an unknown. It must be remembered that the rules regarding probe spacing must be applied to all combinations of probes used in self checking.

In the present application four probes are used, the frequency being known. Equations (13), (14), and (15) have been programed on a computer. In making measurements the probe output is read for each of the four positions and the readings entered into the computer. Four values for the reflection coefficient are calculated and averaged. In addition the maximum deviation between this average and any of the individual calculations is found. The average is plotted on a Smith Chart by the computer and an error circle, whose radius corresponds to this maximum deviation, is drawn around it. All the impedance data presented in this report were obtained in this manner. The error circle is a direct indication of the self consistency of the experimental data.

As a further check on the accuracy of this method one of the antennas was connected to the reflectometer and its impedance measured. A series of waveguide spacers $\lambda_g/32$ thick were then introduced between the antenna and the reflectometer. The result is shown in Fig. 42. With an ideal probe section, this data would fall on a circle whose center is at the center of the Smith Chart and whose radius is the reflection coefficient of the load. In any practical measuring system the points will fall on a circle whose center is displaced from the center of the Smith Chart. The distance from the chart center to the data circle center is a measure of the reflections from the probe section itself (due to presence of the probe, flange alignment, etc.), i.e., the residual reflections. These measurements indicated a residual VSWR of

$$\sqrt{\frac{VSWR_{\max}}{VSWR_{\min}}} \approx 1.008.$$

This residual VSWR is close to that attainable with the best coaxial slotted line available and in practice represents a considerable improvement over such a line since 7 mm connectors typically have VSWR's

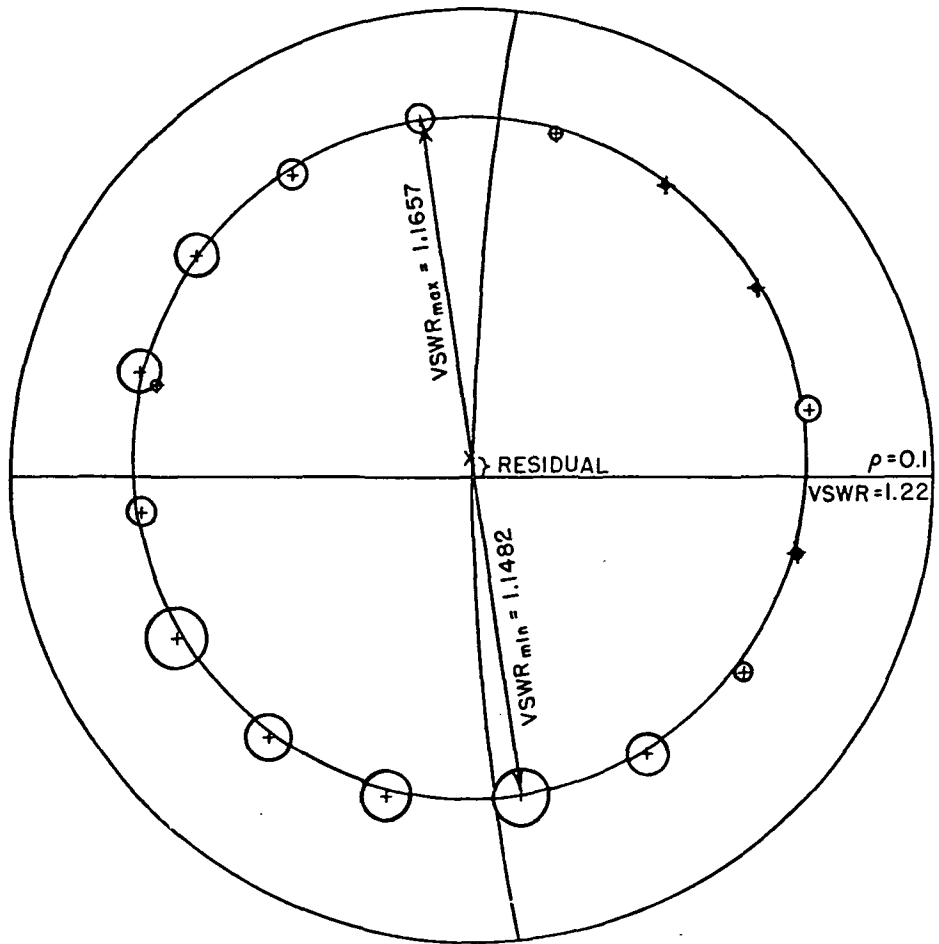


Fig. 42. Residual VSWR measurement for the 4 probe reflectometer (circular waveguide model).

of the order of 1.02 and waveguide to coaxial adapters are usually much worse (typical manufacturer specs "less than 1.25:1").

One further comment should be made in connection with the accuracy of this technique. An examination of the sensitivity of the reflection coefficient to errors in probe voltages was made by differentiating the expressions for V^2 , ρ and θ with respect to one of the probe outputs. It was observed that the derivatives of θ and of the product term ρV^2 were well behaved but the derivatives of ρ and V^2 separately were proportional to $1/1-\rho$. The accuracy with which ρ and V^2 can be determined decreases with increasing ρ ; and thus the method appears unsuitable for measuring anything but the phase angle of loads approaching $\rho = 1$. However, since it was planned to measure the resistive loss in the various antennas by closing them with a metal cap and observing the resulting reflection coefficient it was imperative to find a way around this restriction. A closer look at the derivatives in question showed that they were also proportional to the distance from the minimum of any two out of a group of three probes. This is because of the uncertainty of determining the exact depth of the minimum with a single probe on a steeply sloping standing wave. Placing two probes near the minimum takes care of this uncertainty. (Alternatively a single probe may be placed exactly at the minimum, in which case of course it provides the level of the minimum point directly, the other probes providing the remainder of the information.) Thus it is still possible to obtain accurate measurements for the higher VSWRs. In measuring high reflection coefficients for resistive loss determination, the procedure adopted was to place one of the probes at the standing wave minimum by using waveguide spacers (variable in $\lambda_g/32$ steps) and making a final adjustment by varying the frequency slightly, since the exact frequency of the measurement was generally not critical. To avoid problems with the crystal law a precision attenuator was placed in the feed line to the reflectometer in addition to a fixed attenuator pad in the circular waveguide between the probe section and the feed point. When the probe was moved to the high level positions attenuation was inserted to bring the probe output back to the same level. The attenuator readings were then used to calculate the reflection coefficient. An alternative method which was found to give very similar results was to use an r.f. coupled probe and a precision receiver.

B. Impedance Measurements

Reflection measurements were found to be quite straightforward using the four probe technique and measurements of the S-band antennas were made using the appropriate square or circular probe section. Measurements were not made on the square X-band horns because a probe section was never constructed for this guide size. The frequency was always measured independently with a cavity wavemeter so that the fourth probe provided the necessary redundancy for checking the accuracy of the measurement. The results are shown in Figs. 43-45.

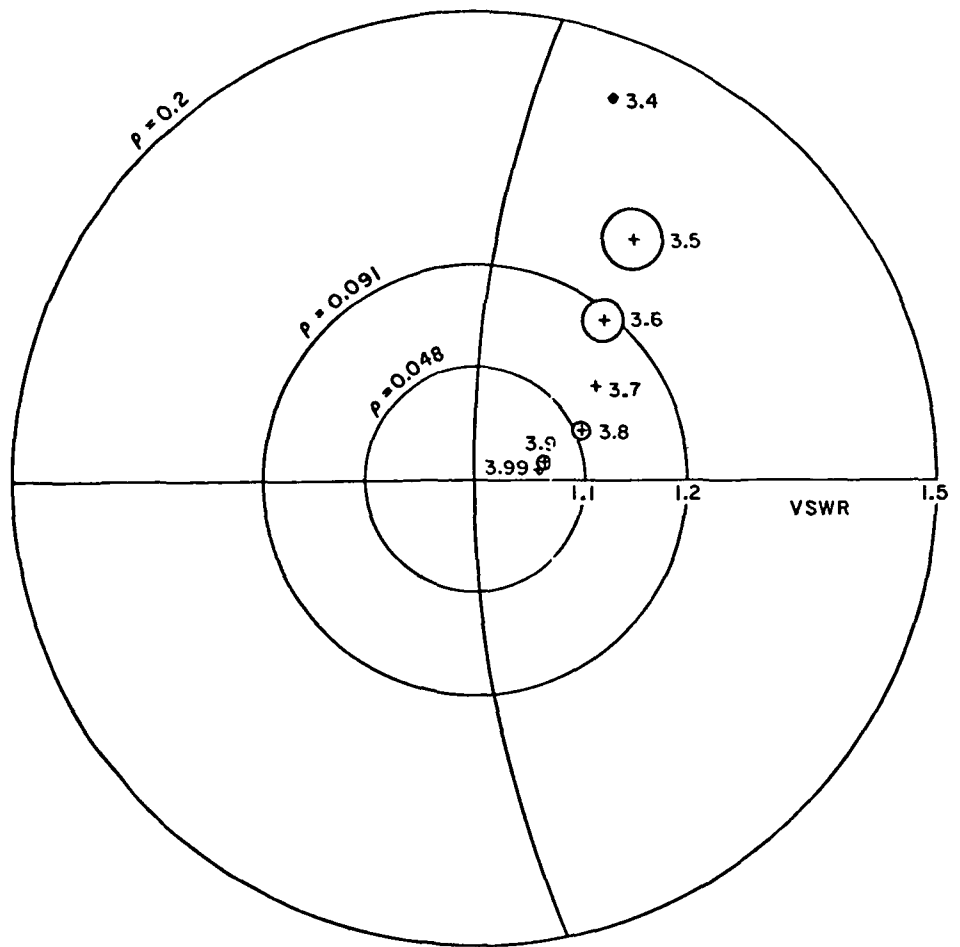


Fig. 43. Impedance of the conical corrugated horn, first two slots covered. (The numbers next to the points are frequencies in GHz).

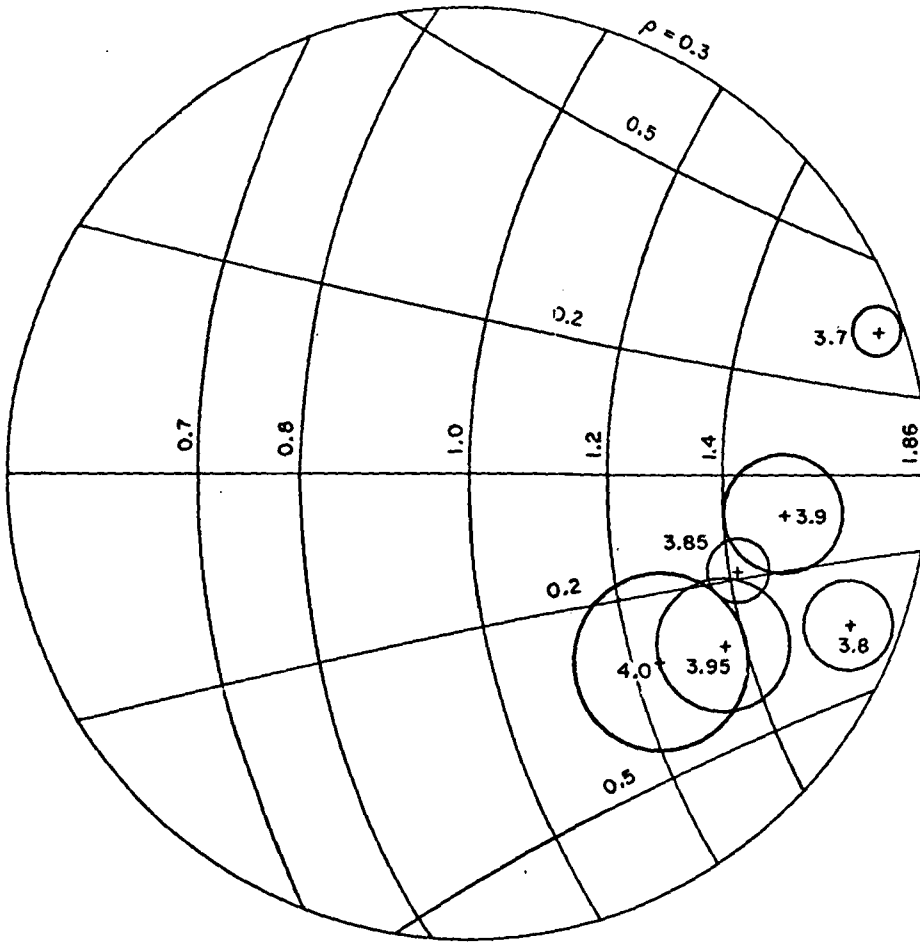


Fig. 44. Impedance of the pyramidal corrugated horn, 55° flare angle and 6 teeth per wavelength. (The numbers next to the points are frequencies in GHz).

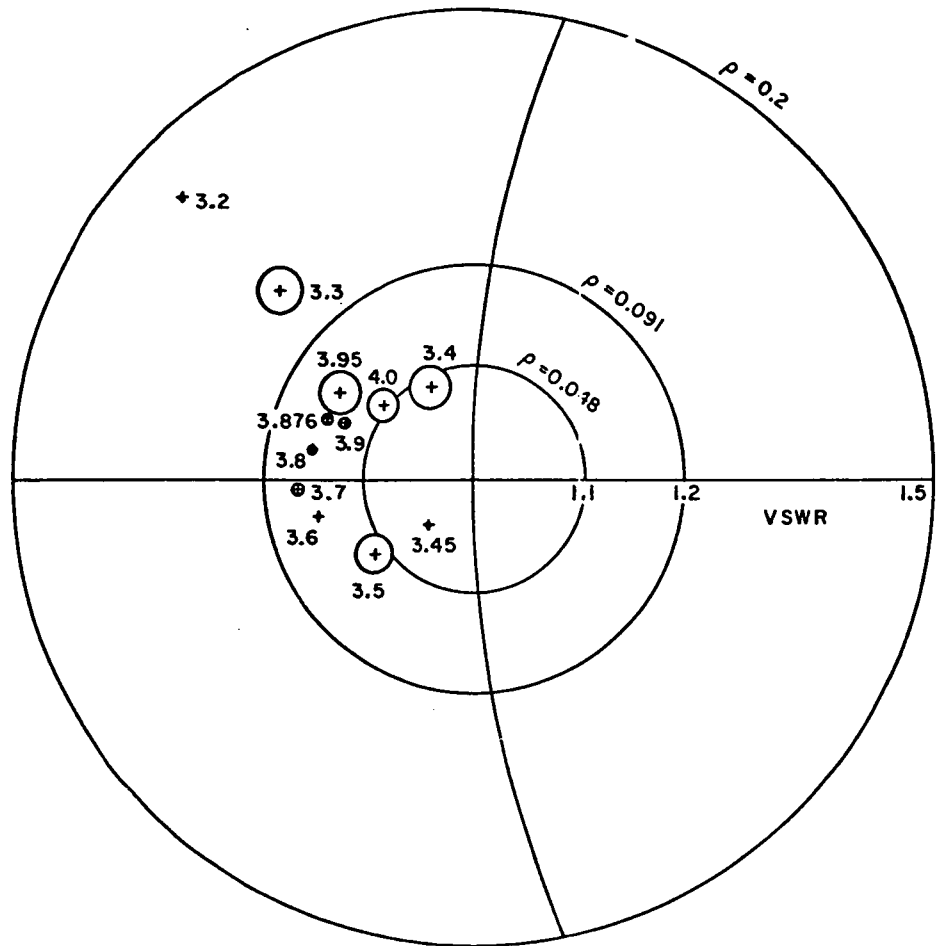


Fig. 45. Impedance of the conical dual mode horn. (The numbers next to the points are frequencies in GHz).

The VSWR of the conical corrugated horn is already below 1.1 in the frequency range 3.8 to 4.0 GHz thus the reflection loss is less than 0.01 dB. With some matching this range could probably be extended since the impedance points are all to one side of the circle. In any case with the accuracy obtained (the circles in the figure indicate the uncertainty in the measurement) the reflection loss, even where greater than 0.01 dB is known to well within the required accuracy.

The impedance of the pyramidal corrugated horn (Fig. 44) is less satisfactory. However, this particular antenna was also unsatisfactory as regards its radiation pattern characteristics.

Between 3.7 and 4.0 GHz, where its pattern characteristics were most satisfactory, the conical dual mode antenna shows a VSWR of between 1.1 and 1.17 (Fig. 45). Thus the loss is a little over 0.01 dB. This could probably be improved by matching. Again, however, the accuracy with which this loss is known is well within the required limit.

C. Resistive Loss Measurements

A number of methods for measuring the resistive loss in the horn walls were tried. All of them involved closing the aperture of the antenna with a short circuiting cap. Since it was desired that the reflected fields should be nearly identical to the incident fields to avoid introducing other modes, the ideal cap should match the phase front at the aperture. As aperture field measurements had shown the phase front of the conical corrugated horn to be almost perfectly spherical it was selected for the first tests. The less regular phase fronts of the other antennas would have made construction of a matching reflector extremely difficult. Accordingly a spherical end cap was built for the conical corrugated horn.

The first method tried for measuring loss was to make the shorted antenna into a cavity. This was achieved by adding a transition to rectangular waveguide and a sliding short circuit. A loosely coupled probe was then used to excite the cavity and to measure its Q factor, by observing the location of the sliding short circuit at the half power points either side of the resonant position. However, it was found that the loss in the sliding short-circuit was much greater than that in the antenna and also rather unstable. This method was therefore abandoned.

The next approach was to look for a method of measuring the reflection coefficient of the shorted antenna. The loss in reflected power in this situation will then be twice the loss in the forward power if the antenna were radiating. It has already been stated that the multiprobe reflectometer is not suitable for measuring very high reflection coefficients unless two of each group of three probes are close to the minimum point. This means that three out of four probes must be close to the minimum if the self checking capability is to be retained. The method shown in Fig. 46 was therefore devised. It was

assumed that to a first approximation the change in the standing wave voltage near the minimum would be the same if either a single test probe were moved slightly along the waveguide or the probe were left fixed and the frequency changed by a very small amount. Using a phase locked transmitter with a frequency offset capability it was possible to vary the frequency precisely over a range of ± 1 MHz around the center frequency. One of the four original probe positions was therefore placed near a standing wave minimum by suitable choice of frequency and the available waveguide spacers. This single probe was then measured as if it were a multiple probe by varying the frequency. Additional measurements were also taken for the other probe positions which were of course away from the null. The reflection coefficient was then calculated from the resulting probe outputs.

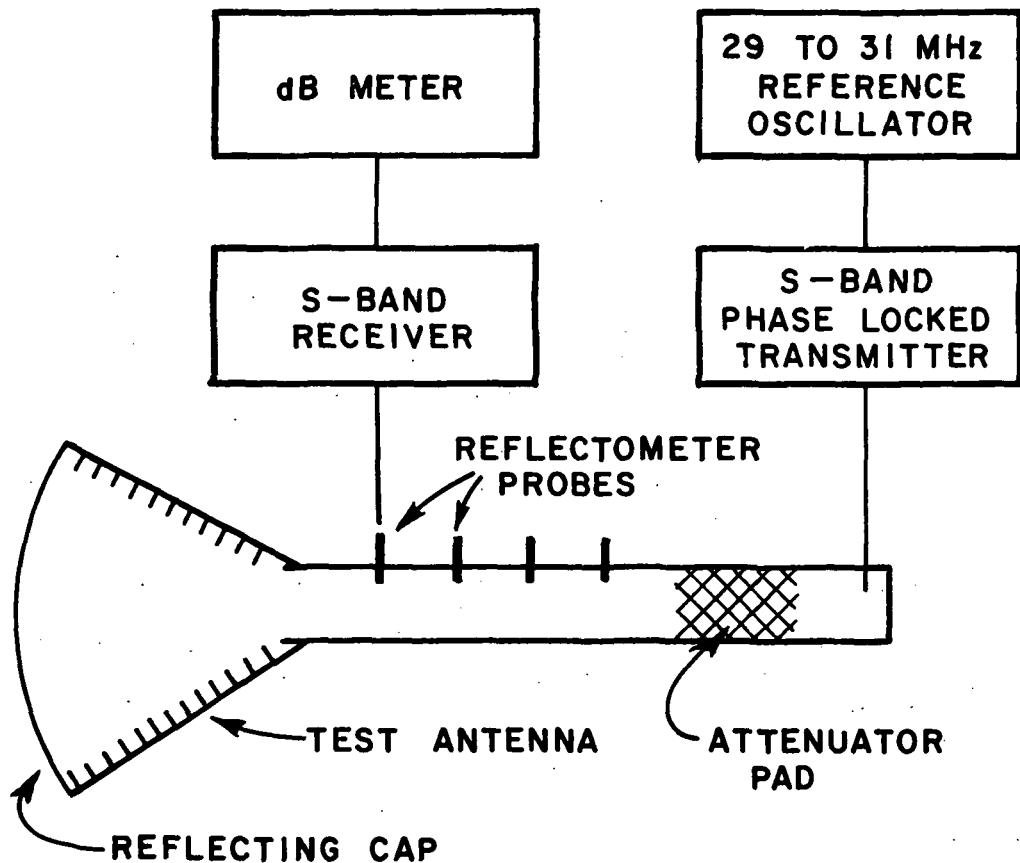


Fig. 46. Block diagram of efficiency measuring equipment.

Satisfactory measurements were obtained by this method, however, there were some reservations regarding its use. At some frequencies spurious nulls were observed on the standing wave pattern due to reflections from the throat of the horn (Fig. 47). Such nulls do not of course exist on the fixed frequency standing wave pattern but

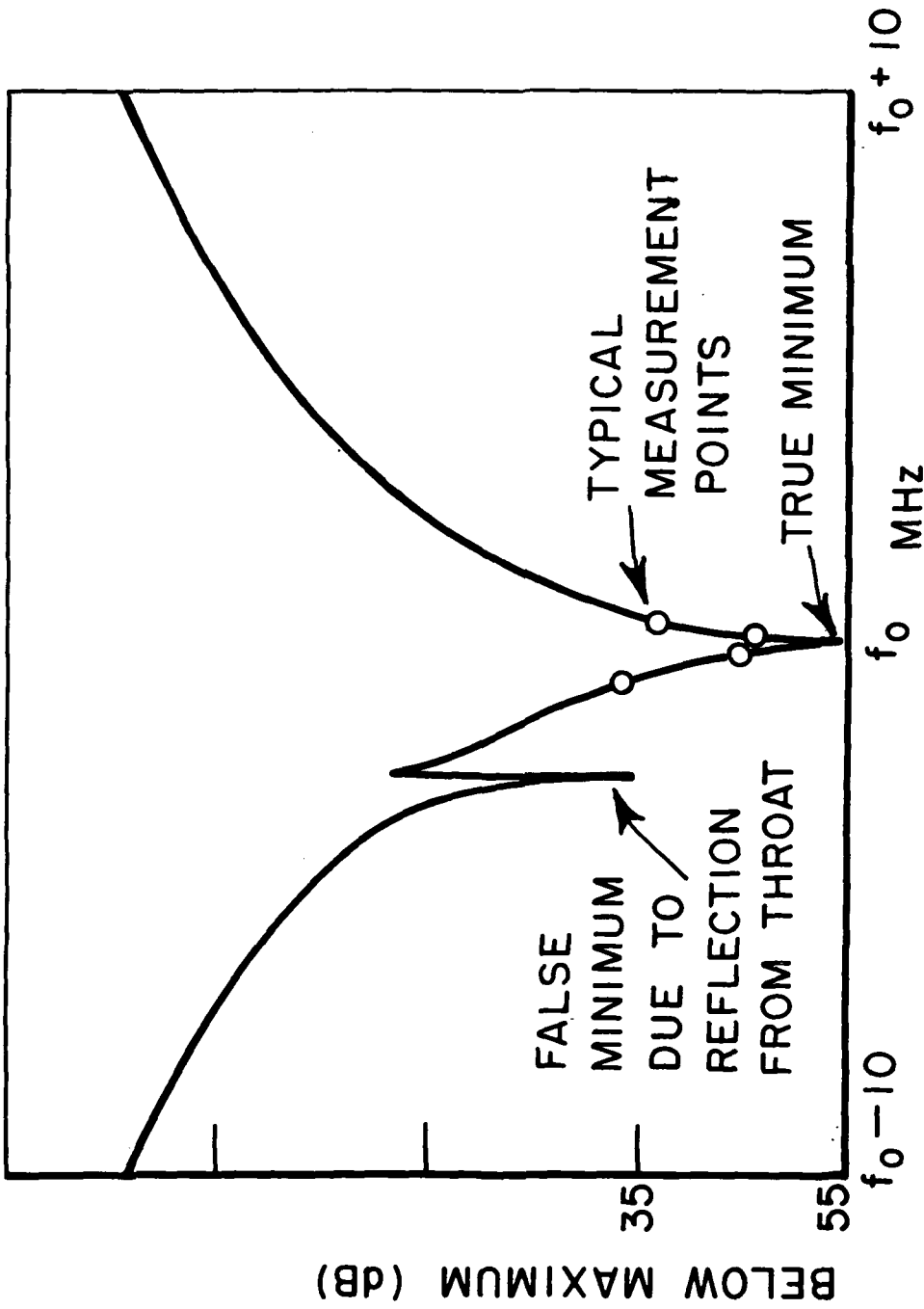


Fig. 47. Null curve from which efficiency is calculated.

only on the psuedo standing wave produced when the frequency is changed. It was not difficult to distinguish the one null from the other. However, when they occurred close together there was some concern that there might be distortion in the shape of the true null. It was found that this problem could be avoided if the waveguide spacers and fine frequency control were used only to place one of the probe positions exactly in the null (care had still to be taken to avoid the spurious nulls). The four probe positions were then read in the usual way except that a precision attenuator was used to measure the level for the null position by the substitution method, thus avoiding excessive dependence on the crystal law. The advantage of the redundant fourth probe is lost with this method. However, repeatability of results and the fact that the same detector is used in each of the four probe positions gave a high level of confidence to the results.

The measured data for the two conical horns is shown in Fig. 48. The loss shown in the figure is half the measured loss, in other words it is the one way loss which would exist with the antenna radiating. The loss of the shorted waveguide is also shown. If the loss in this shorting plate is assumed to be equal to that in the antenna shorting cap; the waveguide is common to both measurements; then the antenna loss is simply the total loss observed minus that for the shorted guide. The shorted guide showed a loss of 0.0065 dB. The conical corrugated horn was measured with both the spherical cap and a flat shorting plate to determine how much the plate contour affected the loss measurement. The loss curve shifted up by 0.0025 dB for the flat plate if one ignores the two high points around 3.75 GHz in Fig. 48, which are assumed to be due to excitation of some higher order mode by the flat plate. Taking the extreme variations for the conical corrugated horn (including both shorting plates except for the two points near 3.75 GHz) and subtracting the loss for the shorted guide gives a resultant loss for the horn of $0.016 \text{ dB} \pm 0.0058$, well within the required accuracy of 0.01 dB.

Since the shape of the shorting plate had been found to make only a minor difference in the loss measurement for the conical corrugated horn and because of the complex phase front of the conical dual mode horn it was felt that the use of the flat plate was justified in this case. The results for the conical dual mode horn are also shown in Fig. 48. Performing the same calculation as before gives a loss of $0.0125 \text{ dB} \pm 0.0033$.

Similar data for the pyramidal dual mode horn are shown in Fig. 49. A flat shorting plate was again used and it is evident that more of a moding problem existed for the square geometry both for the horn and waveguide alone. If one assumes that the high loss points are the result of modes which would not exist in the radiating condition then the results are very similar to those for the conical horns. If the worst possible interpretation is put on the data then the horn loss is still no worse than $0.02 \text{ dB} \pm 0.01$.

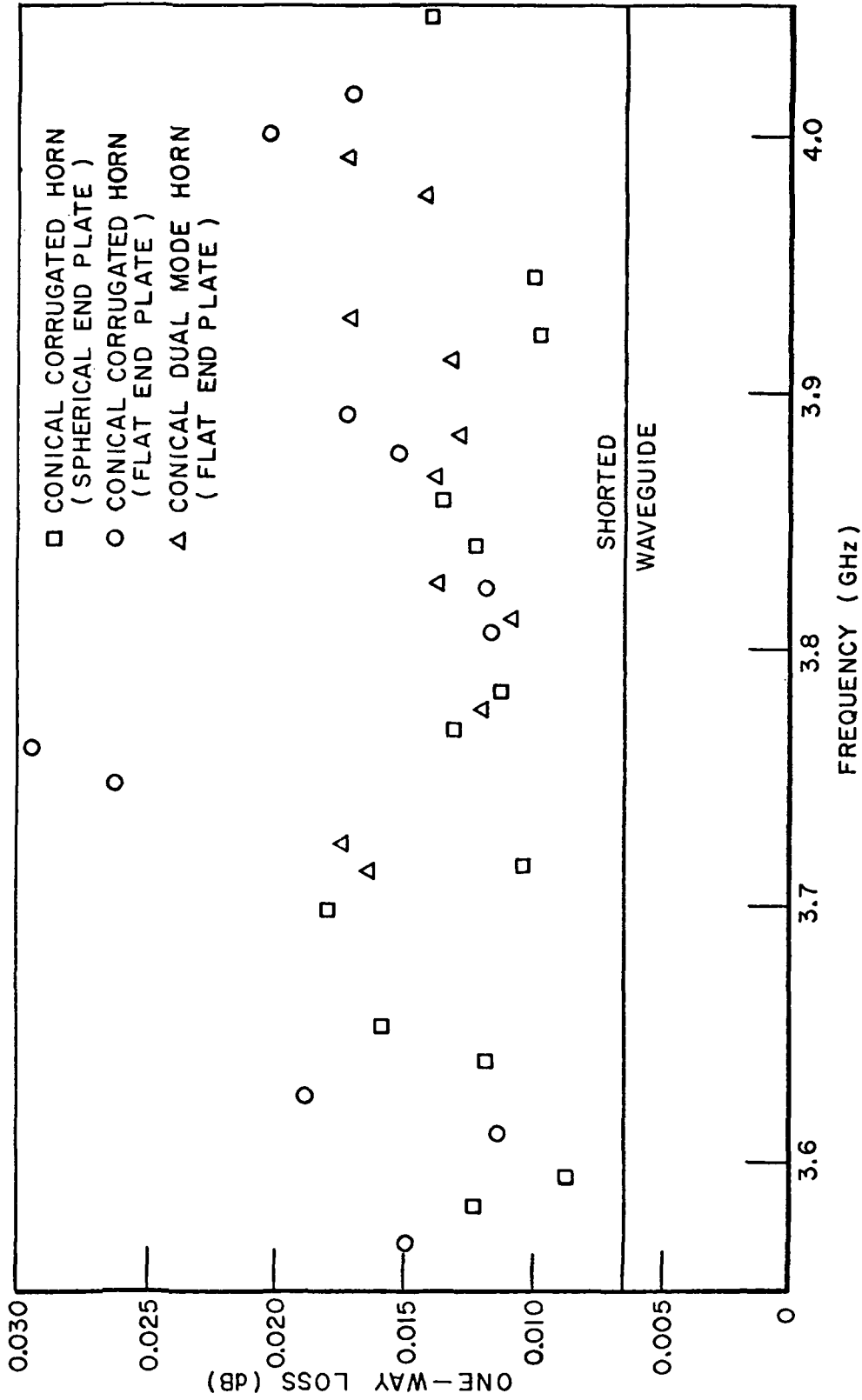


Fig. 48. Resistive loss for the two conical horns.

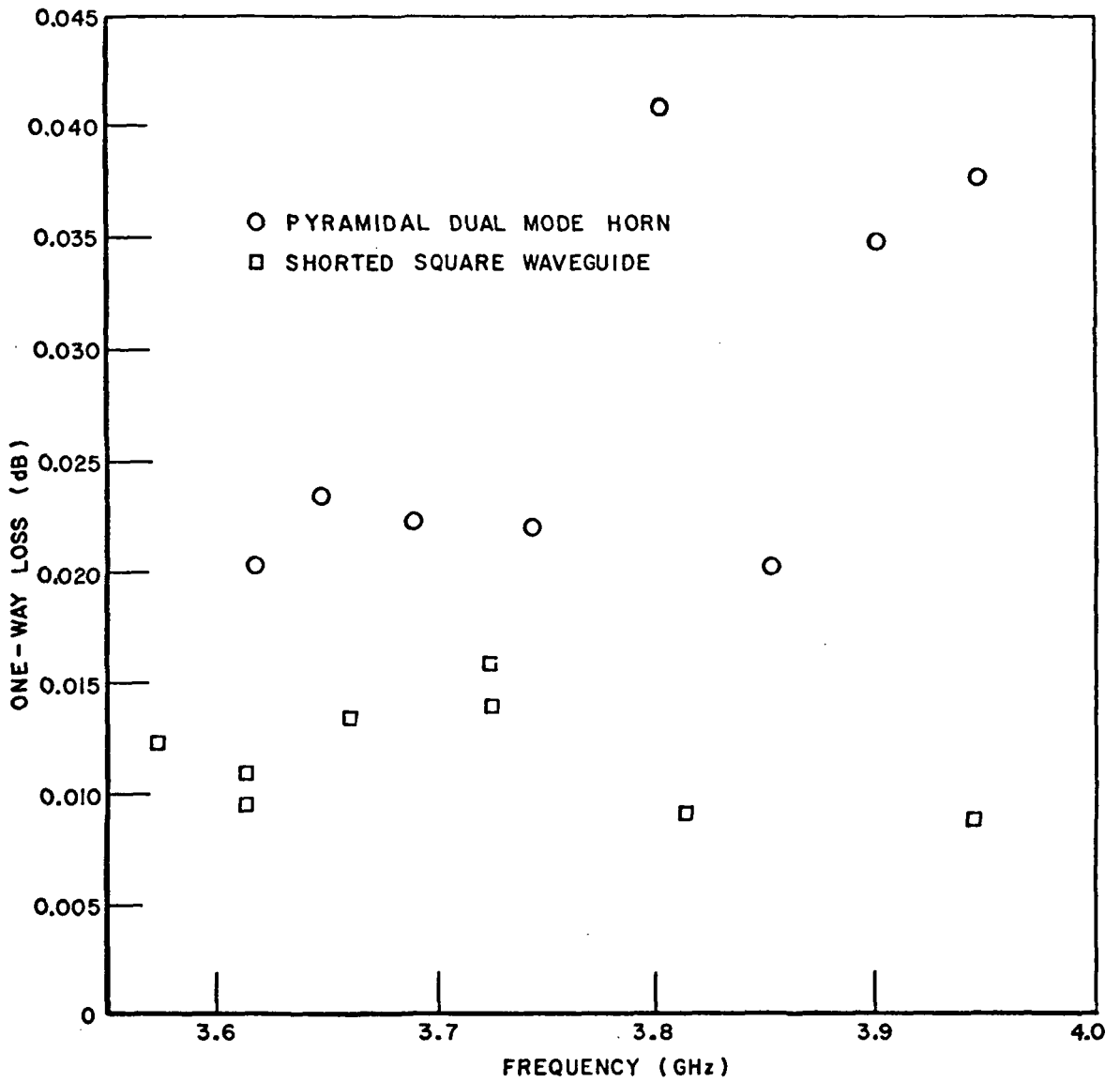


Fig. 49. Resistive loss for the square dual mode horn.

D. Beam Efficiency Measurements

The major problem in determining beam efficiency is the same as that in calculating directivity from radiation pattern measurements. It is first necessary to record sufficient radiation patterns to give an adequate three dimensional representation over the complete sphere. The recorded patterns must then be integrated as a function of angle from the beam axis to provide the data necessary for an efficiency calculation. In the present program, with several types of antenna being evaluated, the number of radiation patterns to be recorded is formidable in itself. Integration of the patterns becomes impracticable unless both reading of the patterns and the integration can be performed with a digital computer. Accordingly it was decided that the pattern data should be recorded directly into an instrumentation computer in real time without any intermediate pattern recordings. Once in the computer a conventional pattern plot, on any desired scale, could readily be obtained by outputting the stored data to an X-Y plotter. The data were also immediately available for any desired computation. The pattern recording and data processing system is illustrated in Fig. 50.

All pattern recording and data processing is performed by a single computer program on command from the teletype. Eighteen commands are currently recognized by the program. In operation two calibration points are first given to the computer using the precision attenuator in the transmitting arm (Fig. 50) and with the receiving antenna stationary. In the record mode the computer senses the pedestal rotation through a microswitch which opens and closes for every degree of rotation. At each switch closure the computer records the receiver output. The process continues until 360 points have been recorded. The receiver has a dynamic range of only 40 dB. Since patterns with a dynamic range of 50 dB or greater are required for the present purpose the parallel polarized pattern is recorded in two stages. The pattern is first recorded with 20 or 30 dB of attenuation in the transmitter. This provides the main beam information. The attenuation is then removed (the amount being indicated to the computer via the teletype) and a second pattern is recorded. The receiver will now saturate in the main beam. The computer automatically merges the two patterns into a single extended range pattern. At this point the pattern may be smoothed, normalized or centered (if recording was not started at the center of the main beam) on command from the teletype and written on the disc file. If the cross polarized pattern is required, it is recorded next. This may be done with any appropriate attenuator setting at the transmitter. The pattern will be kept in its correct relationship to the parallel polarized pattern by the computer. Both the transmitting and test antennas are now rotated about their axes and a second set of patterns recorded. In the present work patterns were recorded every $22\frac{1}{2}$ degrees.

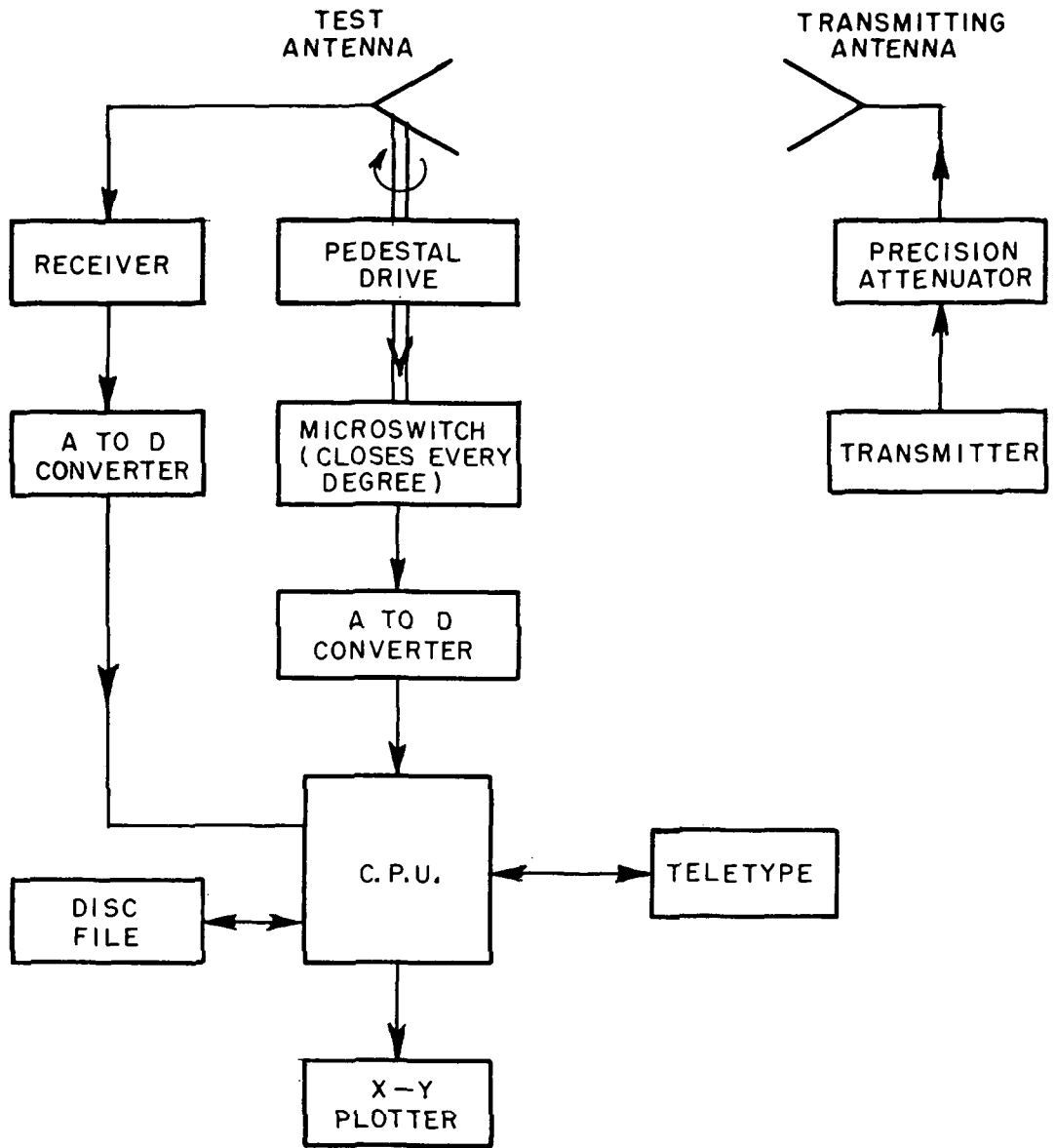


Fig. 50. Computer controlled radiation pattern recording and processing system.

Patterns may be drawn on the X-Y plotter at any time using any desired scale limits. They may be superimposed on the same plot in any combination. When a complete set of patterns is stored on the disc file they may be analyzed to obtain the beam efficiency. The patterns are first averaged, parallel and cross polarization being treated separately. If the cross polarized energy is to be treated as desirable it is added to the parallel polarized pattern at this point and the resulting pattern renormalized. The analysis section of the program is then invoked and the parallel and cross polarized (if being treated as undesirable) file names entered. The patterns are now integrated and an efficiency curve calculated expressed as percent of power within a given angle from the beam axis. This curve may be plotted or stored on the disc. Half power beamwidth, directivity and efficiency at twice the half power beamwidth are printed on the teletype.

This last parameter has been used in this program as a figure of merit for the antenna since the patterns in general do not have sharp nulls and hence a well defined beam edge. Examination of the efficiency curves suggests that it may not, however, be the most appropriate figure. The curves for the horn antennas exhibit a definite knee around 97%. This knee could be identified mathematically as the point where the curvature is sharpest (i.e., the second derivative highest). It may well be that this is the point that should be defined as the beam edge for radiometer antennas, the efficiency at this point would then be a more realistic figure of merit.

V. NEAR FIELD STUDIES

During this program the possibility was raised of using the horn antennas, which had been developed, for radiometric studies of water in a ripple tank. As it was thought possible that the antennas might be used under near field conditions some measurements were made to evaluate the near field properties.

In the case of the two conical horns it was found that their radiation patterns remained essentially the same as in the far field for ranges down to about 30 inches or 3 aperture widths. (The usual $2D^2/\lambda$ criterion for this antenna gives a far field range of 66 inches.) To demonstrate the near field effect patterns were accordingly measured at one third and two thirds of this distance or 10 and 20 inches. These patterns together with the beam efficiency curves are shown in Figs. 51-62. The cross polarized radiation has been treated as undesirable in the efficiency calculations.

For comparison purposes similar measurements were made on a 2 foot diameter paraboloid operating at 10 GHz. This is not the same paraboloid as that shown earlier in this report. Since the measurements were made indoors it was not possible to satisfy the usual far field criteria.

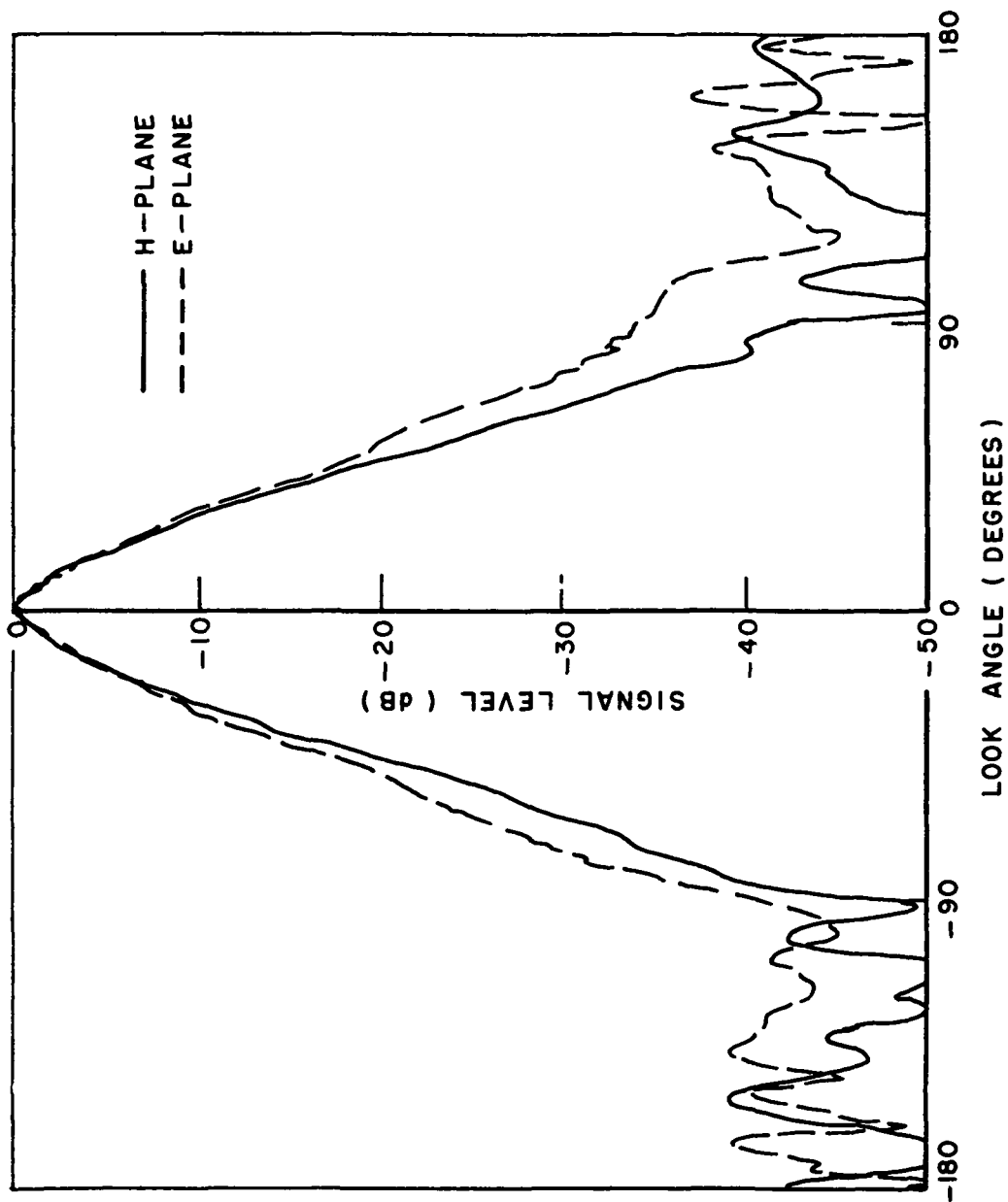


Fig. 51. Radiation patterns of the conical corrugated horn (20 inch range, 3.7 GHz).

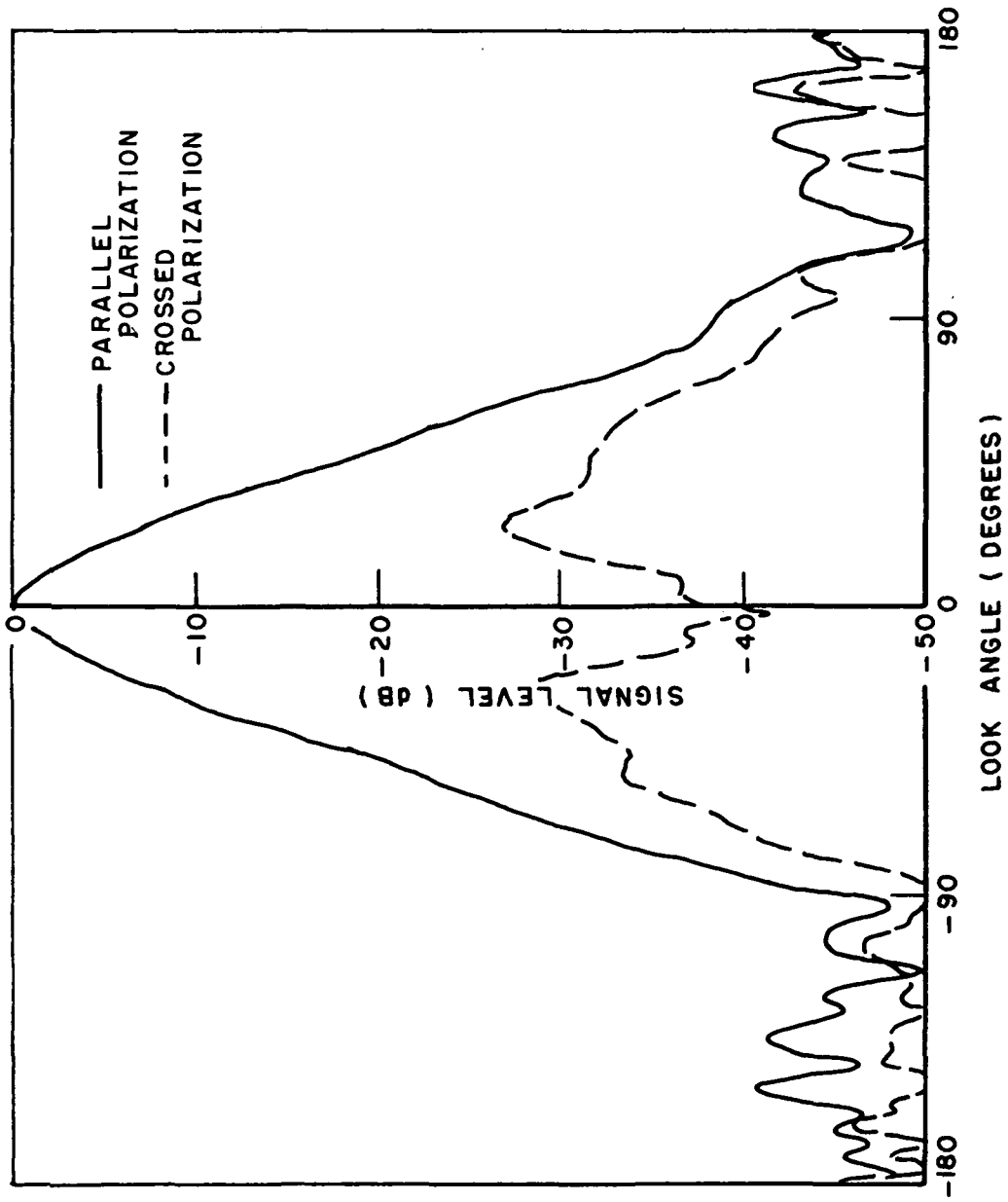


Fig. 52. Average patterns of the conical corrugated horn (20 inch range, 3.7 GHz).

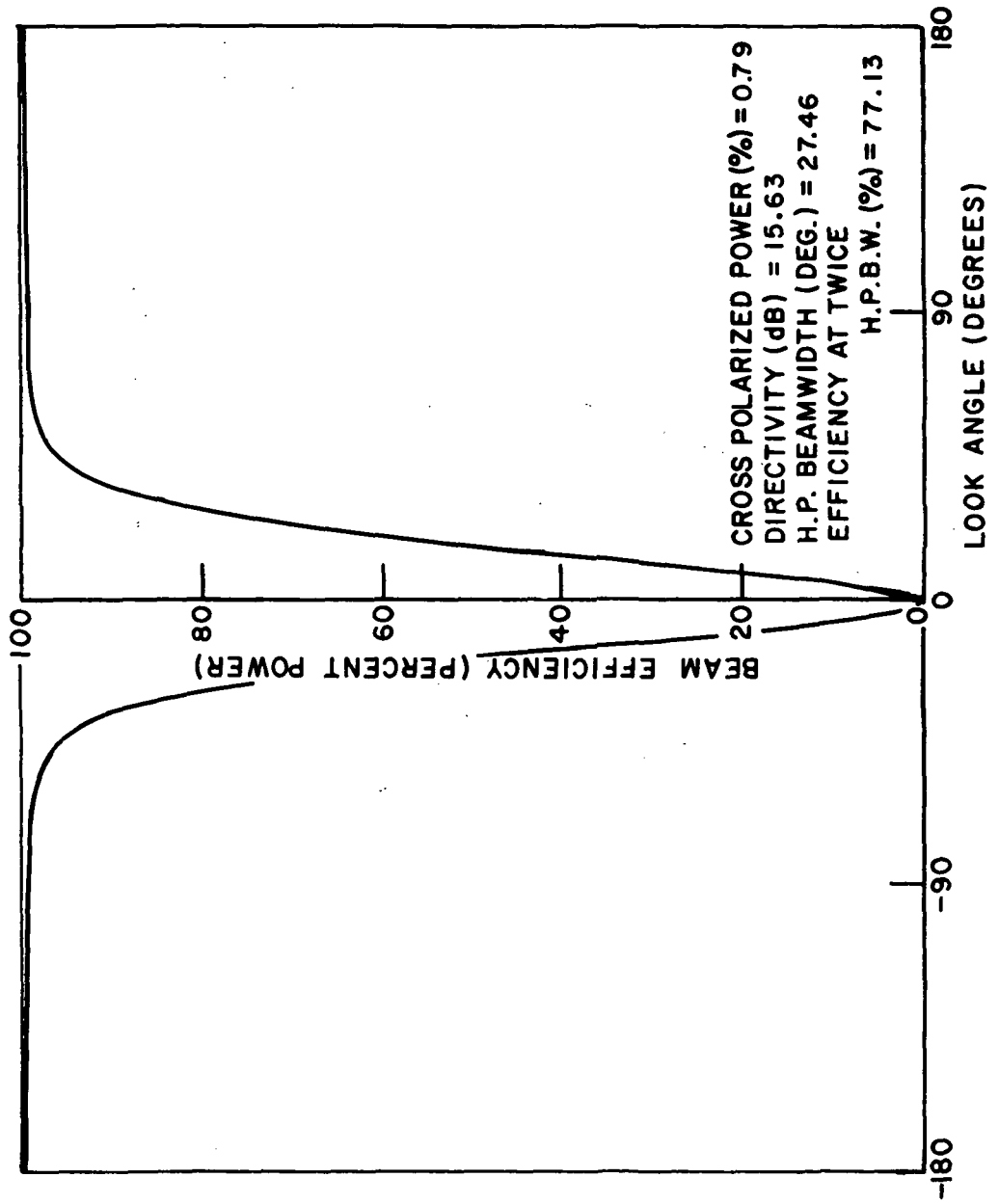


Fig. 53. Beam efficiency of the conical corrugated horn (20 inch range, 3.7 GHz).

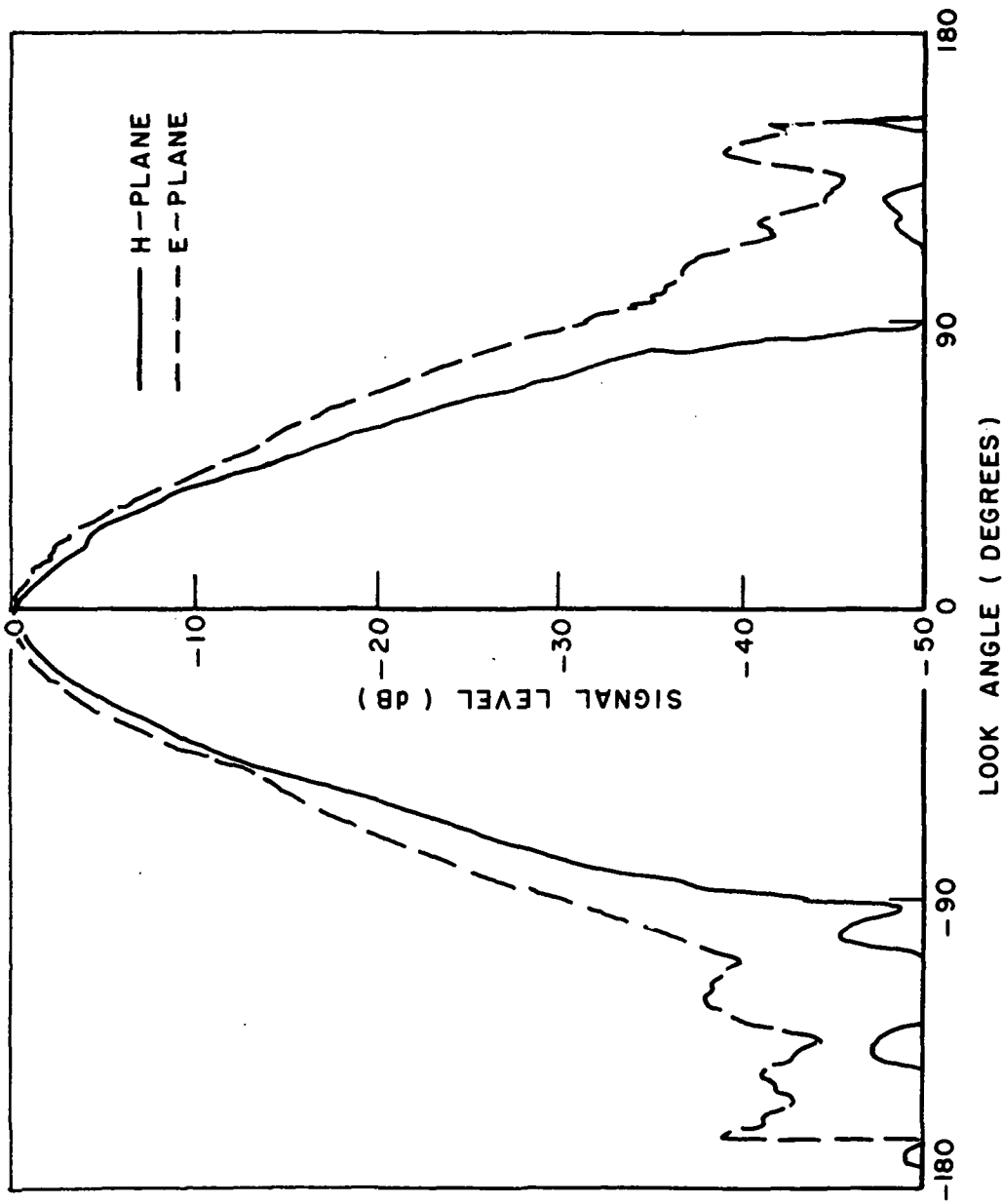


Fig. 54. Radiation patterns of the conical corrugated horn (10 inch range, 3.7 GHz).

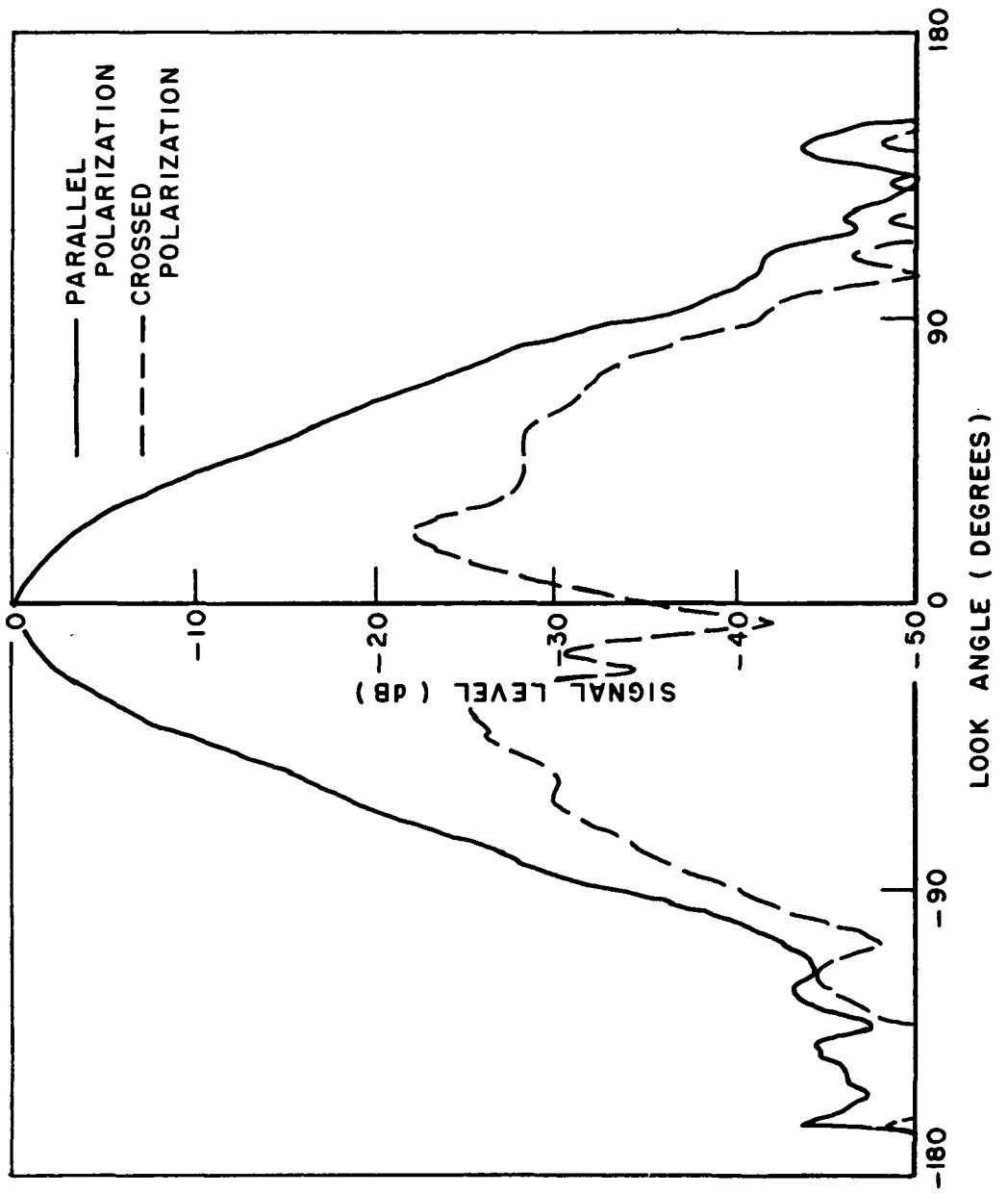


Fig. 55. Average patterns of the conical corrugated horn (10 inch range, 3.7 GHz).

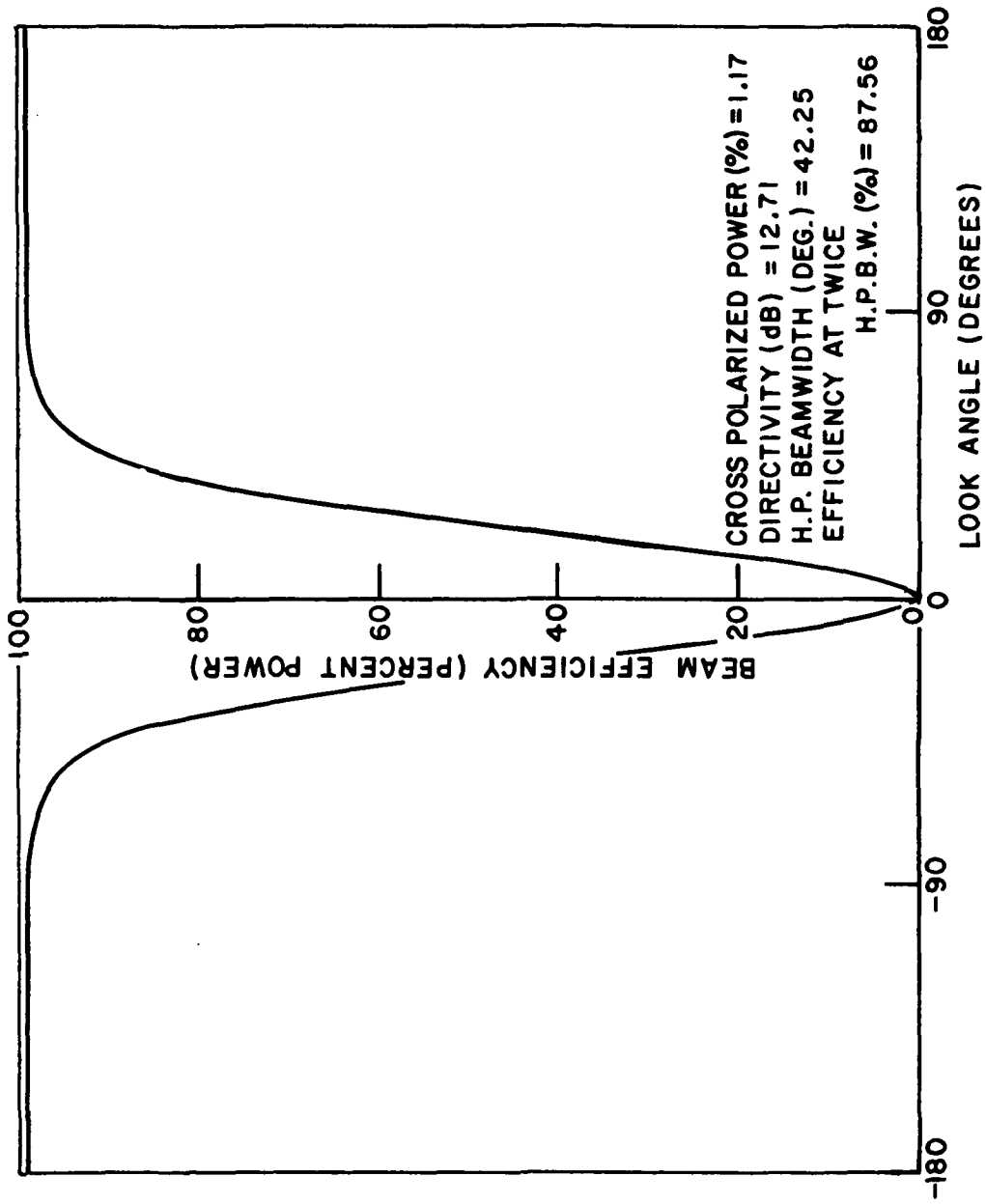


Fig. 56. Beam efficiency of the conical corrugated horn (10 inch range, 3.7 GHz).

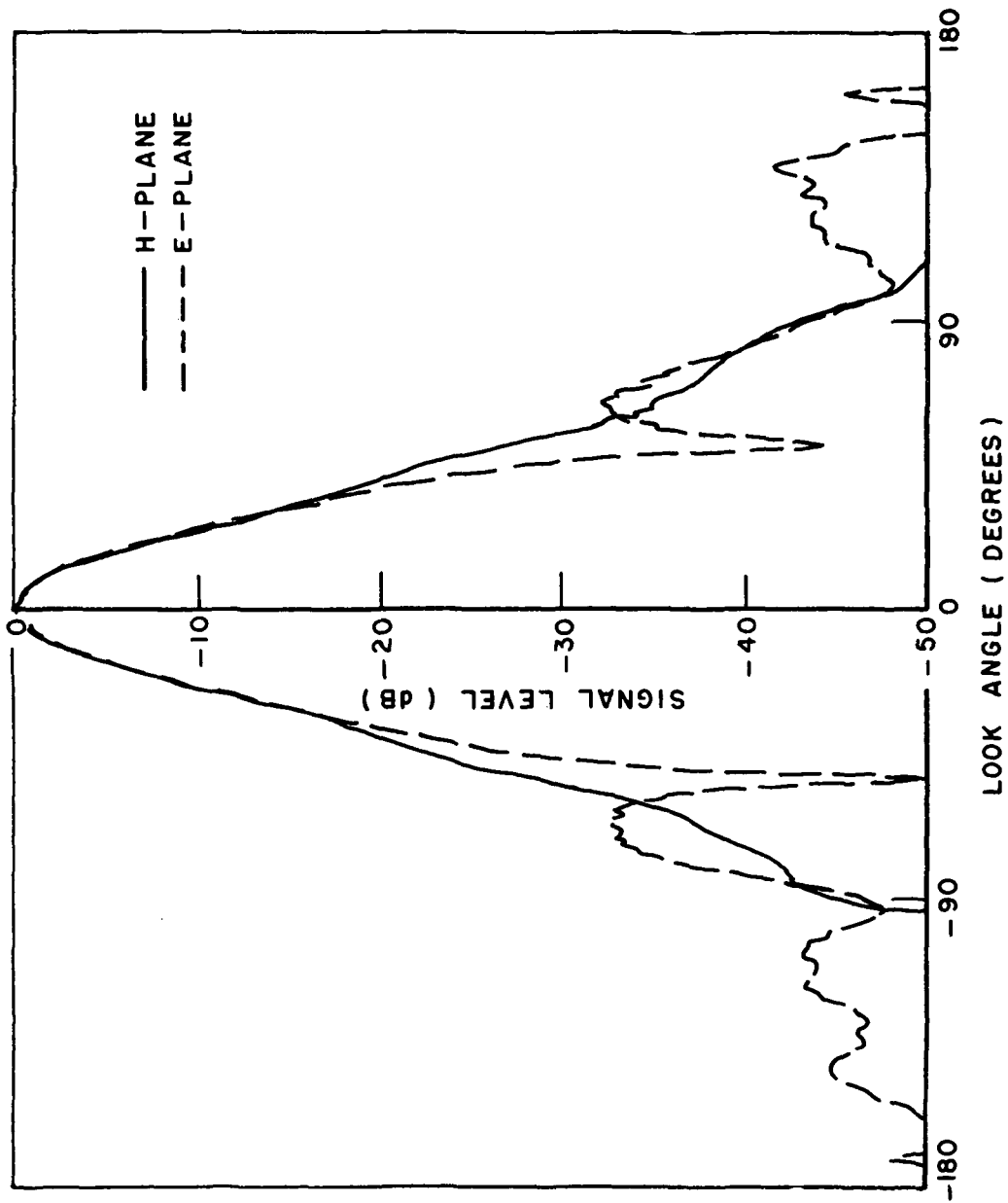


Fig. 57. Radiation patterns of the conical dual mode horn (20 inch range, 3.8 GHz).

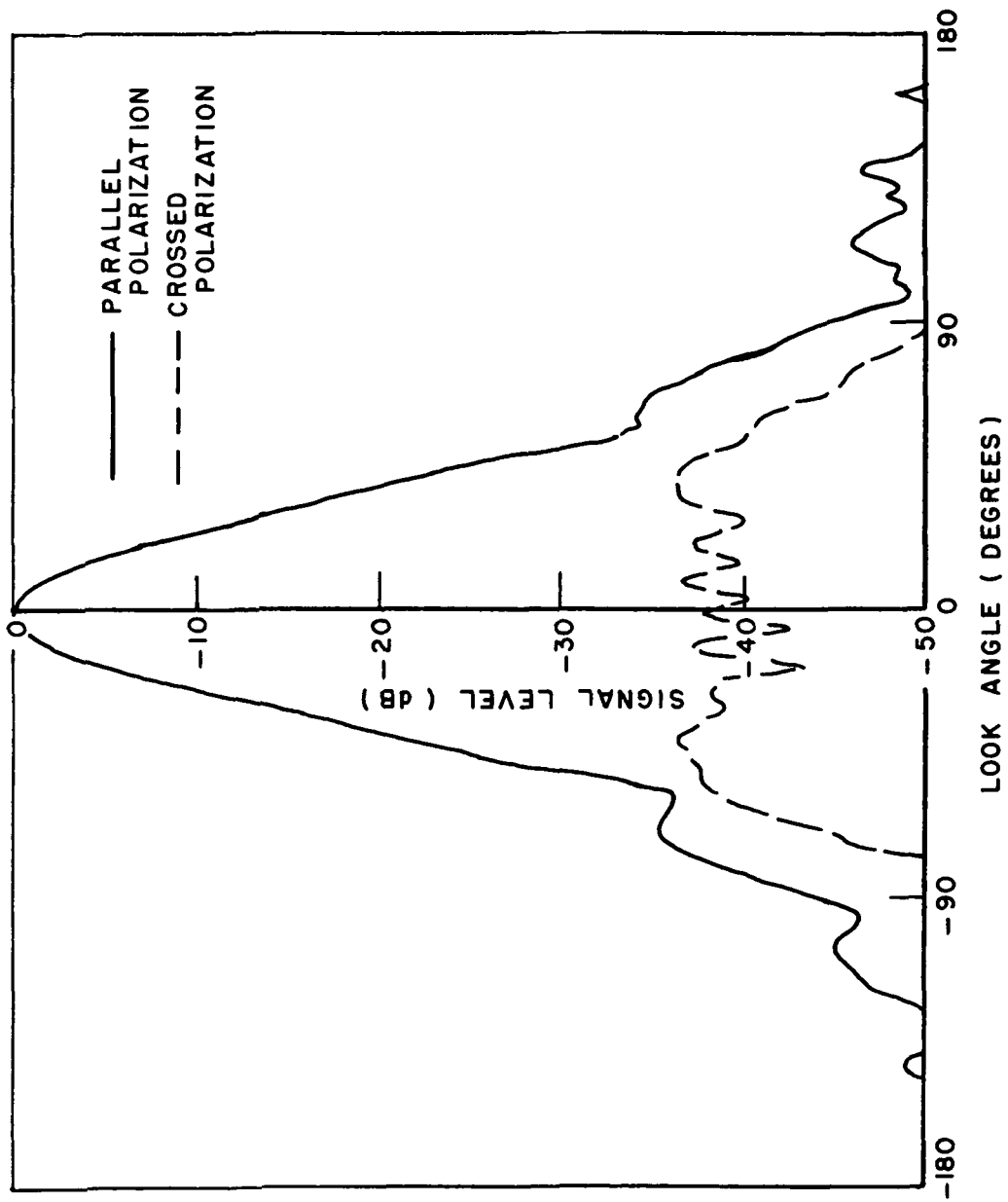


Fig. 58. Average patterns of the conical dual mode horn (20 inch range, 3.8 GHz).

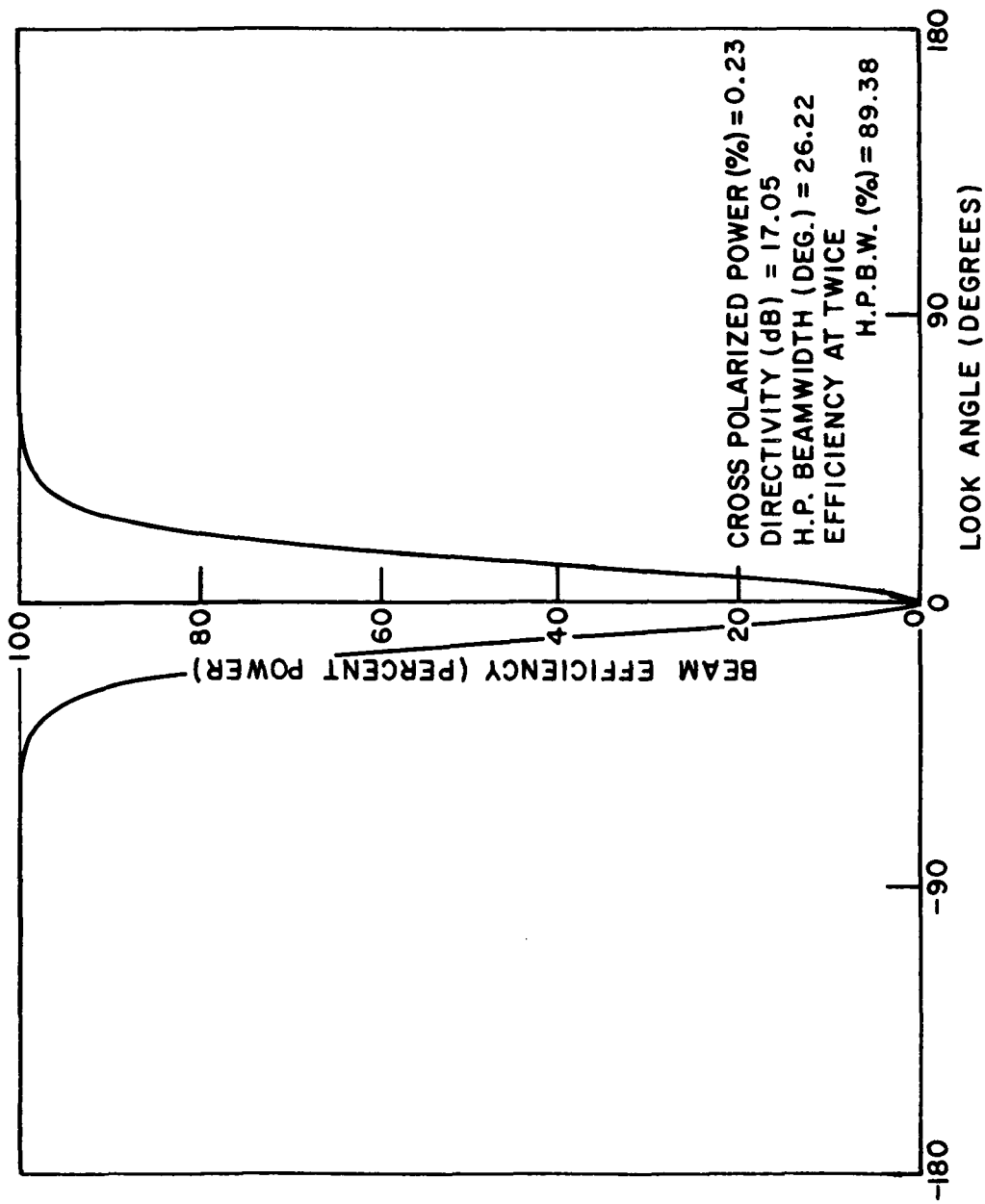


Fig. 59. Beam efficiency of the conical dual mode horn (20 inch range, 3.8 GHz).

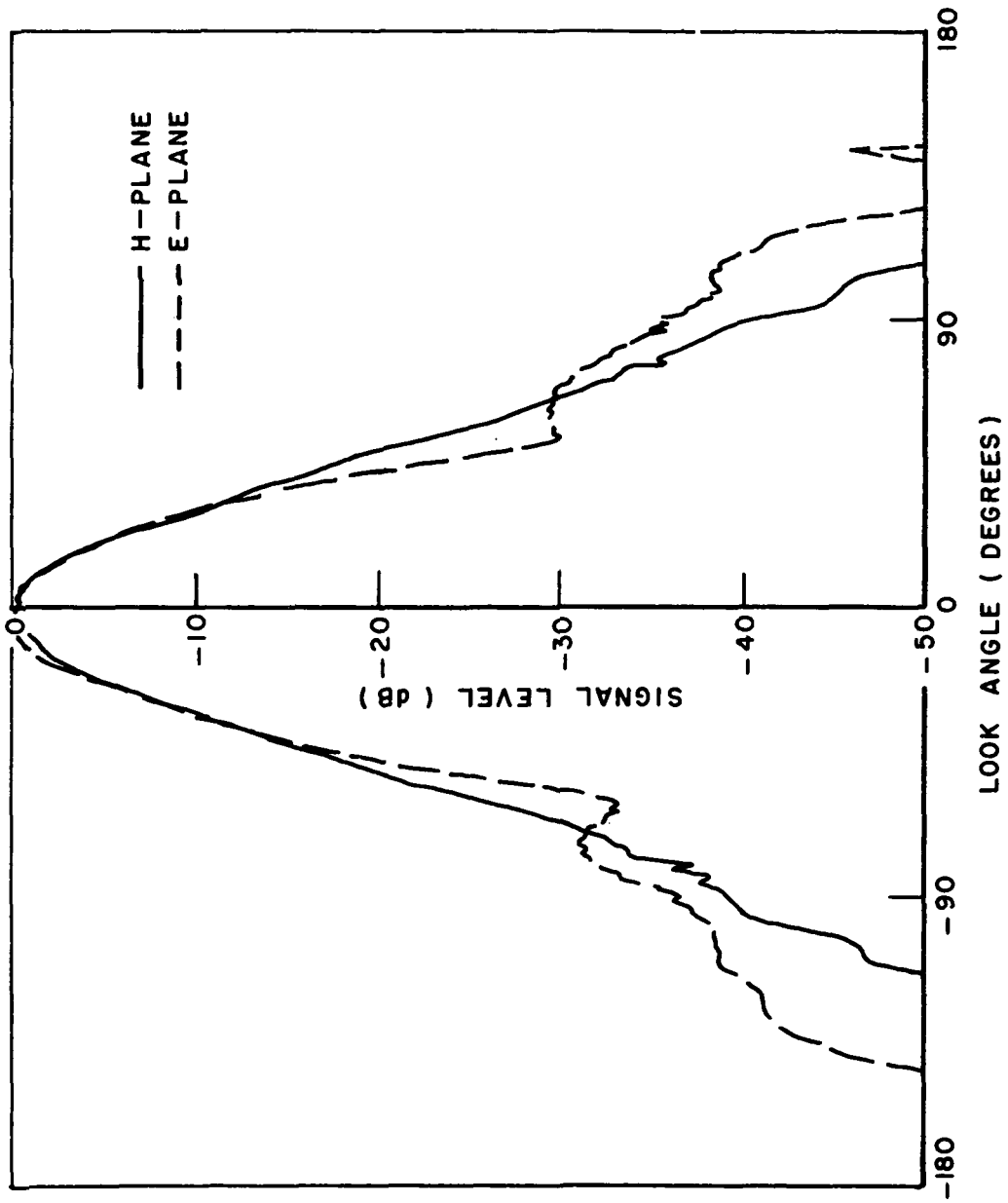


Fig. 60. Radiation patterns of the conical dual mode horn (10 inch range, 3.8 GHz).

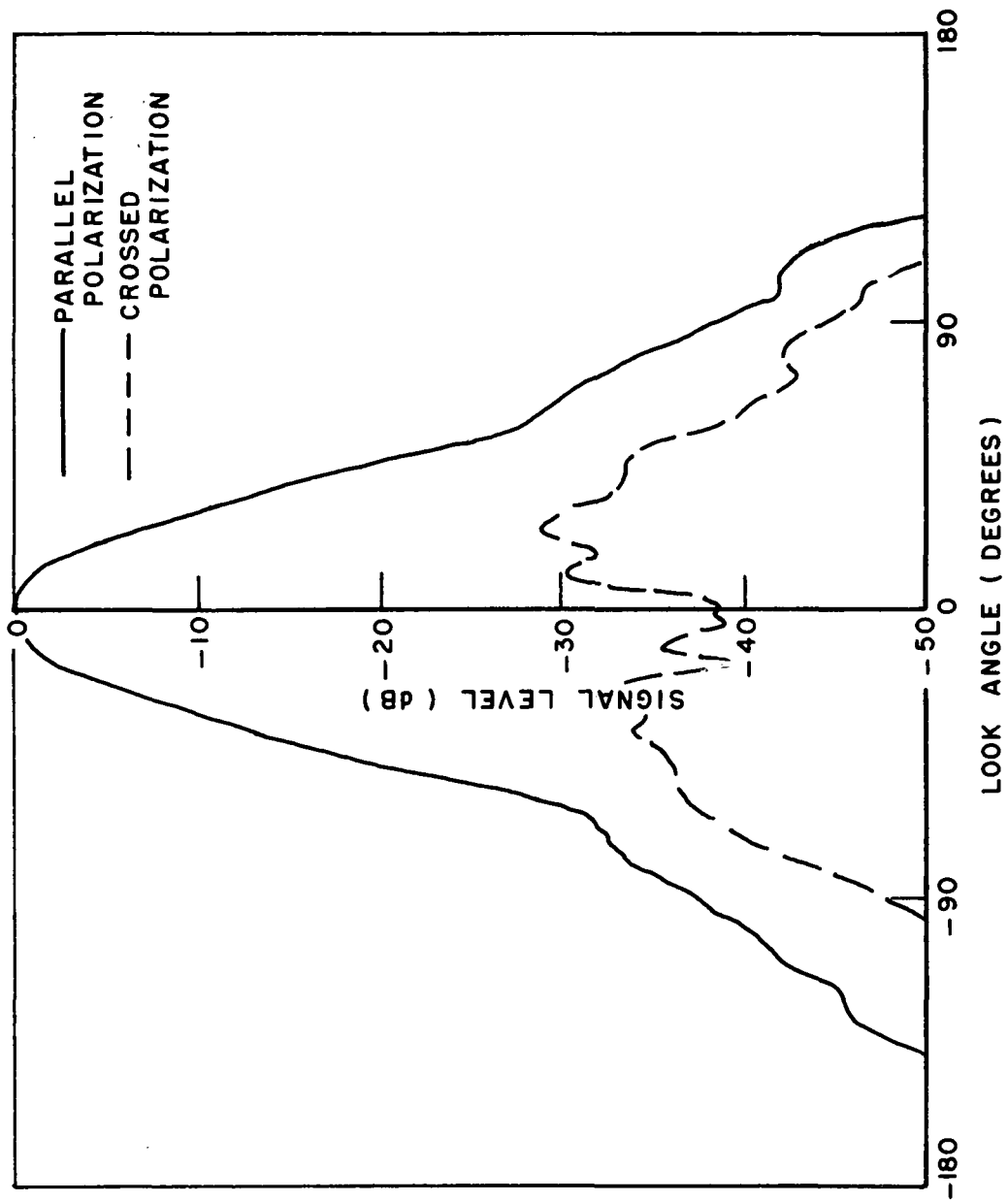


Fig. 61. Average patterns of the conical dual mode horn (10 inch range, 3.8 GHz).

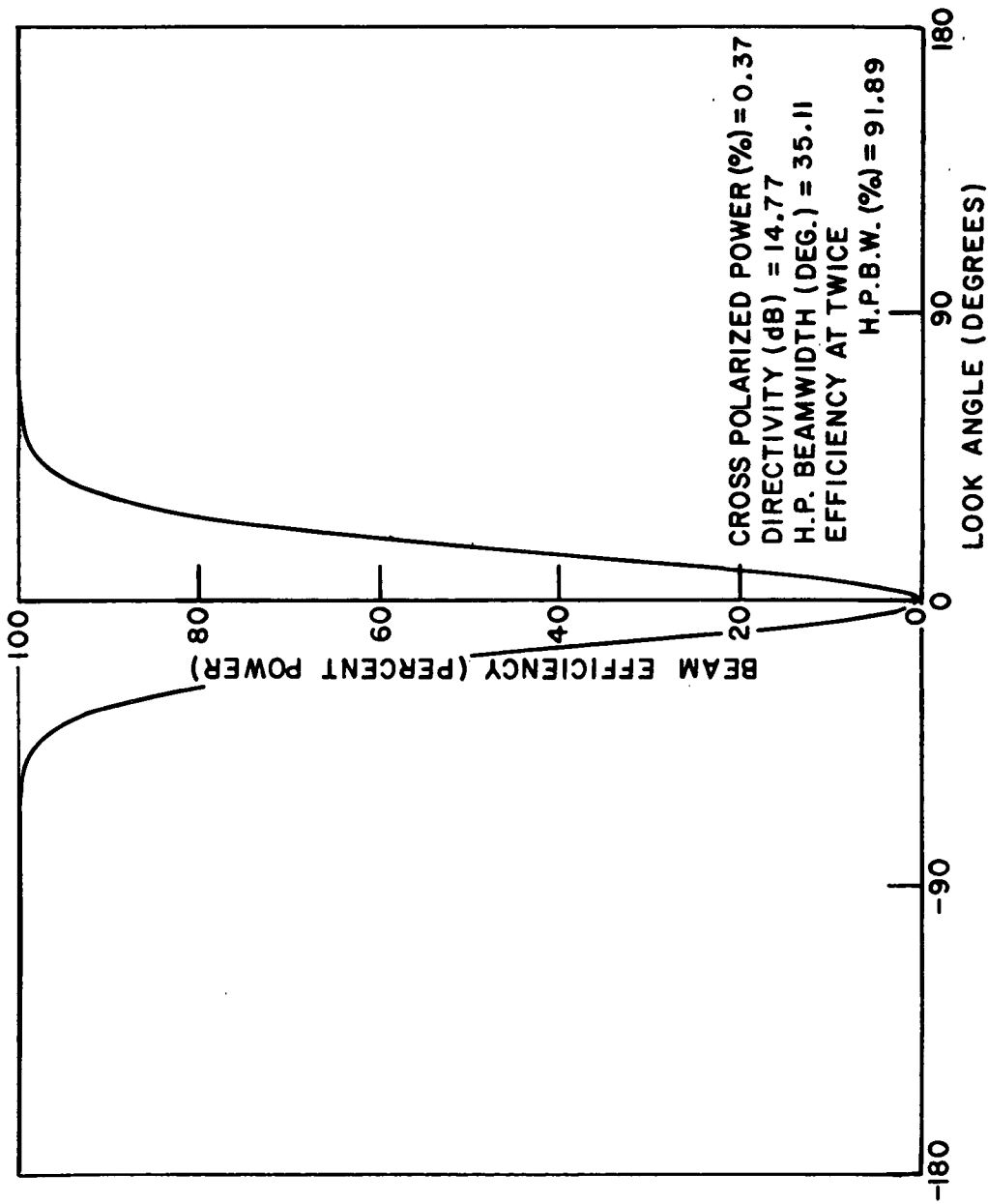


Fig. 62. Beam efficiency of the conical dual mode horn (10 inch range, 3.8 GHz).

The maximum range available was 28 feet. The patterns and beam efficiency curve at this range are shown in Figs. 63-65. The beam efficiency should be regarded with some reservations since the beam width of this antenna was 4 degrees and the computer only samples the pattern at a rate of 1 point per degree. Patterns at ranges of 7.5 feet and 2.7 feet are shown for this antenna in Figs. 66-71. Here the beam has broadened sufficiently that the efficiency calculation should be accurate.

In addition to the near field amplitude measurements of the corrugated and dual mode conical horns (Figs. 51-62) some phase patterns were also recorded. An open-ended rectangular waveguide was used as the transmitting antenna. For some of the patterns the test antenna was rotated about an axis through apex of the horn and for others about an axis in the aperture plane (Fig. 72). The resulting phase patterns are shown in Figs. 73-77.

VI. RADOME LOSS MEASUREMENTS

Another question arose during this program, namely the effect of a radome on the antenna system losses. If the antenna is to be used for radiometric studies aboard an aircraft it is necessary that it be covered with a radome to protect it from weather and to preserve the aerodynamic contour of the aircraft. The major concern here was not any loss which might originate in the radome itself since this could be measured and calibrated out if it proved to be significant. More uncertain was the loss due to rain, oil or dirt deposits on the radome.

To investigate this problem an experiment was set up as shown in Fig. 78. It consists of a conventional waveguide slotted line terminated in a short circuit. One quarter of a guide wavelength from the short circuit, which was easily removable, was a thin mylar diaphragm clamped between two waveguide flanges. The system was operated vertically with the short uppermost. On top of the mylar was placed a rectangle of filter paper cut to fit the waveguide. The filter paper was weighed on a chemical balance having first been heated to drive out any residual moisture. It was then moistened with water, and weighed again, the object of the filter paper being to ensure a uniform distribution of water. As quickly as possible it was placed in the waveguide and a VSWR reading taken. The waveguide was then opened and the filter paper allowed to dry slightly. It was weighed again and another VSWR measurement taken. This process was repeated until the paper was completely dry. The loss in reflected power was calculated from the VSWR readings. Since the water is at a standing wave maximum and couples only to the E-field the observed loss will be four times what it would be if the same forward power were being transmitted into a matched load. Thus a quarter of the observed loss was plotted against the amount of water on the filter paper (Fig. 79). The fact that coupling was only to the E-field was verified by placing half a wavelength of waveguide beyond the diaphragm and repeating the measurement. No increase in loss was observed in this case when water was added. The same measurement was repeated using lubricating oil on the diaphragm.

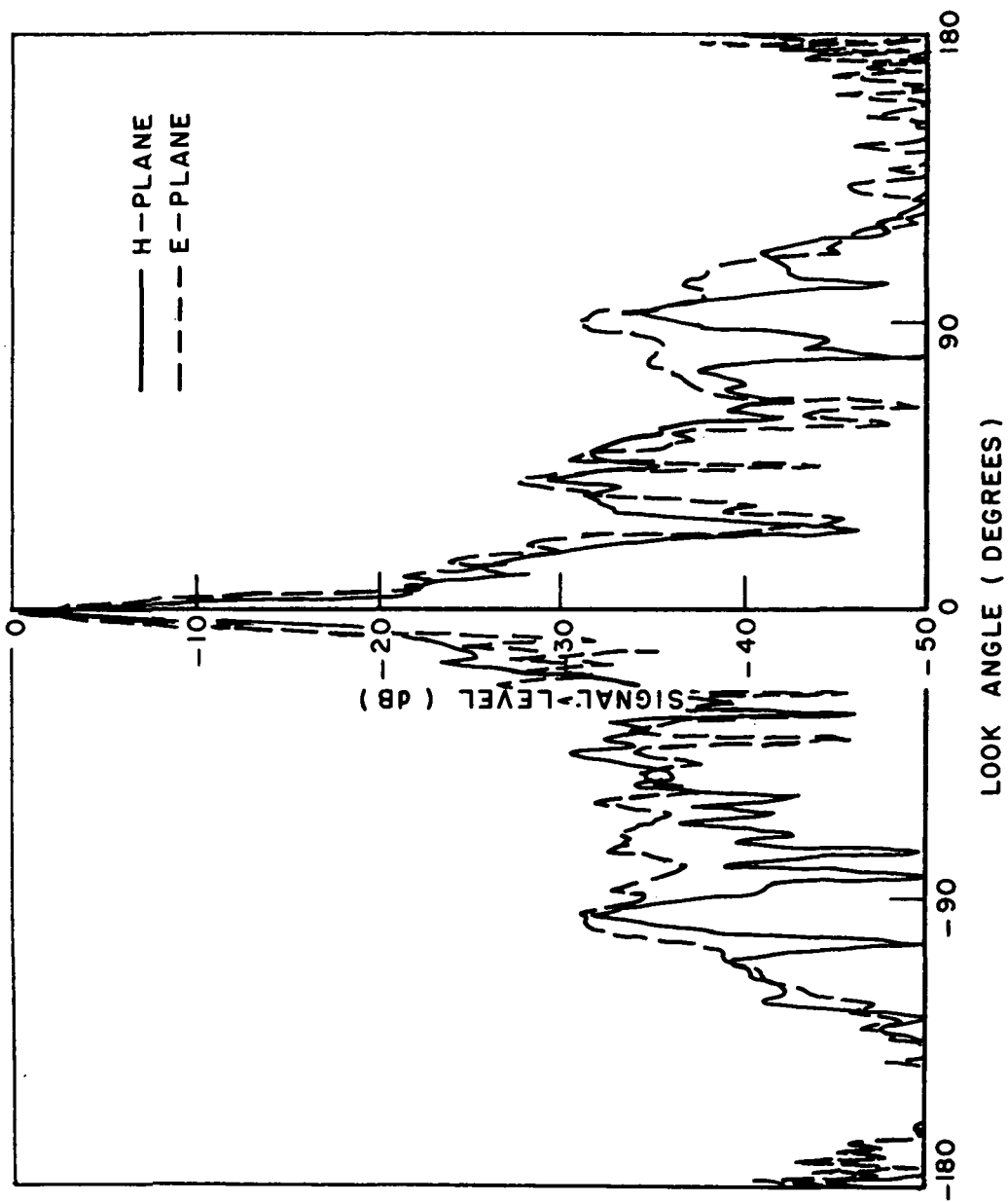


Fig. 63. Radiation patterns of a 2 ft diameter paraboloid (10 GHz, 28 ft range).

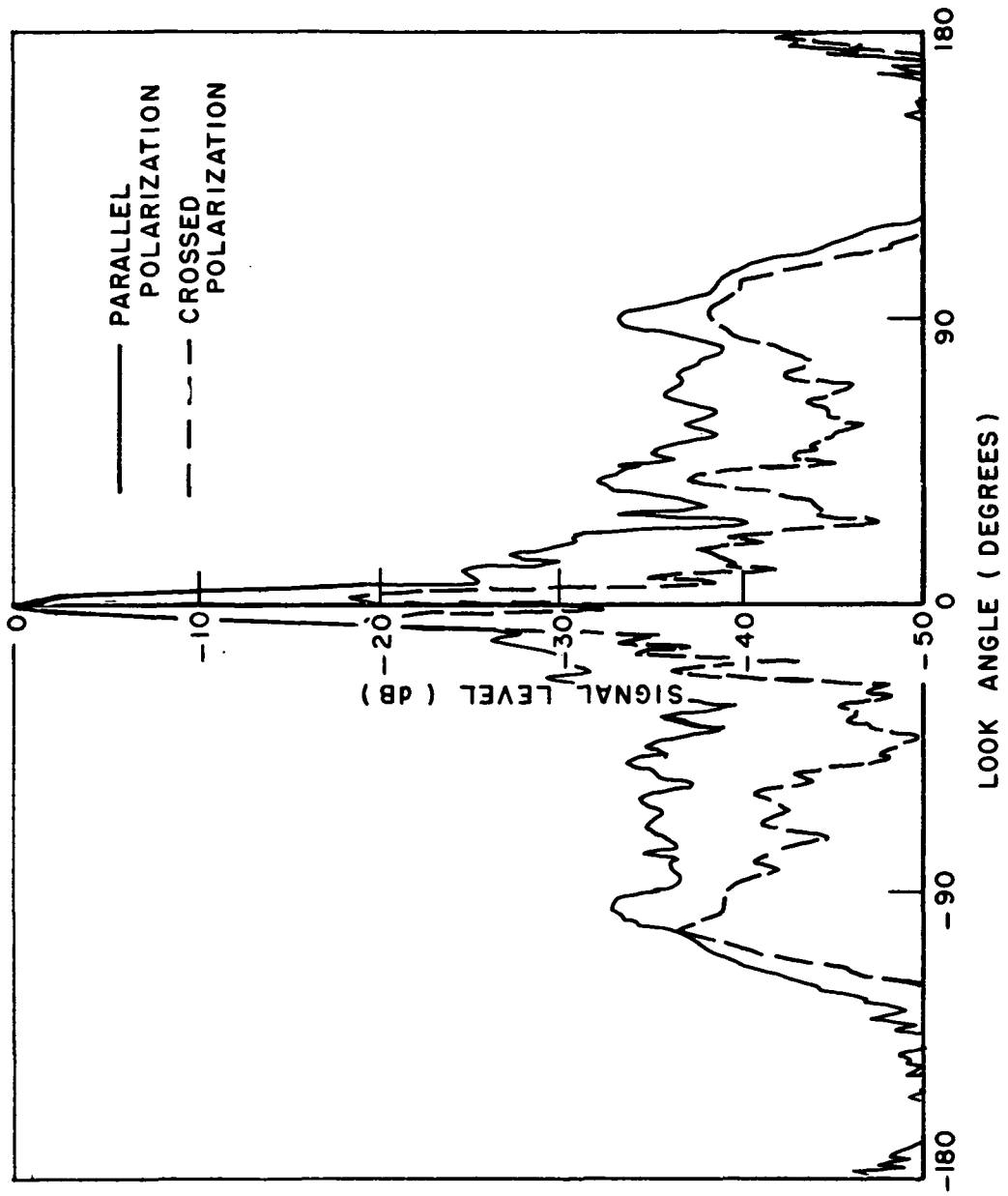


Fig. 64. Average patterns of a 2 ft diameter paraboloid (10 GHz, 28 ft range).

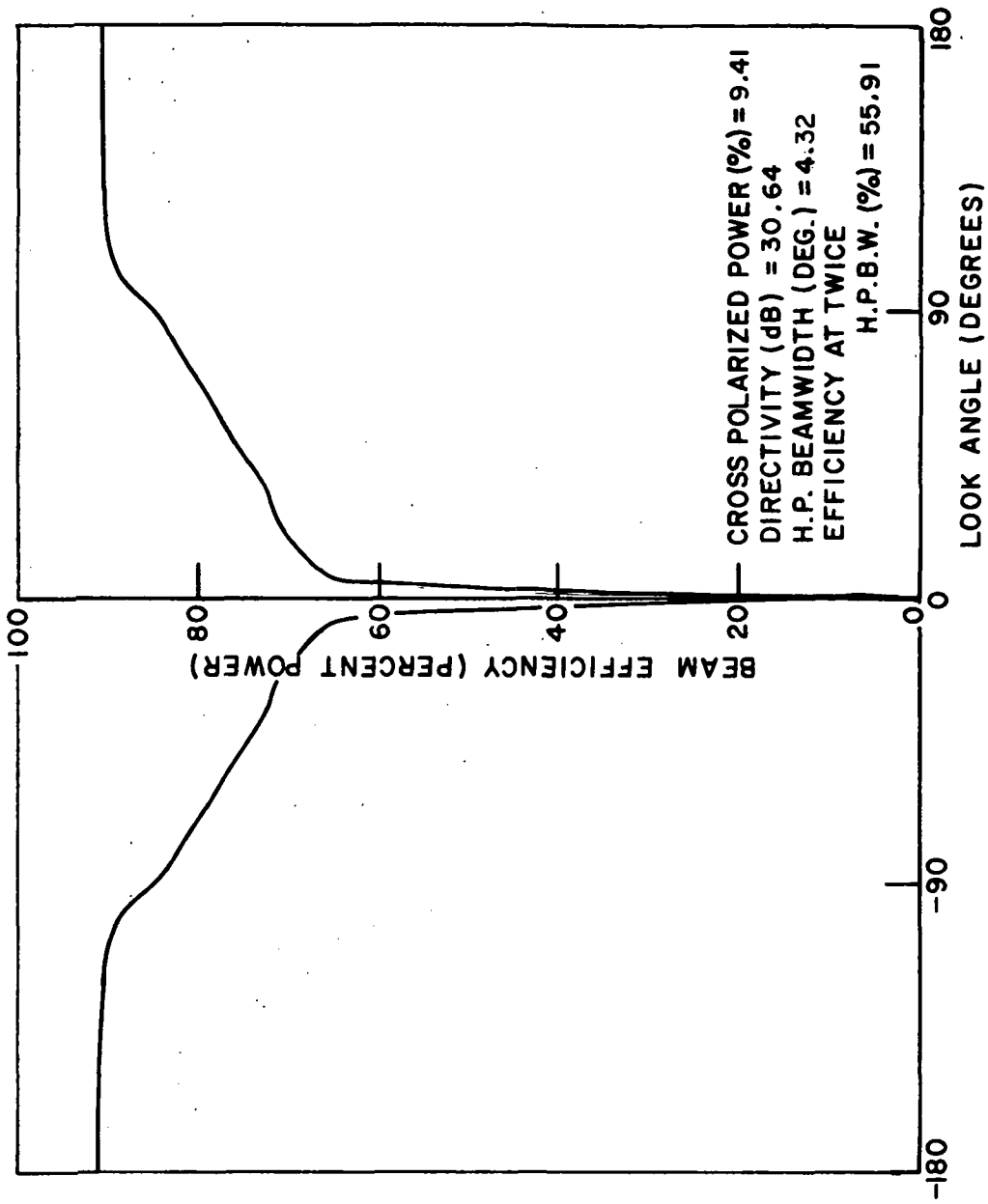


Fig. 65. Beam efficiency of a 2 ft diameter paraboloid (10 GHz, 28 ft range).

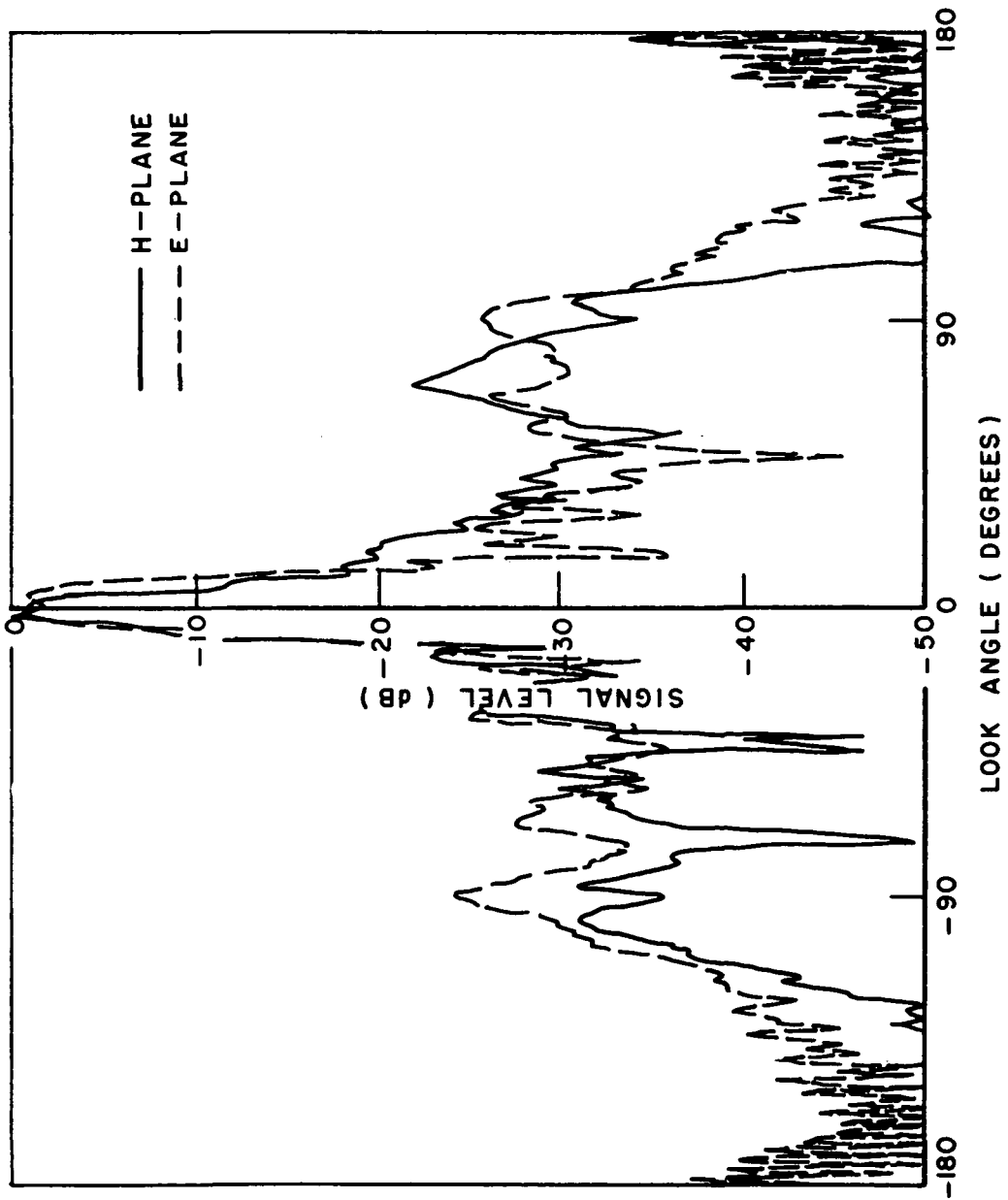


Fig. 66. Radiation patterns of a 2 ft diameter paraboloid (10 GHz, 7.5 ft range).

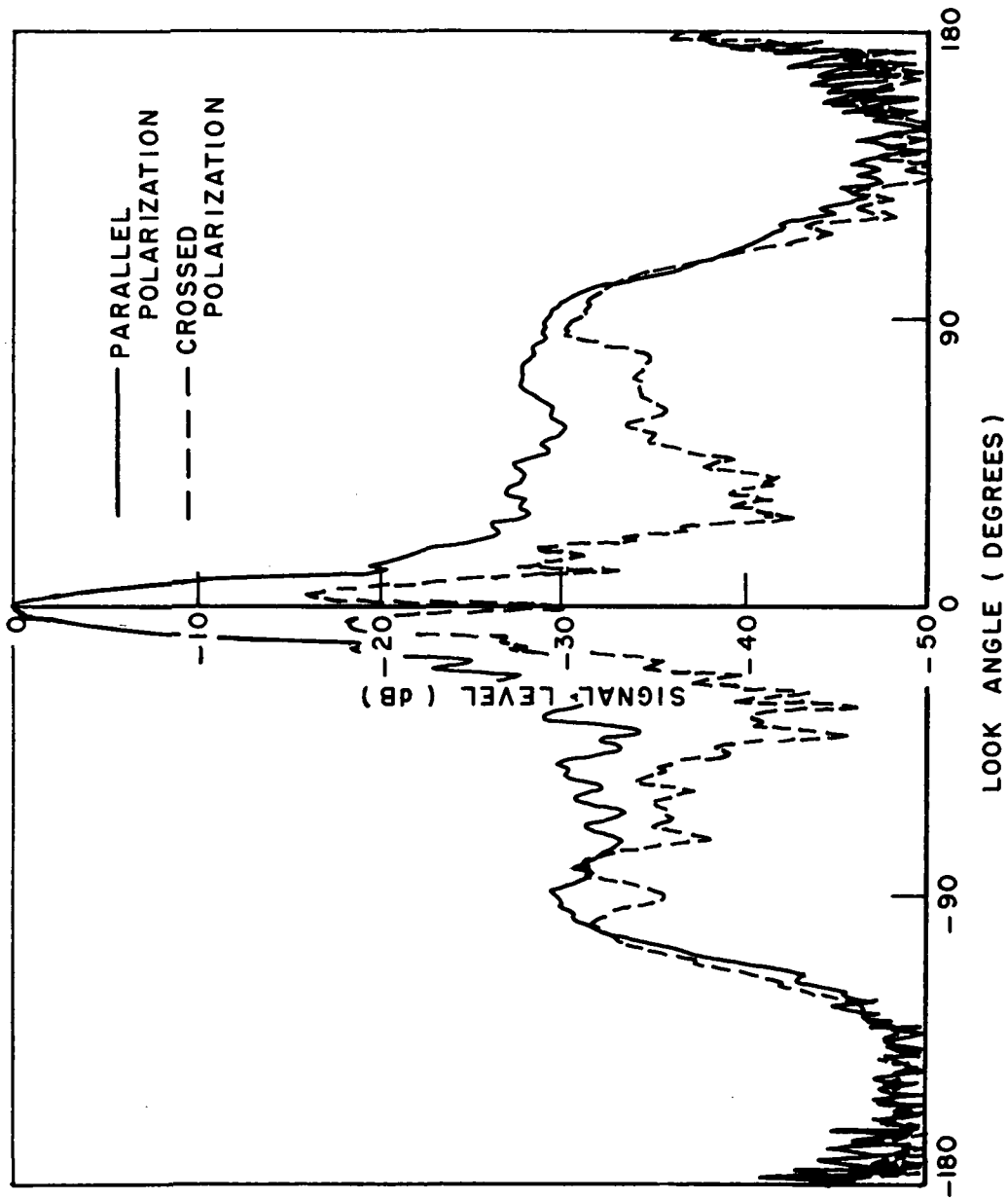


Fig. 67. Average patterns of a 2 ft diameter paraboloid (10 GHz, 7.5 ft range).

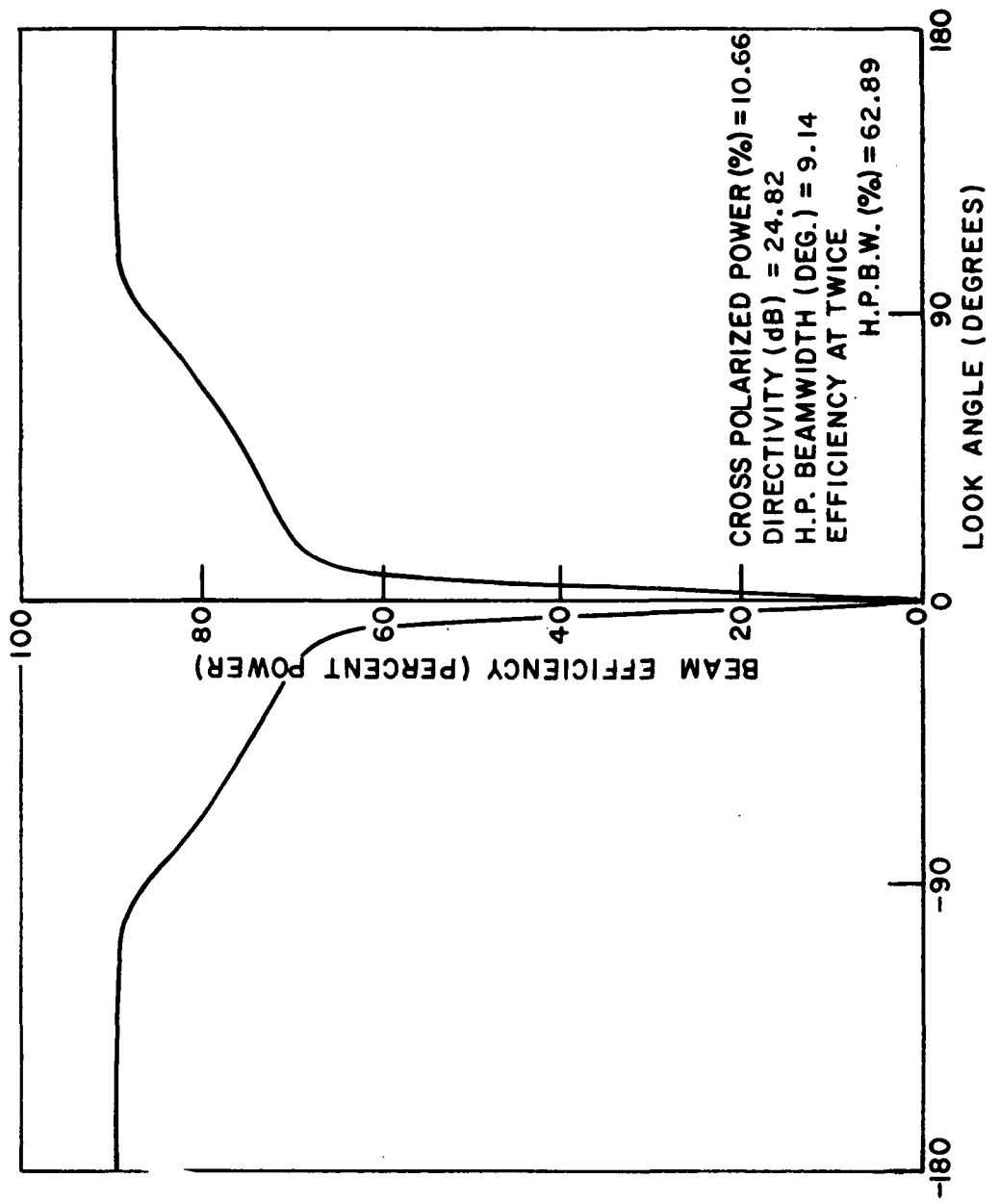


Fig. 68. Beam efficiency of a 2 ft diameter paraboloid (10 GHz, 7.5 ft range).

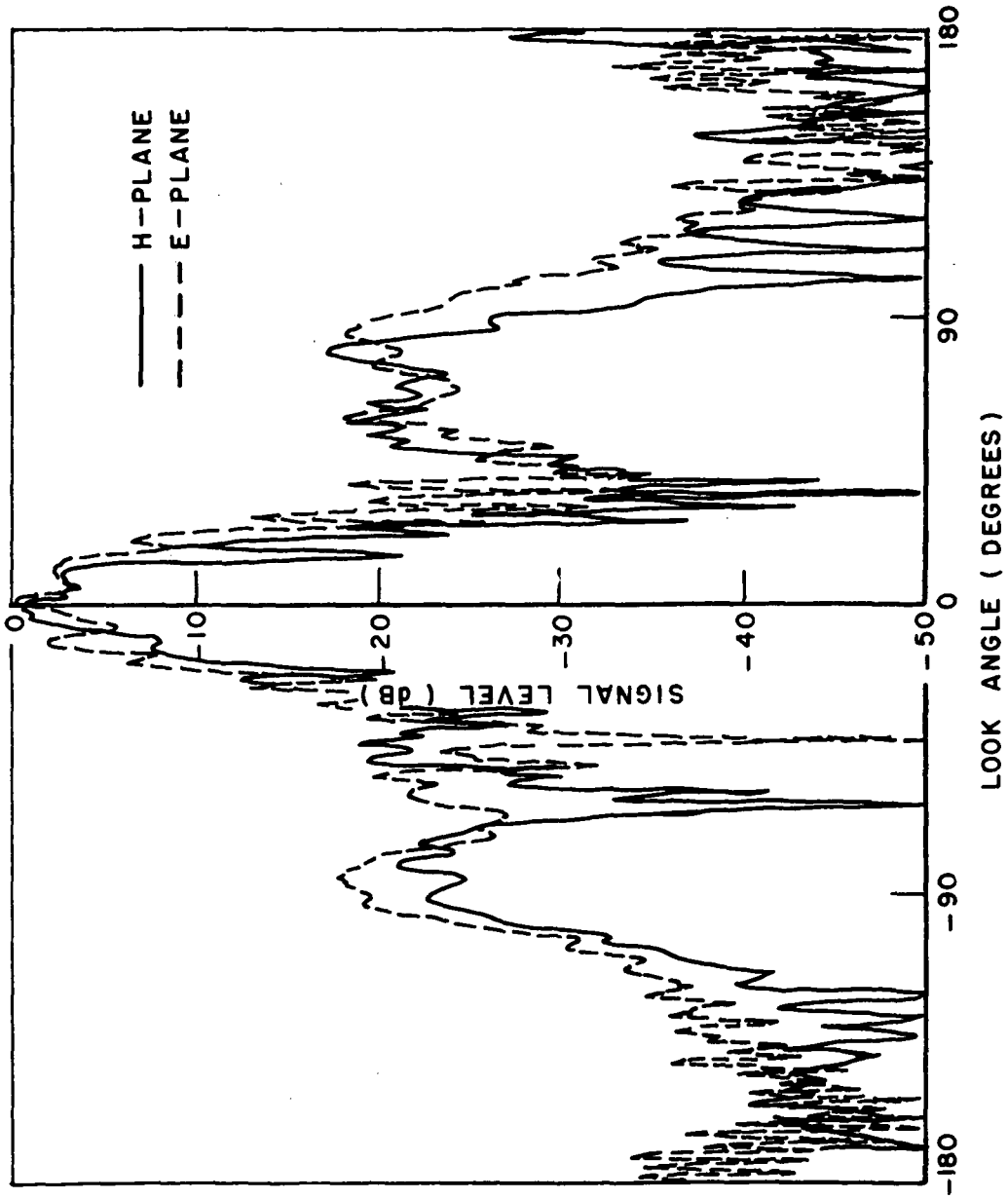


Fig. 69. Radiation patterns of a 2 ft diameter paraboloid (10 GHz, 2.7 ft range).

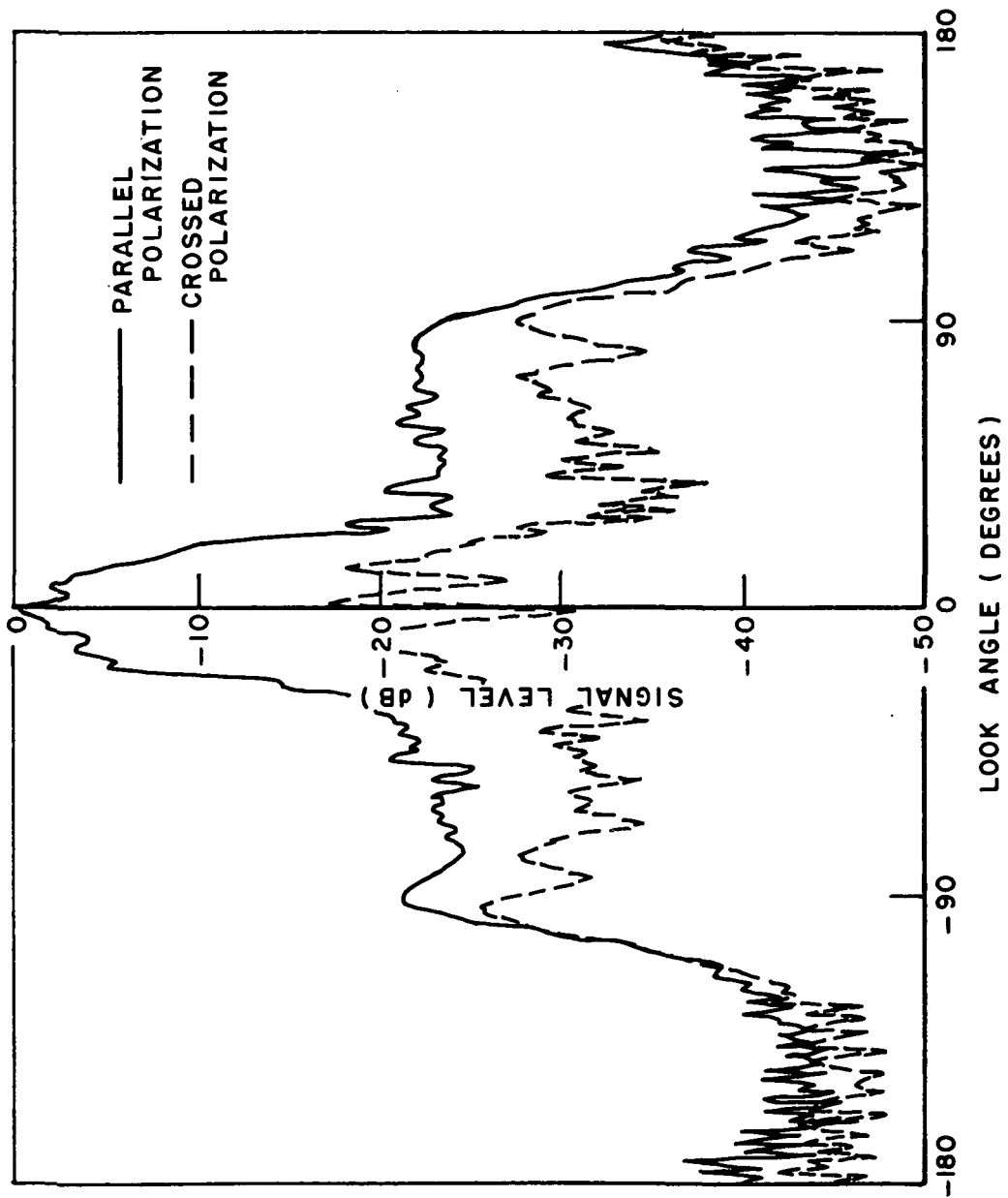


Fig. 70. Average patterns of a 2 ft diameter paraboloid (10 GHz, 2.7 ft range).

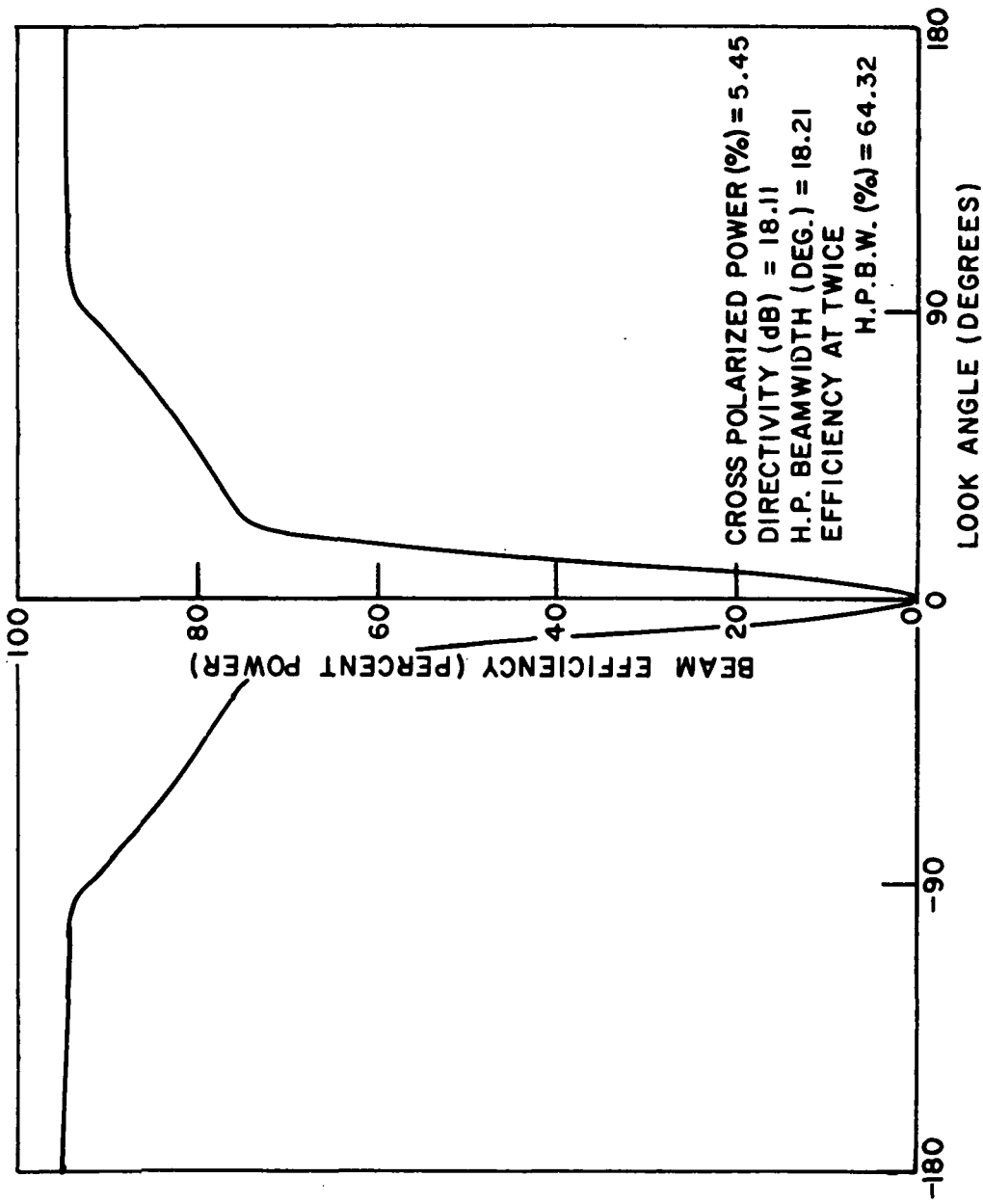
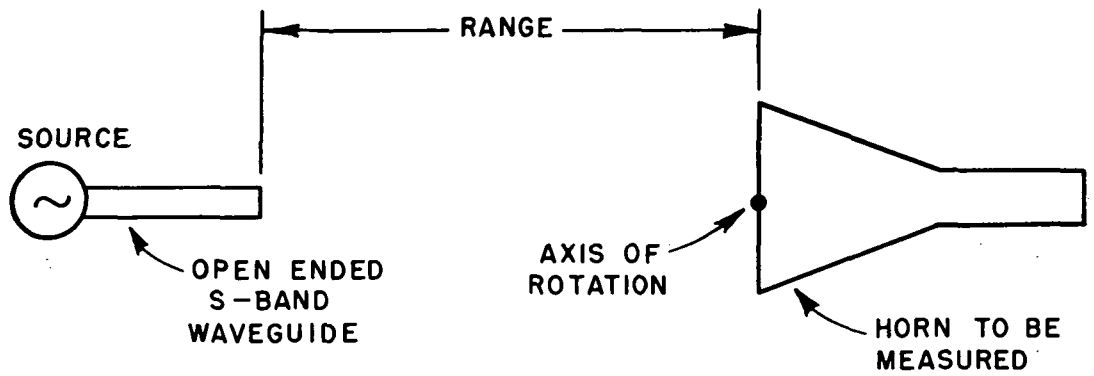
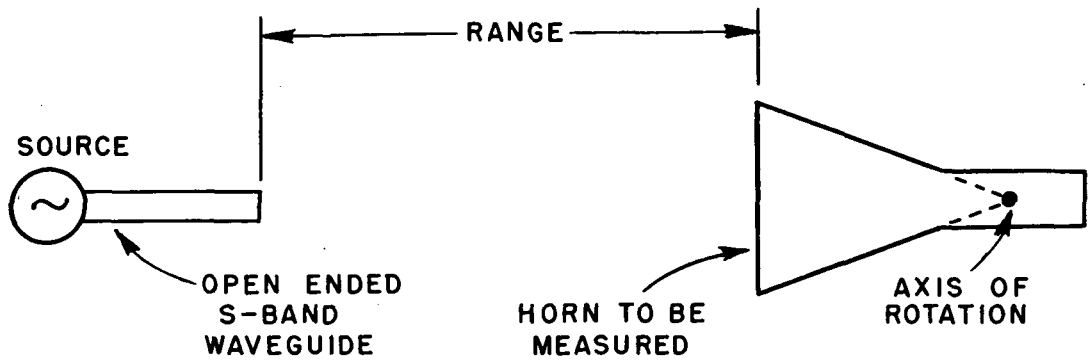


Fig. 71. Beam efficiency of a 2 ft diameter paraboloid (10 GHz, 2.7 ft range).



(a) ROTATION ABOUT APERTURE



(b) ROTATION ABOUT APEX

Fig. 72. Experimental arrangement for near field phase measurements.

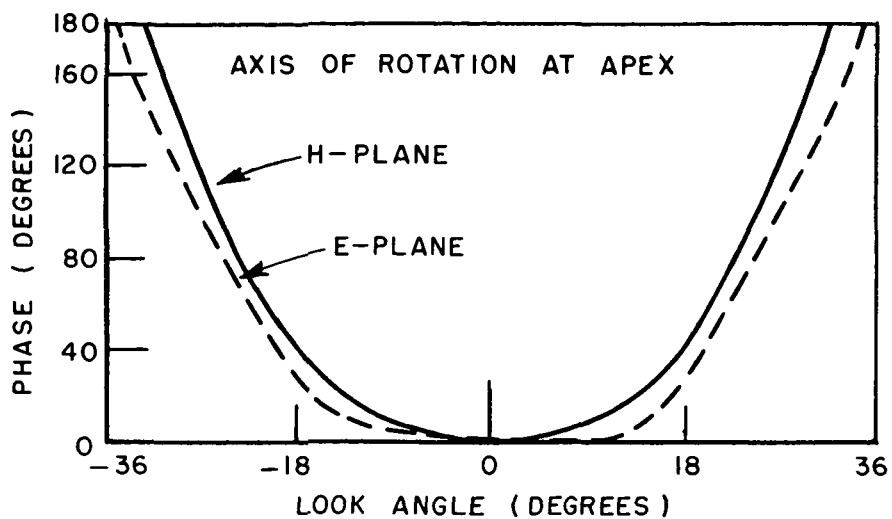


Fig. 73. Phase of the conical corrugated horn (20 inch range, 3.7 GHz).

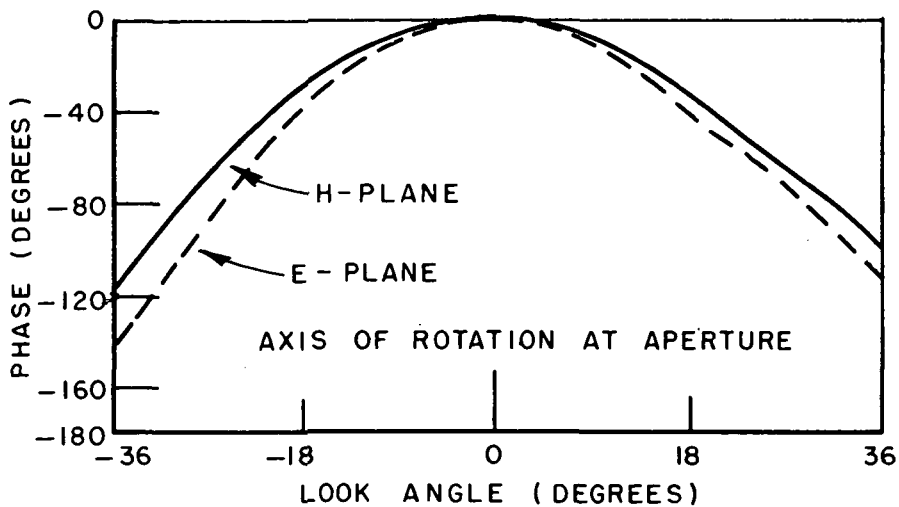


Fig. 74. Phase of the conical corrugated horn (20 inch range, 3.7 GHz).

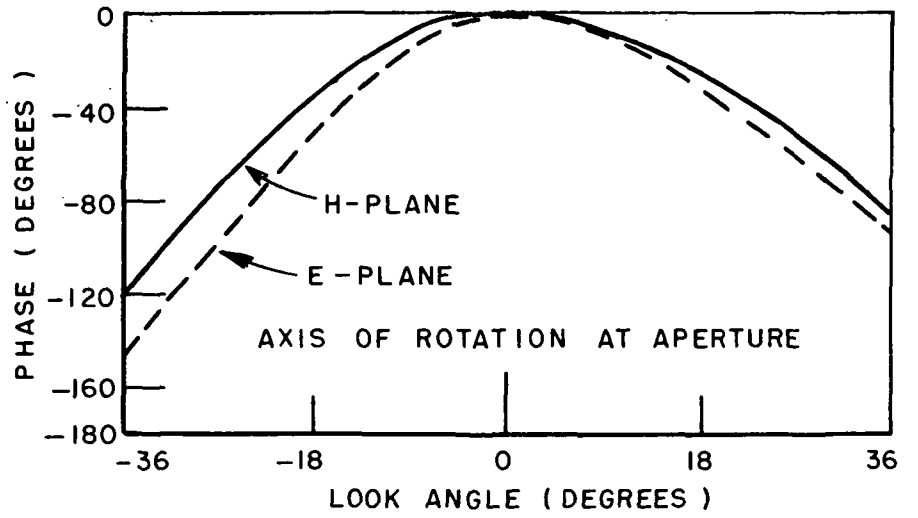


Fig. 75. Phase of the conical corrugated horn (10 inch range, 3.7 GHz).

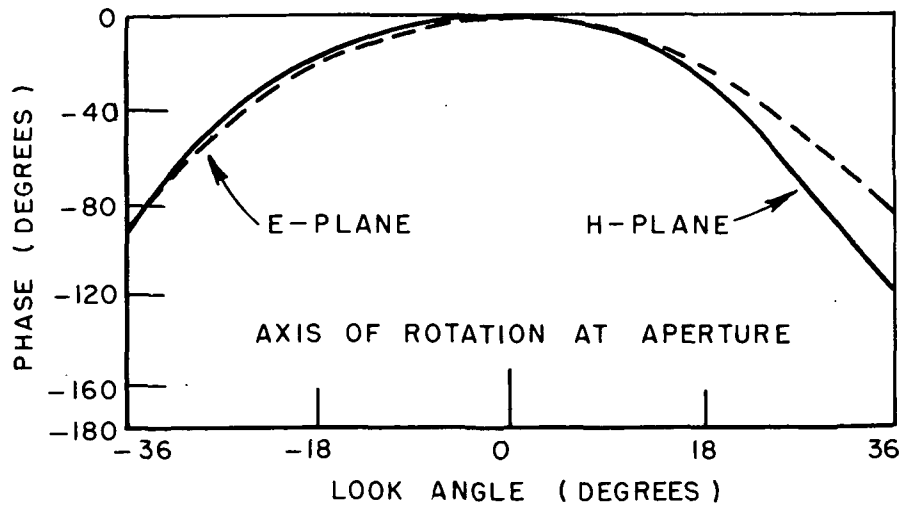


Fig. 76. Phase of the conical dual mode horn (20 inch range, 3.8 GHz).

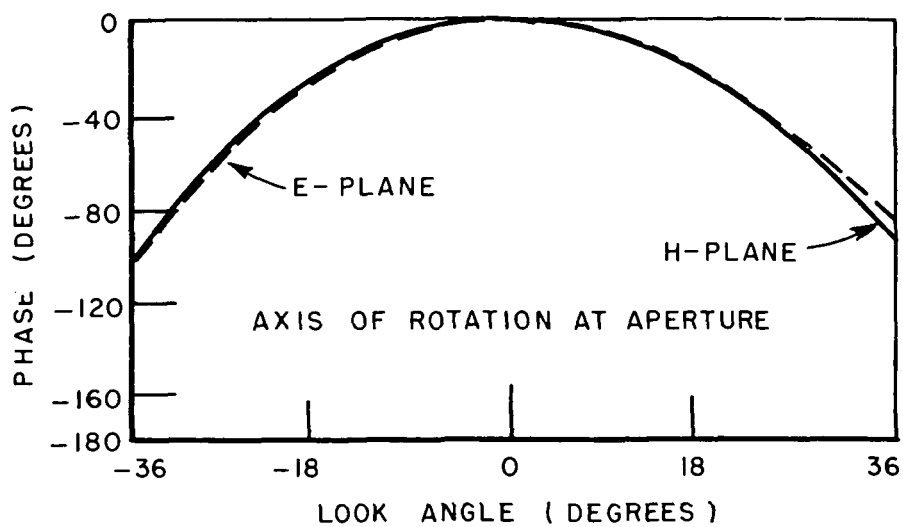


Fig. 77. Phase of the conical dual mode horn (10 inch range, 3.8 GHz).

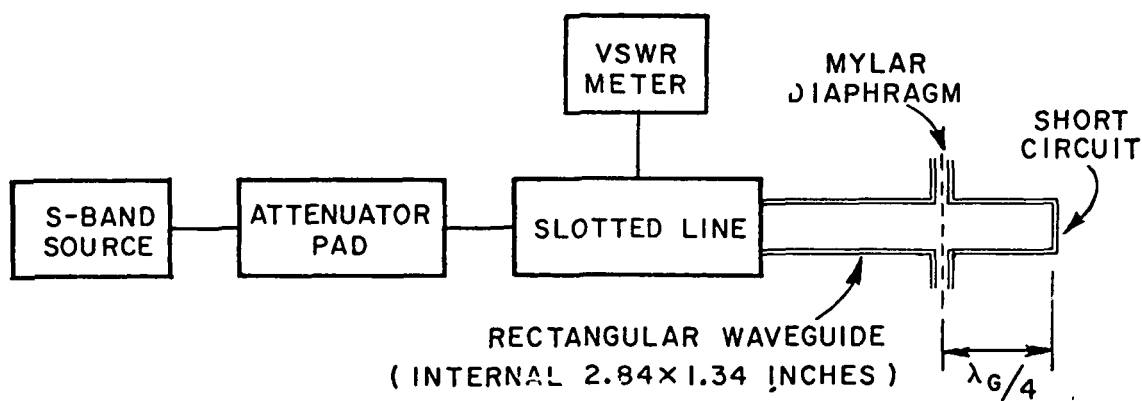


Fig. 78. Loss due to water and oil on a waveguide window.

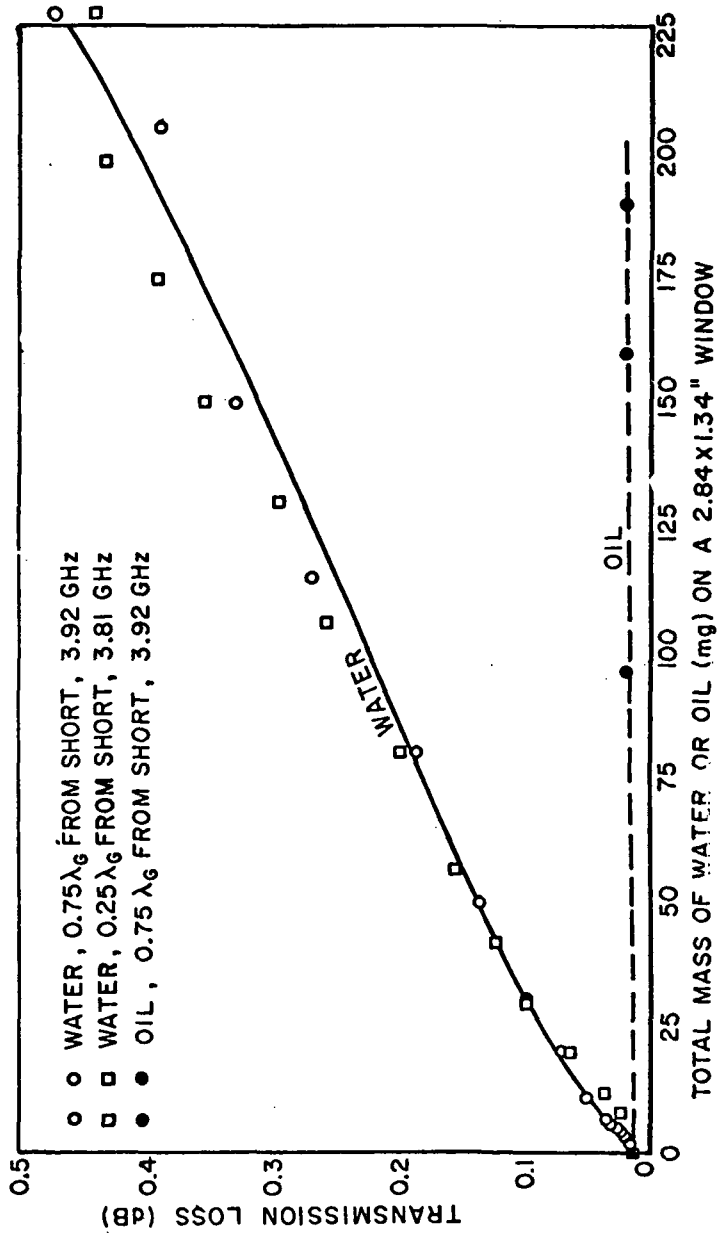


Fig. 79. Loss due to water and oil on a waveguide window.

A similar set of measurements of VSWR were then made with the short circuit replaced by a precisely matched load (Fig. 80). The object of this measurement was to see if there was correlation between reflection and loss due to the radome.

Following this initial test the next step was to repeat the measurements for an antenna. The conical dual mode horn was selected for this purpose because of its smaller flare angle. An open web of nylon threads was constructed a quarter wavelength from the aperture by drilling small holes through the horn walls for attachment purposes. The guide wavelength for the modes of interest is very nearly equal to the free space wavelength at this point in the horn. The horn was mounted vertically and a mylar diaphragm and filter paper were placed on the supporting web. The horn mouth was closed with a flat plate and VSWR measurements were made, as in the earlier loss measurements on this horn, using the four probe reflectometer in circular waveguide. Similar data were taken for various amounts of water on the filter paper as had been done in the rectangular guide. The oil measurement was omitted this time as it was felt that the initial tests had shown this to produce negligible loss. The comparative results for the horn and rectangular guide for the case of water are shown in Figs. 81-82. To permit a direct comparison the water density has been expressed in milligrams per 3.8 sq. in. of area (i.e., the area of the rectangular guide). Some difference may be seen between the two cases but this is to be expected since the modes are not identical.

The next question considered was the possible effect of contamination in the water, particularly due to salt spray. The horn measurements were therefore repeated using distilled water and a salt solution. Tap water was used for the first measurements. The three results are compared in Figs. 83-84. Because of the difficulty of controlling evaporation over the large area of filter paper a uniform salt concentration was not maintained. Instead a 0.3 molal solution was prepared initially. The paper was then allowed to dry as before to obtain successive readings. Thus the amount of salt remained constant but the concentration increased. The total amount of salt present is indicated by the intercept on the horizontal axis of Fig. 83 after the water had evaporated, the dry salt producing negligible attenuation.

In order to determine whether or not it is possible to measure radome loss in flight by monitoring the VSWR, the transmission loss and VSWR, for various conditions of the horn window, were plotted against each other in Fig. 85. It is evident that if the water is pure or nearly so a definite relationship exists between the loss and VSWR. However, if an unknown amount of salt is present it is not possible to infer the one from the other. Nevertheless, if the radome is initially clean it should be possible to estimate the loss due to rain on the window by a VSWR measurement if the distribution of water is fairly uniform.

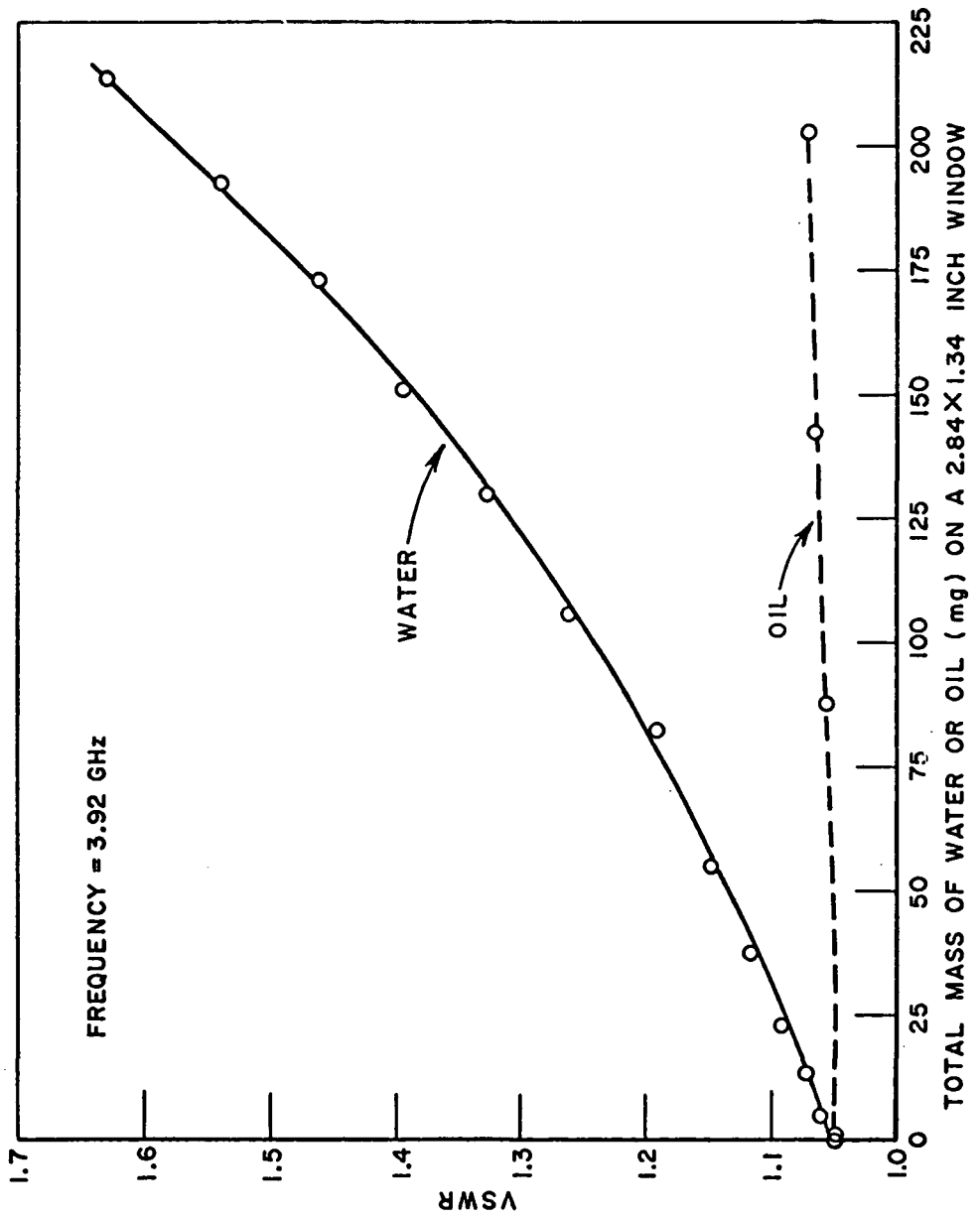


Fig. 80. VSWR due to water and oil on a waveguide window.

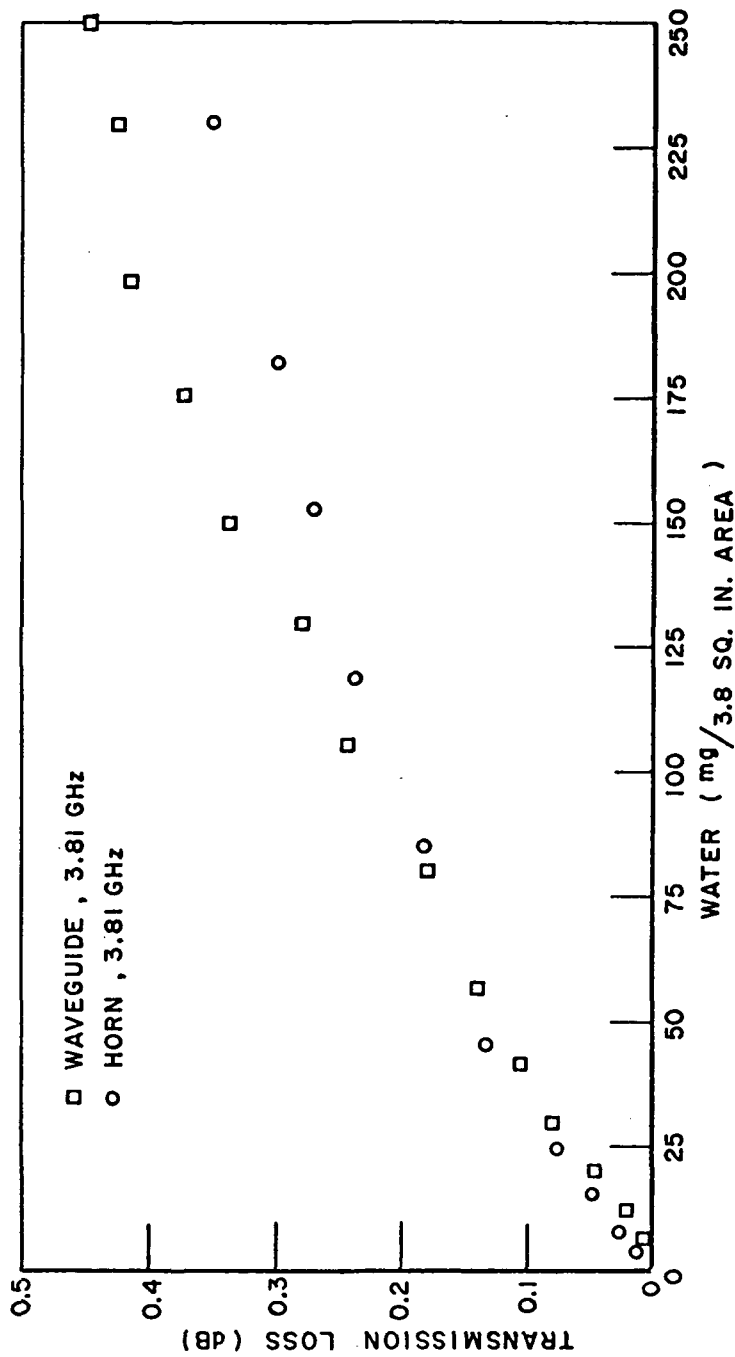


Fig. 81. Comparative loss measurements due to a water covered window for the conical dual mode horn and rectangular waveguide.

C-2

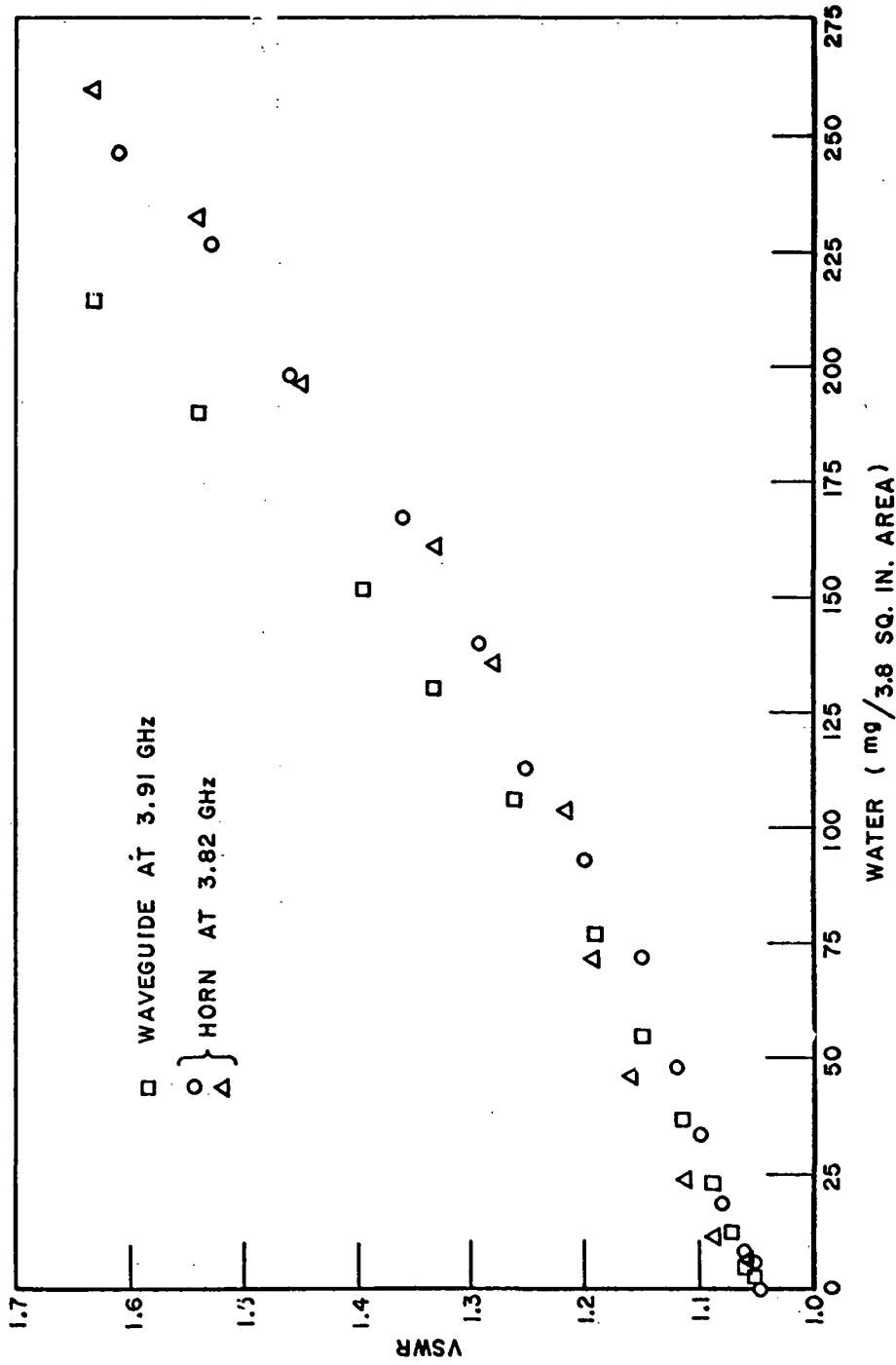


Fig. 82. Comparative VSWR measurements due to a water covered window for the conical dual mode horn and rectangular waveguide.

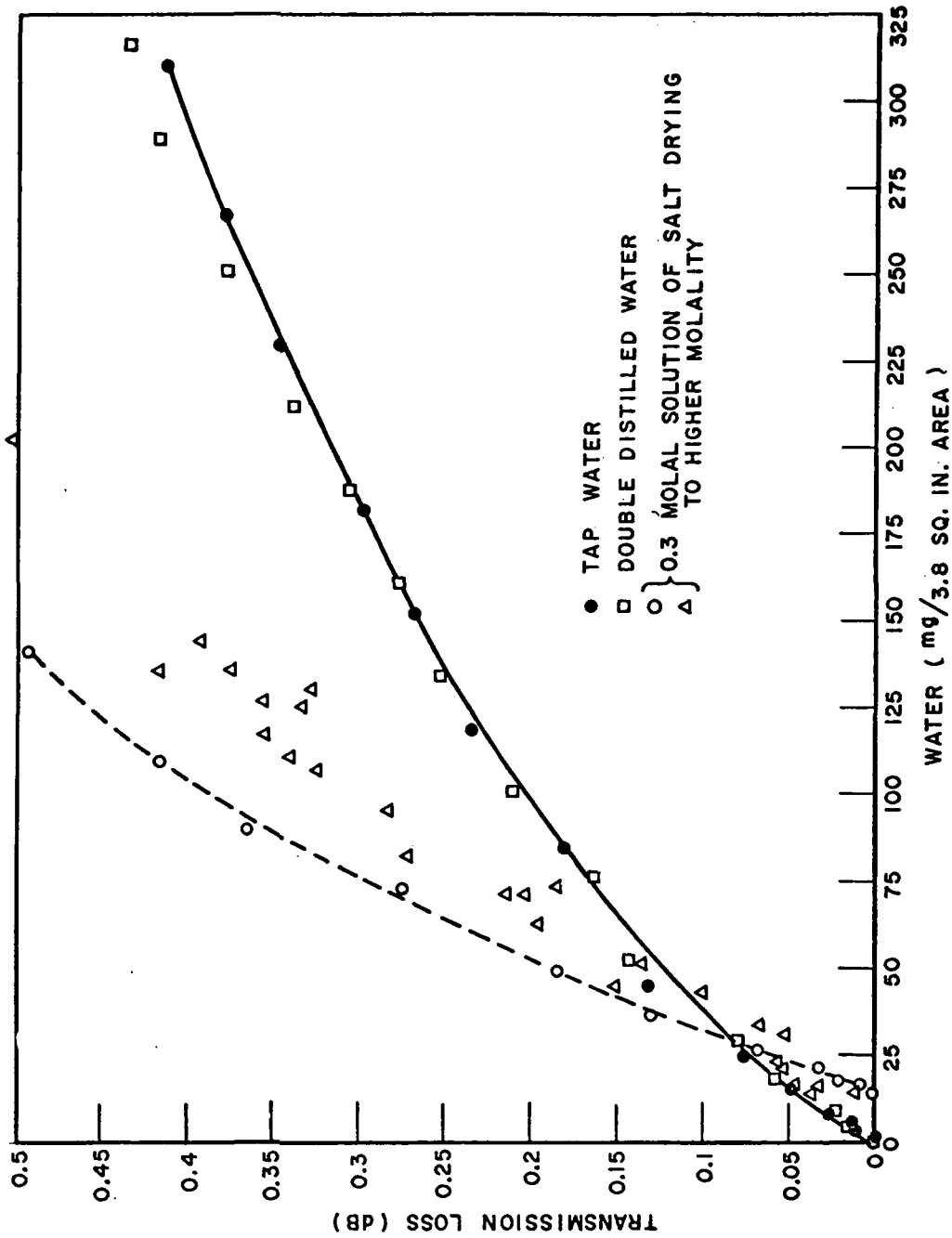


Fig. 83. Showing the effect of water purity on loss due to a water covered window over the conical dual mode horn (3.82 GHz).

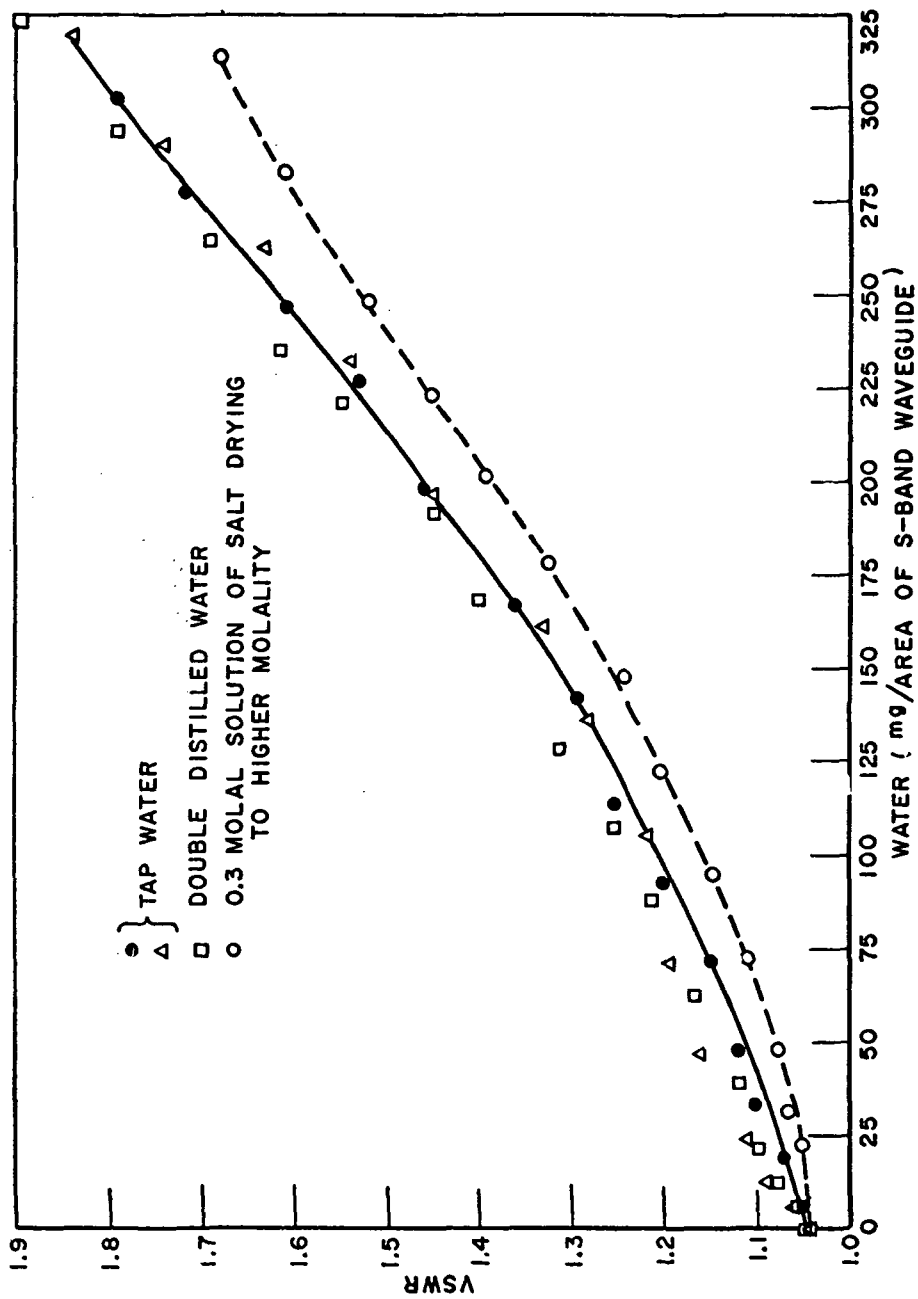


Fig. 84. Showing the effect of water purity on VSWR due to a water covered window over the conical dual mode horn (3.82 GHz).

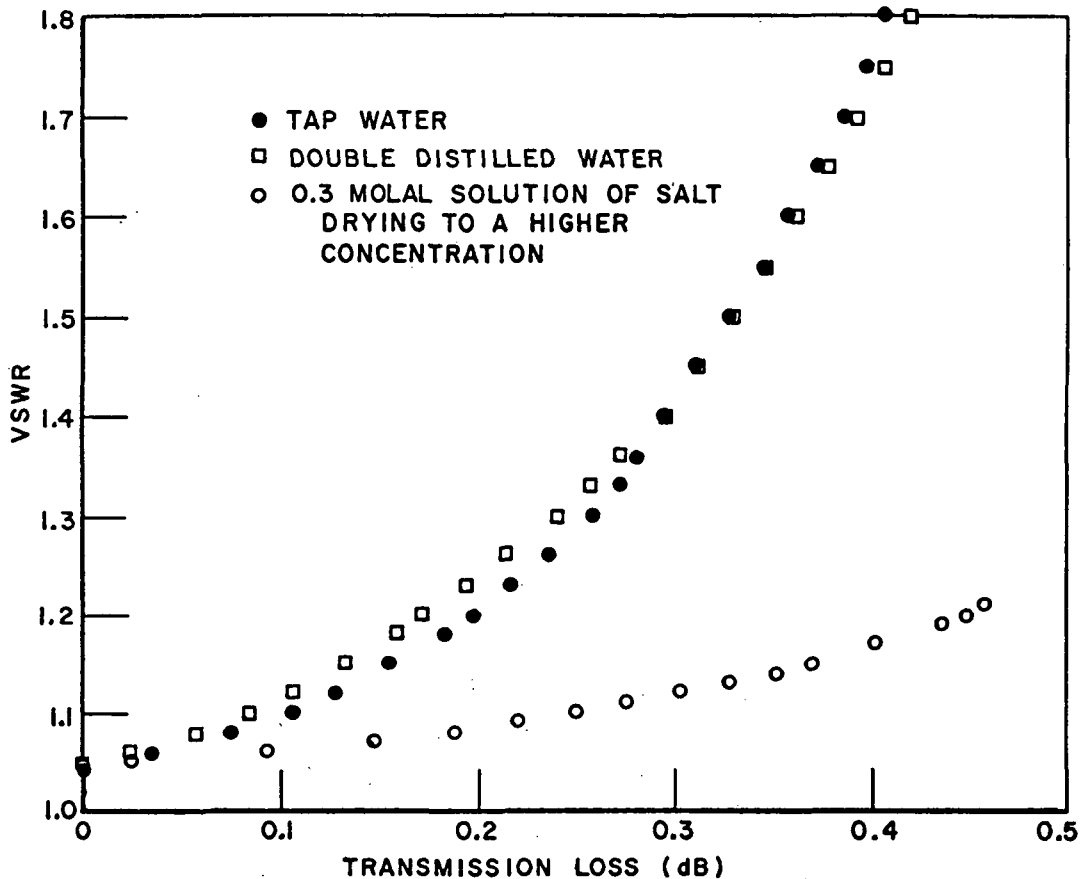


Fig. 85. Comparison of transmission loss and VSWR for various conditions of the window of the conical dual mode horn.

One further form of possible contamination was investigated briefly. The mylar window in a rectangular waveguide was first smeared with oil. The window was then covered with "road dust" and as much dust as did not adhere to the oil was blown off. The general appearance of the window is illustrated qualitatively in Fig. 86. Carbon scraped from the tail pipe of an automobile was added to the dust for some tests. The highest equivalent radome loss observed was about 0.005 dB which may be considered negligible.



Fig. 86. Approximate appearance of the waveguide window when coated with oil and road dust.

VII. GEOMETRICAL DIFFRACTION THEORY APPLIED TO DUAL MODE HORN DESIGN

In order to provide a better insight into the operation of the various horn types and ultimately to develop design procedures and make loss estimates for the dual mode geometries without resorting to empirical techniques, the geometrical theory of diffraction has been applied to the dual mode horn structures.

The geometric theory of diffraction analysis of the near fields of the dual mode horns has yielded some useful results but has proved to be rather cumbersome because of the large number of rays which must be considered in the analysis. The calculated aperture distribution for the pyramidal dual mode horn agrees fairly well with measured results in both the E-plane and H-plane. The conical dual mode horn analysis has not been completed but should yield similar results since the analysis is similar to the pyramidal dual mode horn. An outline of the analysis and some initial results appear here. A more detailed discussion of this work along with computer programs and additional calculated results will appear in a future report.

A. The Pyramidal Dual Mode Horn

The horn considered is composed of two pyramidal sections separated by a mode generating step discontinuity. The slant length of the two sections is 8.39 cm for the section between the waveguide and the step and 36.3 cm for the other section. The step height is 1.03 cm and the flare angle of each section is 10° . The computations have been made at a wavelength of 8 cm (3.75 GHz) to obtain both the E-plane and the H-plane aperture distributions. The fields incident on the horn-waveguide junction are assumed to be due to the dominant TE_{01} waveguide mode propagating in a square waveguide 4.42 cm on a side. In the E-plane, this mode is represented as a TEM wave propagating along the axis of the waveguide while the H-plane representation is the familiar plane wave pair bouncing between the waveguide walls. Figures 87 and 88 show the incident rays considered in the H-plane and E-plane respectively. The incident field at an edge is a combination of the diffracted fields from all the other unshadowed edges plus the direct waveguide incident field, if it is not shadowed. These incident rays after diffracting at the edge combine to form the internal horn fields. The rays used to determine the aperture fields in both the E- and H-plane are shown in Fig. 89 for a typical observation point. The various forms of the V_B diffraction coefficient⁷ were used in computing the aperture distributions shown in Figs. 90 and 91. Figure 90 shows measured and calculated aperture fields in the H plane along with a cosine distribution for comparison, since the H plane fields should be nearly sinusoidal. The measured data were obtained using a nulled backscatter system and moving a very small sphere across the aperture and recording the relative level of the reflected signal. The corresponding E-plane results are shown in Fig. 91. Here the cosine distribution is shown just for comparison with the H-plane data. While the agreement between measured and calculated H-plane aperture distributions is excellent, the agreement in the E-plane is only fair. This is not too surprising since the E-plane is the one where the mode generating step is effective and the small height of the step ($\sim \lambda/8$) makes the G.T.D. analysis somewhat questionable even when the near field form is used for the interaction between the two wedges which form the step. These results, however, should be adequate for an approximate loss calculation.

B. The Conical Dual Mode Horn

The conical dual mode horn considered here is the same one treated elsewhere in this report. The slant length and flare angle of the conical section between the 2.8 cm radius circular waveguide and the mode generating step are 6.0 cm and 10.4° respectively. The second conical section has a 39 cm slant length with a 10.4° flare angle and is separated from the first section by a 1.0 cm ($\lambda/8$) step ($\lambda = 8$ cm, $f = 3.75$ GHz). The circular waveguide is operated in its dominant TE_{11} mode which may be represented as a conical bundle of plane waves emanating from the waveguide axis. In a given plane containing the waveguide axis, this mode picture is similar to the plane wave pair picture usually associated with the H-plane of the TE_{01} rectangular waveguide mode. Details of this analysis and computed results will appear in a future report.

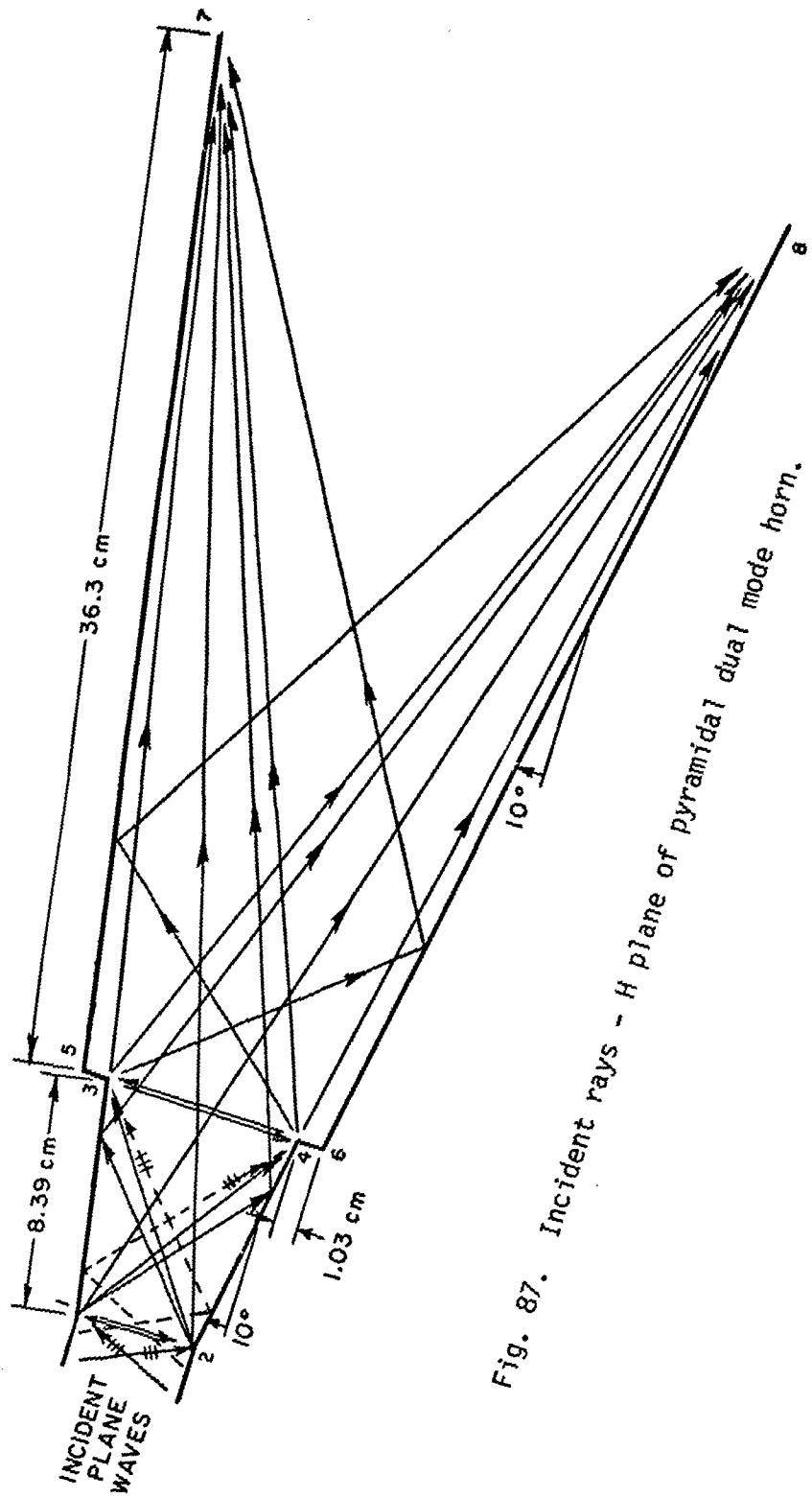


Fig. 87. Incident rays - H plane of pyramidal dual mode horn.

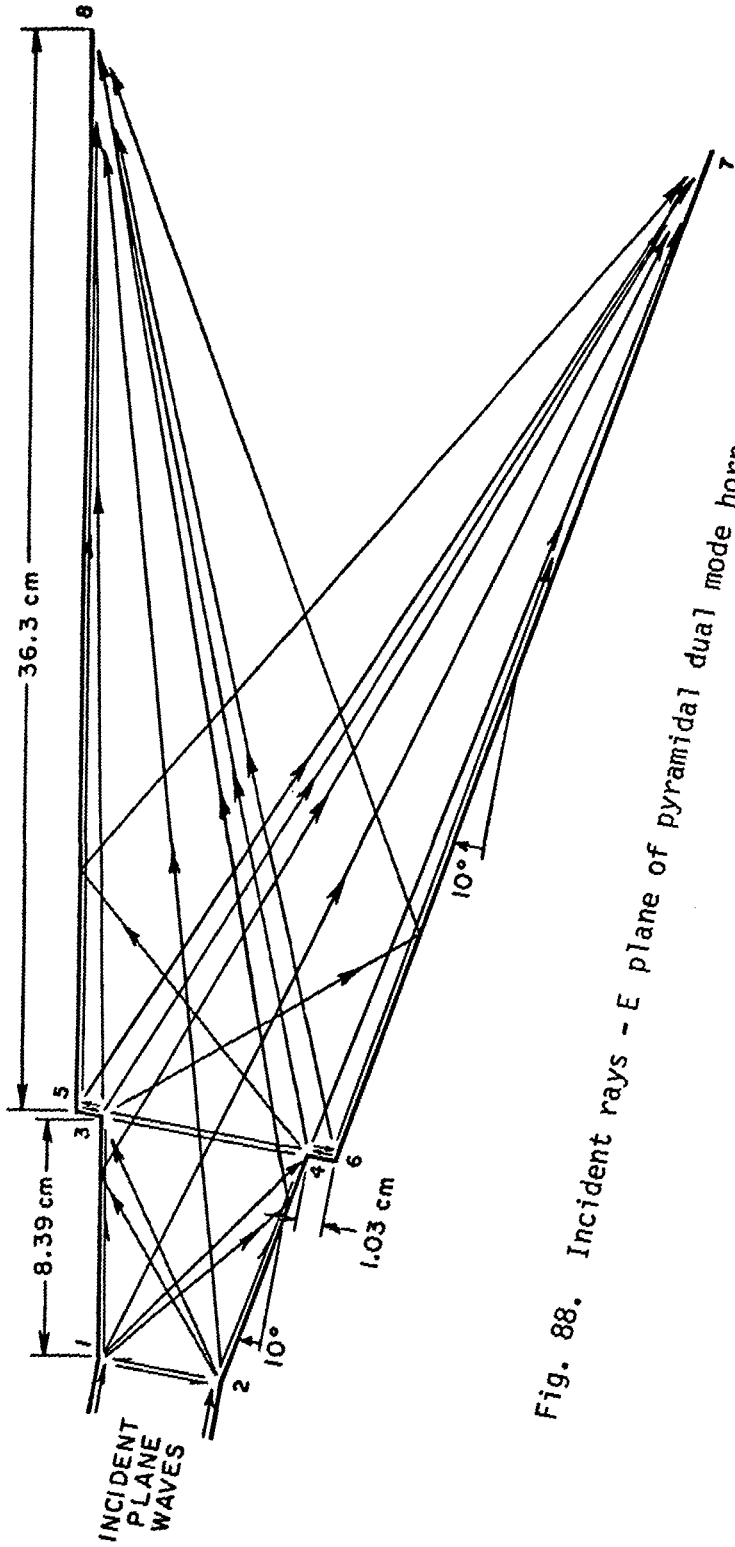


Fig. 88. Incident rays - E plane of pyramidal dual mode horn.

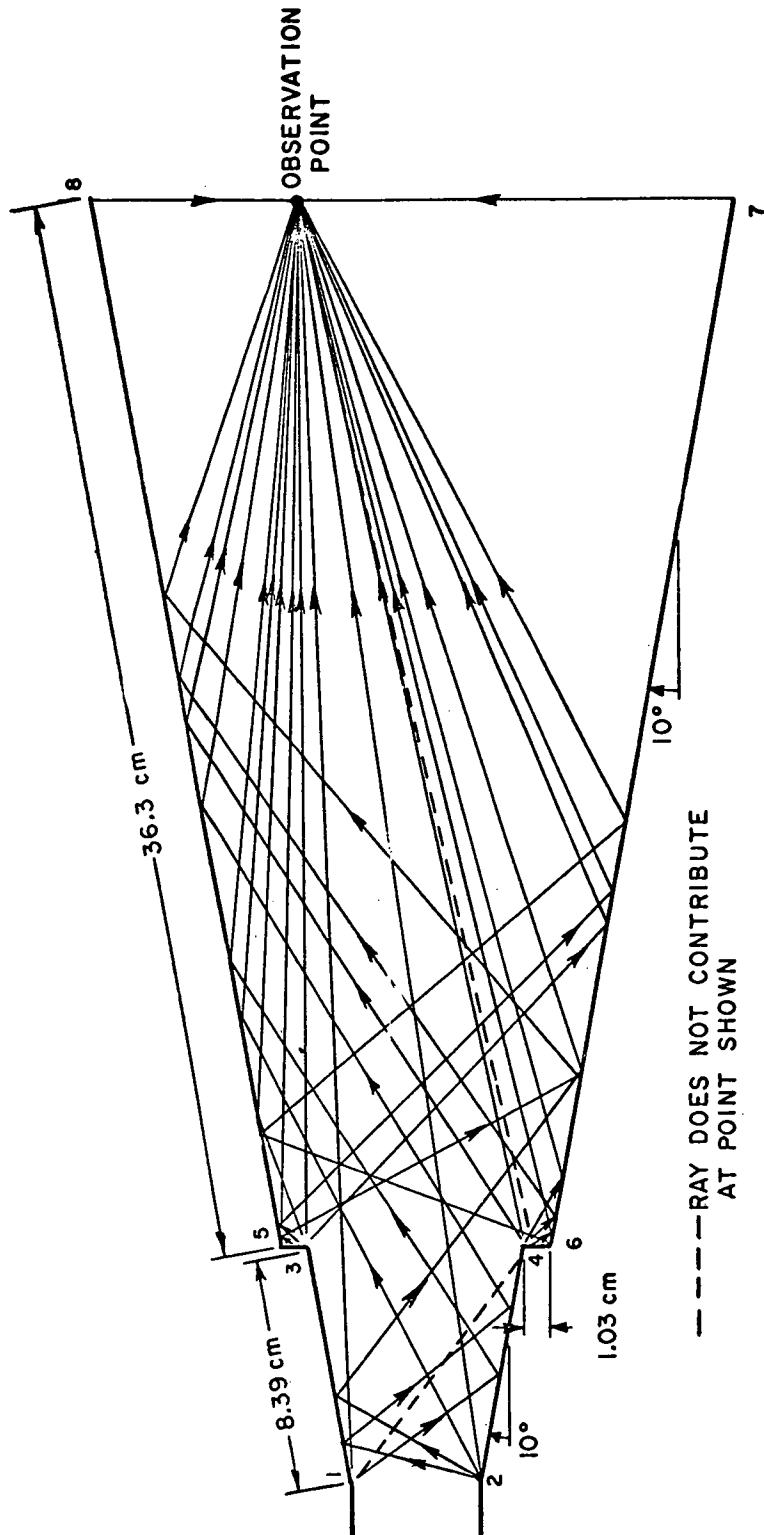


Fig. 89. Diffracted rays - H plane and E plane of the pyramidal dual mode horn.

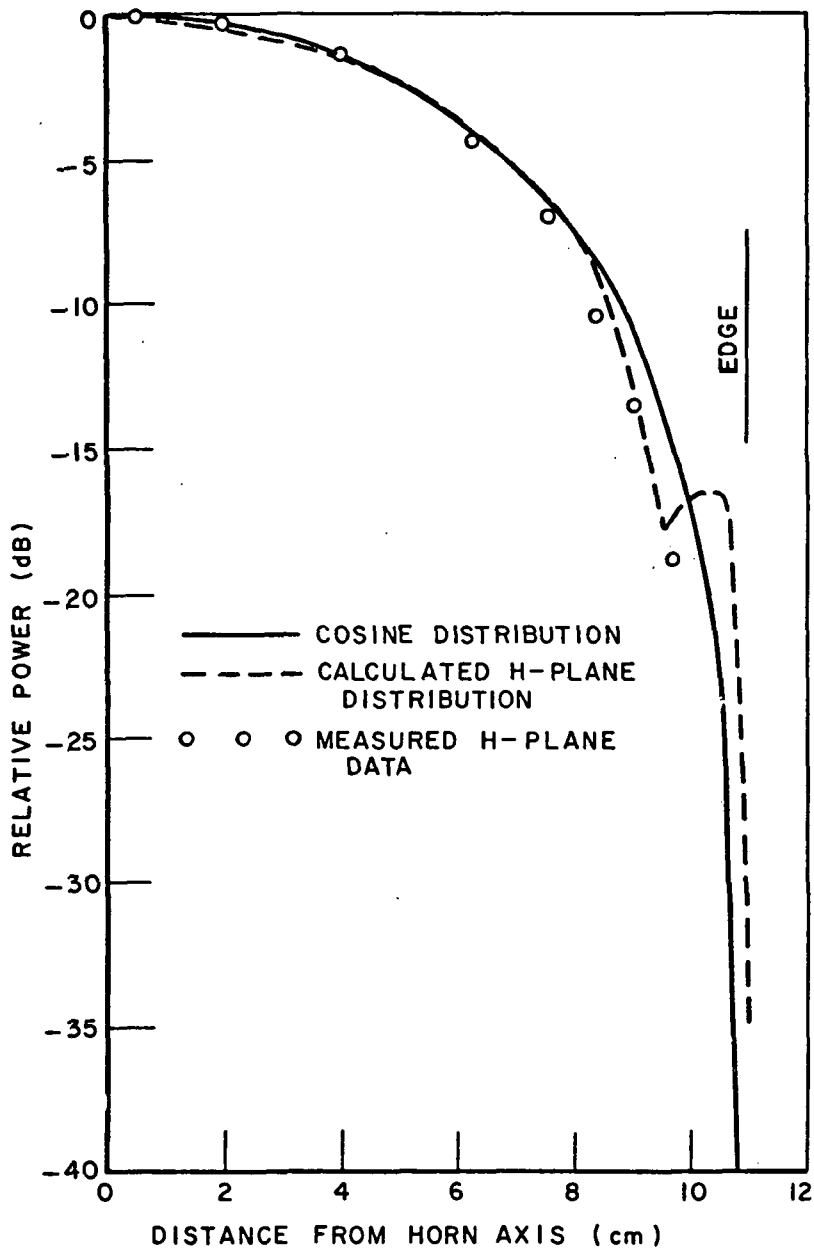


Fig. 90. H-plane aperture distribution of the pyramidal dual mode horn using rays of Figs. 87 and 89.

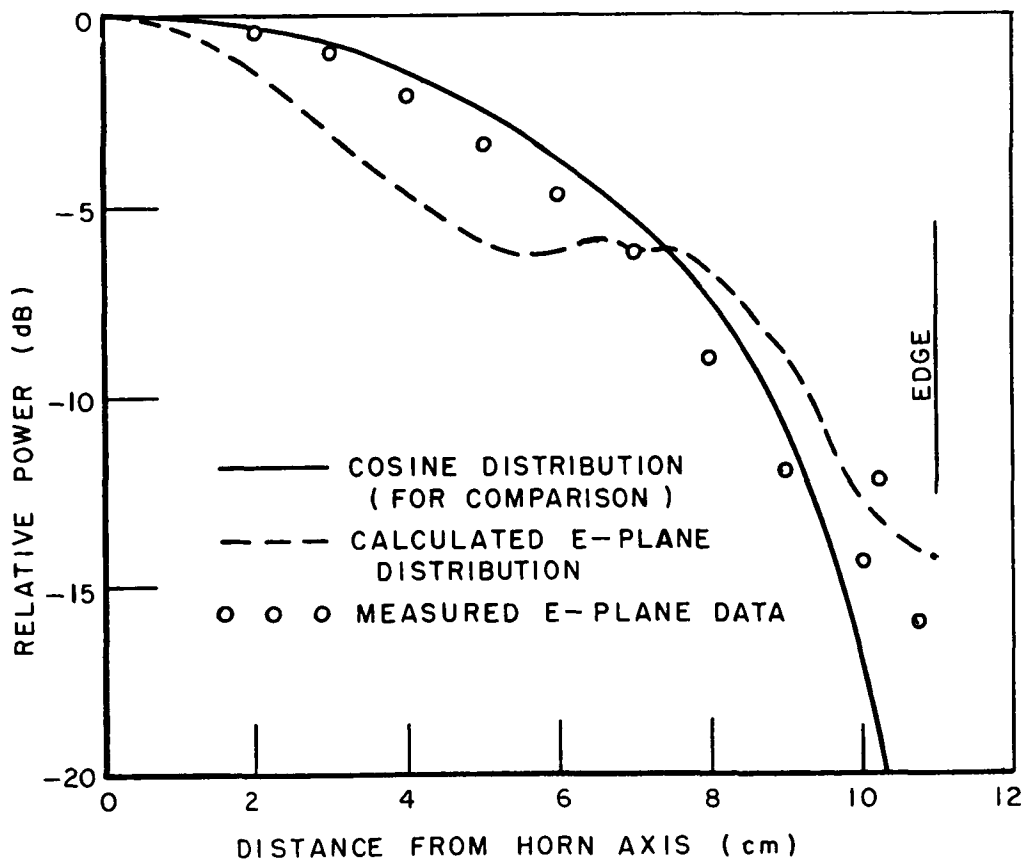


Fig. 91. E-plane aperture distribution of the pyramidal dual mode horn using rays of Figs. 88 and 89.

VIII. CONCLUSIONS

This work has shown that the criteria for the design of high performance radiometer antennas are considerably different from those for communications antennas. Of major importance is the radiation pattern which must have very low side and backlobes. It has been shown that the popular "half-power-beamwidth" has little meaning for a radiometer antenna nor does the full beamwidth in radiation patterns which have essentially no nulls. Rather the beamwidth should be defined in terms of the fraction of the radiated power (the antenna considered as transmitting) contained within a given angle. Beam efficiencies based on this definition have been measured for a number of horn antennas. The efficiency curves exhibit a natural knee around 97% efficiency where the second derivative of included power versus angle from the beam axis reaches a maximum. This would seem to be a logical point to define as the beam edge, the included power at this point being a figure of merit

for the antenna. The antennas designed and tested under this program, namely pyramidal and conical horns using both corrugated walls and dual mode techniques to produce the required beam shape, have proved far superior to such conventional antennas as the paraboloid.

In addition to having a clean radiation pattern it is essential that the reflection coefficient and wall losses of a good radiometer antenna be low. More important still is to know the residual losses to a high degree of accuracy so that correction can be made. Multi-probe reflectometer techniques have been developed under this program to the point where it is possible to measure these losses to better than 0.01 dB of the forward power when the antenna is transmitting. This is better than 1⁰K for a radiometer antenna if the losses are assumed to occur at an ambient temperature of 300⁰K. This technique avoids the need to construct special slotted lines for the circular and square waveguides used and also avoids the unacceptable approach, when this sort of accuracy is needed, of using a transition to a conventional sized slotted line.

The program has also seen the development of the geometrical theory of diffraction to the point where it is possible to calculate radiation patterns for dual mode horn geometries. This should permit future designs without the need for empirical adjustment of the mode forming system. The method also offers promise for calculating reflection and absorption losses directly.

While the program has produced major improvements in antenna design for radiometer applications, the antennas developed have been relatively low gain. Future work should be directed towards more directive antenna systems. Such systems might include the horn reflector antenna which offers no benefit in low gain systems. The techniques so far developed offer many possibilities for improving higher gain systems.

REFERENCES

1. Lawrie, R. and Peters, L., Jr., "Modification of Horn Antennas for Low Sidelobe Levels," The Ohio State University, IEEE - GAP, September 1966, Vol. AP-14, No. 5.
2. Narashimhan, M.S., "Corrugated Rectangular Horns," personal communication.
3. Jeuken, M.E.J., "Frequency Independence and Symmetry Properties of Corrugated Conical Horn Antennas with Small Flare Angles," Theoretical Electrical Engineering Group, Eindhoven University of Technology, Eindhoven, The Netherlands, 8 December 1970.
4. Clarricoats, P.J.B., "Analysis of Spherical Hybrid Modes in a Corrugated Conical Horn," Electronics Letters, 1 May 1969, Vol. 5, No. 9, p. 189.
5. Potter, P.D., "A New Horn Antenna with Suppressed Sidelobes and Equal Beamwidths," Microwave Journal, June 1963, pp. 71-78.
6. Jakes, W.C., Jr., "Horn Antennas," in Jasik, H., editor, Antenna Engineering Handbook, McGraw-Hill Book Co., 1961, pg. 10-12.
7. Rudduck, R. and Tsai, L.L., "Application of Optical Methods to Microwave Problems," Short Course 1969, Department of Electrical Engineering, ElectroScience Laboratory, The Ohio State University, section IV.

NATIONAL AERONAUTICS AND SPACE ADMINISTRATION
WASHINGTON, D.C. 20546

OFFICIAL BUSINESS
PENALTY FOR PRIVATE USE \$300

FIRST CLASS MAIL

POSTAGE AND FEES PAID
NATIONAL AERONAUTICS AND
SPACE ADMINISTRATION
451



POSTMASTER: If Undeliverable (Section 158
Postal Manual) Do Not Return

"The aeronautical and space activities of the United States shall be conducted so as to contribute . . . to the expansion of human knowledge of phenomena in the atmosphere and space. The Administration shall provide for the widest practicable and appropriate dissemination of information concerning its activities and the results thereof."

—NATIONAL AERONAUTICS AND SPACE ACT OF 1958

NASA SCIENTIFIC AND TECHNICAL PUBLICATIONS

TECHNICAL REPORTS: Scientific and technical information considered important, complete, and a lasting contribution to existing knowledge.

TECHNICAL NOTES: Information less broad in scope but nevertheless of importance as a contribution to existing knowledge.

TECHNICAL MEMORANDUMS: Information receiving limited distribution because of preliminary data, security classification, or other reasons. Also includes conference proceedings with either limited or unlimited distribution.

CONTRACTOR REPORTS: Scientific and technical information generated under a NASA contract or grant and considered an important contribution to existing knowledge.

TECHNICAL TRANSLATIONS: Information published in a foreign language considered to merit NASA distribution in English.

SPECIAL PUBLICATIONS: Information derived from or of value to NASA activities. Publications include final reports of major projects, monographs, data compilations, handbooks, sourcebooks, and special bibliographies.

TECHNOLOGY UTILIZATION PUBLICATIONS: Information on technology used by NASA that may be of particular interest in commercial and other non-aerospace applications. Publications include Tech Briefs, Technology Utilization Reports and Technology Surveys.

Details on the availability of these publications may be obtained from:

SCIENTIFIC AND TECHNICAL INFORMATION OFFICE

NATIONAL AERONAUTICS AND SPACE ADMINISTRATION

Washington, D.C. 20546